Alma Mater Studiorum – Università di Bologna

DOTTORATO DI RICERCA IN

Biologia cellulare e molecolare

Ciclo XXXII

Settore Concorsuale: 05/L1

Settore Scientifico Disciplinare: BIO/18 GENETICA

Harnessing the power of *Drosophila* model to obtain new insights on *MYC* and *ABCC1* cellular functions: from neuroblastoma to autism spectrum disorder

Presentata da: Dott.ssa Sara Monticelli

Coordinatore Dottorato

Prof. Giovanni Capranico

Supervisore

Prof.ssa Elena Maestrini

Co-supervisore

Dott. Roberto Bernardoni

Esame finale anno 2020

ABSTRACT

MYCN amplification is a genetic hallmark of the childhood tumour neuroblastoma. MYCN-MAX dimers activate the expression of genes promoting cell proliferation. Moreover, MYCN seems to transcriptionally repress cell differentiation even in absence of MAX. We adopted the *Drosophila* eye as model to investigate the effect of high MYC to MAX expression ratio on cells. We found that dMyc overexpression in eye cell precursors inhibits cell differentiation and induces the ectopic expression of *Antennapedia* (the wing Hox gene). The further increase of MYC/MAX ratio results in an eye-to-wing homeotic transformation. Notably, dMyc overexpression phenotype is suppressed by low levels of transcriptional co-repressors and MYCN associates to the promoter of *Deformed* (the eye Hox gene) in proximity to repressive sites. Hence, we envisage that, in presence of high MYC/MAX ratio, the "free MYC" might inhibit *Deformed* expression, leading in turn to the ectopic expression of *Antennapedia*. This suggests that MYCN might reinforce its oncogenic role by affecting the physiological homeotic program.

Furthermore, poor neuroblastoma outcome associates with a high level of the MRP1 protein, encoded by the *ABCC1* gene and known to promote drug efflux in cancer cells. Intriguingly, this correlation persists regardless of chemotherapy and *ABCC1* overexpression enhances neuroblastoma cell motility. We found that *Drosophila* dMRP contributes to the adhesion between the dorsal and ventral epithelia of the wing by inhibiting the function of integrin receptors, well known regulators of cell adhesion and migration. Besides, integrins play a crucial role during synaptogenesis and *ABCC1* locus is included in a copy number variable region of the human genome (16p13.11) involved in neuropsychiatric diseases. Interestingly, we found that the altered dMRP/MRP1 level affects nervous system development in *Drosophila* embryos. These preliminary findings point out novel ABCC1 functions possibly defining ABCC1 contribution to neuroblastoma and to the pathogenicity of 16p13.11 deletion/duplication.

CONTENTS

PREFACE

For over 100 years, *Drosophila melanogaster*, commonly called the fruit fly, has been representing one of the most extensively used model organisms in biomedical research. Rapid generation time, low cost and valuable genetic tools have made *Drosophila* an extremely flexible model suitable for multiple research areas ranging from genomics to cell and developmental biology. The fruit fly began to be used for scientific purposes in the early 1900s when Thomas Hunt Morgan's experiments on white-eye mutants laid the bases for the demonstration of the chromosomal theory if inheritance. Between 1970s and 1980s the intensive study of *Drosophila* embryology led to the discovery of specific sets of genes regulating several aspects of development. A number of those genes, e.g. the Hox genes, turned out to be shared among virtually all species and their homologs have been demonstrated to be involved in both human physiological development and pathological conditions. The significant level of conservation between human and *Drosophila* encouraged researchers to use the fruit fly to assess the function of conserved genes and to address basic and applied questions on cell biology especially attempting to model human diseases.

During my PhD I adopted this excellent model system to assess the impact of a high MYC to MAX expression ratio on cell proliferation and differentiation. The most studied members of the MYC family, c-MYC and MYCN, are known to have a substantial activity as oncogenes. The deregulated expression of MYCN drives multiple human tumours affecting nervous hematologic and neuroendocrine systems. Among others, the genomic amplification and overexpression of MYCN represents a robust prognostic marker of the childhood tumour neuroblastoma. Upon dimerization with its binding partner MAX, MYCN activates the transcription of several target genes promoting cell proliferation and inhibiting cell differentiation. Besides, MYCN seems to play an important role as transcriptional repressor of pro-differentiation genes, even though the underlying mechanisms and the requirement of MAX are still elusive. Therefore, during the first part of my PhD I evaluated the impact of a high MYC to MAX expression ratio on cell physiology.

Among the genes transcriptionally activated by MYCN, there is another significant prognostic marker of poor neuroblastoma outcome, *ABCC1*, encoding the multidrug associated protein 1 (MRP1). MRP1 is an ATP-binding cassette transporter which promotes the efflux of multiple drugs out of cancer cells thus contributing to the development of multidrug resistance. Intriguingly, high ABCC1 level is associated with unfavourable neuroblastoma prognosis even in absence of chemotherapeutic treatments and its overexpression has been demonstrated to

enhance neuroblastoma cell motility. Moreover, the human *ABCC1* locus is included in a well-known copy number variable region of the short arm of the chromosome 16 (16p13.11). Duplications and deletions of this region are associated with several neuropsychiatric conditions such as autism spectrum disorders, schizophrenia and cognitive impairment. Moreover, a copy number variant analysis previously conducted in our laboratory identified the 16p13.11 duplication in a sample of autism-affected individuals. Although *ABCC1* has been reported to be expressed in the nervous system, its physiological role has been very poorly explored yet. Hence, in the last part of my PhD program I started the investigation of ABCC1 physiological functions and its possible role during neurodevelopment.

PART I – High MYC/MAX ratio affects cell differentiation by altering Hox genes expression

INTRODUCTION

1.1 Neuroblastoma

1.1.1 Main clinical features

The extracranial solid tumour neuroblastoma is one of the most extensively studied tumour in cancer research. Accounting for 7-10% of all childhood cancers and for 15% of all paediatric cancer death, it represents the most common and deadly tumour of infancy. At diagnosis, more than half of patients have a metastatic disease principally affecting bone marrow, bones, lymph nodes and liver (brain and lung with lower frequency), while the primary tumour mainly develops in adrenal medulla and in paravertebral sympathetic ganglia (Maris et al. 2007). These last structures are part of the peripheral nervous system and they originate from embryonic neural crest cells (NCCs). After their specification during neurogenesis, NCCs leave the neural tube and migrate ventrally along different paths to eventually differentiate in multiple cell types in response to local cues. NCCs delaminating from the trunk region of neural tube and migrating along the ventral pathway give rise to sympathoadrenal cells, the major cell lineage derived from NCC. Sympathoadrenal cells principally originate sympathetic ganglia neurons and neuroendocrine chromaffin cells of adrenal medulla (Ratner et al. 2016), sites of neuroblastoma onset. Therefore, neuroblastoma can be considered the result of the failure of NCC proper differentiation.

Neuroblastoma frequently appears as an undifferentiated tumour consisting in small neuroblasts with a low or absent level of neural differentiation. Nevertheless, there are cases of partially or totally differentiated neuroblastic tumour, respectively ganglioneuroblastoma and ganglioneuroma. Unsurprisingly, the state of tumour cell differentiation influences tumour malignancy and such histopathological features are important parameters considered during neuroblastoma staging (Brodeur 2003). In 2009 the pre-surgical International Neuroblastoma Risk Group Staging System (INRGSS) has been proposed as an effective alternative to the already established International Neuroblastoma Staging System (INSS). INSS is based on the surgical approach depending on the extent of resection and lymph node sampling, which can

greatly vary from different centres. Differently, INRGSS stratifies neuroblastoma patients before any treatments, providing a worldwide consensus approach for tumour staging. Patients are classified according to clinical criteria and tumour imaging, such as age at diagnosis, histologic category, grade of tumour differentiation, and markers of tumour biology. INRGSS classification system consists of four stages: L1, L2, M and MS. Localized tumours are classified in L1 or L2 according to absence or presence of image-defined risk factors, respectively. While L1 tumours do not involve local structures and are often amenable to resection, L2 are locally invasive tumours and are only rarely resectable at diagnosis. M and MS are metastatic neuroblastomas. The first refers to a widely disseminated tumour, whereas MS stage characterizes children younger than 18 months with skin, liver and bone marrow metastasis and primary L1 or L2 tumour (Cohn et al. 2009). Besides the age at diagnosis and the disease stage, other genomic and cellular features (e.g. tumour histology, MYCN oncogene amplification, cell ploidy, chromosomal aberrations) are evaluated to classify patients into risk groups: very low, low, intermediate or high (Van Arendonk and Chung 2019). Low- and intermediate- neuroblastomas are often associated with a favourable tumour outcome, with a high rate of event free survival (80%-95%). Conversely, 50% of patients affected by high-risk neuroblastoma are susceptible to develop a second malignancy in 5 years (Cohn et al. 2009). The stratification of patients in risk groups is fundamental to predict tumour progression and establish the appropriate therapy. Neuroblastoma prognosis can be highly diversified, ranging from spontaneous regression to widely metastatic and therapy resistant tumour. A reason for that lies in the large number of biological factors affecting tumour onset and progression. Over the past years, much effort has been made to define neuroblastoma features in order to obtain accurate prognosis and provide suitable therapies.

1.1.2 MYCN prognostic marker

Most neuroblastoma cases are sporadic and characterized by different genetic features, such as changing of tumour cell ploidy, allelic loss of tumour suppressor genes and amplification and/or overactivation of oncogenes. Among those, the amplification of the proto-oncogene *MYCN* plays a key role. It occurs with an overall prevalence of 22% and it is associated with rapid progression and poor outcome of the tumour even in presence of a favourable stage of the disease (Cohn et al. 2009). Moreover, *MYCN* amplification is one of the established traits of high-risk neuroblastoma, besides the loss of heterozygosity (consequent to the loss of a parental wild type allele) at one or more loci of the short arm of the chromosome 1 (1p). Although it is

not yet clear whether deletions of 1p could have a prognostic significance independently from *MYCN* amplification, the two events are significantly correlated with each other and are both associated with aggressive neuroblastomas. (Brodeur 2003). Moreover, MYCN is normally expressed by post-migratory neural crest cells and it contributes to the regulation of their expansion and migration along the ventral pathway. The physiological decrease of MYCN level during NCC differentiation toward sympathoadrenal neurons suggests that a low MYCN expression could be required for proper NCC maturation (Zimmerman et al. 1986). Indeed, MYCN overexpression in mature sympathetic neurons is sufficient to trigger cell proliferation and avoid apoptosis normally induced by improper cell cycle re-entry (Wartiovaara et al. 2002). Therefore, a high MYCN expression in neuroblastoma cells could lead to the acquisition of proliferative and antiapoptotic properties favourable to malignant transformation.

In the human genome, MYCN is located in the short arm of chromosome 2. In *MYCN*-amplified neuroblastoma cells it has been detected also in double-minute chromatin bodies (DMs) and in homogeneously staining regions (HSRs): two cytogenetic sites of abnormal gene amplification. Nevertheless, extra copies of MYCN have not been detected in the resident *MYCN* locus (2p24) or in neighbouring chromosomal regions (Corvi et al. 1994). Even though the precise mechanism underlying *MYCN* amplification is still unknown, it seems to rely on the copy of a 2p genomic region including *MYCN* locus and consequent formation of extrachromosomal circular element (DM) or integration in other genomic regions causing a copy number gain (HSR). Notably, *MYCN* amplification is associated with increased MYCN protein level (Seeger et al. 1988) that can be even 100 times higher than normal. Interestingly, even in absence of genomic amplification some neuroblastoma cells show a high amount of MYCN mRNA and protein (Wada et al. 1993). Although little is known about the mechanisms originating this overexpression, MYCN mRNA and protein levels have been shown not to be always strictly correlated. For instance, the activation of PI3K/AKT pathway and Aurora kinase stabilize MYCN protein (Chesler et al. 2006). Protein stabilization and/or alteration of degradative pathways could lead to increased MYCN amount even in presence of physiological genomic copy number and mRNA level.

1.2 The MYC protein family

MYCN is a member of the MYC oncoprotein family composed by c-MYC, L-MYC and MYCN. All these proteins are transcription factors characterized by common structural features. The N-terminal half contains two highly conserved domains for transcriptional

regulation called Myc boxes 1 and 2 (MBI and MBII), through which MYC proteins interact with co-activators or co-repressors. The Myc box 3 and 4 (MBIII and MBIV) located in the central region of c-MYC and MYCN further mediate the transcriptional activity and the apoptosis induction (Cowling et al. 2006). In the same region all MYC family members show a nuclear localization signal (NLS) and a proline rich segment (PEST) involved in rapid MYC degradation. Finally, the C-terminal half of MYC oncoproteins harbours a basic-region/helix-loop-helix/leucine-zipper domain (BR/HLH/LZ) required for protein-protein interaction and DNA binding. In particular, trough the BR/HLH/LZ, MYC proteins interact with the BHLHZ domain of MAX (Myc associated protein X) leading to MYC-MAX heterodimers formation (Conacci-Sorrell et al. 2014)

1.2.1 MYC/MAX/MXD network

MYC-MAX heterodimers (MYC referred to the entire MYC family) promote the expression of target genes harbouring in their regulatory region a specific MYC-MAX binding site, named E-box, defined by the consensus sequence CAC/TGTG: a specific variant of the CANNTG normally bound by bHLH factors. Once the binding has occurred, MYC activates target's expression through different mechanisms. MYC can associate with histone acetyltransferase (HAT) complexes, such as TIP60 (Tat-interactive protein 60kDa, also known as KAT5), which induces an open chromatin conformation resulting in transcriptional activation (Frank et al. 2003). Otherwise, MYC can recruit the transcription elongation factor (P-TEF b) which phosphorylates the C-terminal domain of RNA polymerase II, then promotes RNA elongation (Price 2000). Unlike MYC, MAX can also form homodimers MAX-MAX or complexes with other BR/HLH/LZ proteins such as MXD proteins (Mxd 1-4 also known as Mad), MNT or MGA. MXD proteins interact with repressive factors like Sin3A/Sin3B which associate with histone deacetylases (HDACs) to form the Sin3 repressive complex. The ternary complex MAX-MXD-Sin3 recognizes E-boxes and eventually lead to chromatin condensation and transcriptional repression (Ayer and Eisenman 1993). Many of the target genes positively regulated by MYC-MAX are repressed by MAX-MXD and this balance is essential for the regulation of fundamental cellular processes. MAX dimerization with MYC induces cell growth, cell cycle progression and inhibits differentiation. MYC-MAX dimers are particularly abundant in undifferentiated dividing cells and, consistently, MYC overexpression characterizes different human tumours. Upon differentiation stimuli, the expression of MXD proteins rapidly increases leading to a switch from MYC-MAX dimers to MAX-MXD

complexes. The accumulation of the latter in differentiating cells causes cell-cycle arrest and cell differentiation (Ayer and Eisenman 1993).

1.2.2 MYC repressive function

Besides its role as transcriptional activator, MYC can induce transcriptional repression trough an indirect binding to non-E-box-related sequences that requires the interaction with basal transcription factors, such as SP1 (specific protein 1) or MIZ-1 (Myc-interacting zinc-finger protein-1) and the recruitment of chromatin modifiers. Genes harbouring an initiator element (INRs) YYCAYYYYY (Y refers to T or C pyrimidine base) are bound by several transcription factors including MIZ-1. MIZ-1 protein shows an N-terminal zinc-finger domain accounting for DNA binding and a C-terminal BTB/POZ domain responsible for protein-protein interactions. MIZ-1 can interact with MYC outside its BR/HLH domain but it does not seem to form complexes with other members of the MYC/MAX/MXD network. Upon MYC-MIZ-1 interaction, the stabilized MYC protein regulate the activity of MIZ-1 BTB/POZ domain leading to MIZ-1 targets repression (Eilers and Eisenman 2008). MYC negative targets lacking INR elements can be repressed by MYC-mediated regulation of the activity of the transcription factor SP1. SP1 possesses two transactivation domains (TADs) mediating the interaction with the transcription machinery (such as TATA-binding proteins) and a zinc-finger domain for the binding to GC-rich DNA sequences. The involvement of MAX in this MYC-dependent transcriptional repression is not clear, yet. A ternary complex formed by MIZ-1,c-MYC and MAX binds the promoter of $p15^{INK4b}$ and inhibits the expression of this tumour suppressor gene (Staller et al. 2001). Differently, MAX does not seem to be required in c-MYC-SP1-mediated repression of the anti-proliferative cyclin-dependent kinase inhibitor $p21^{CIP/WAF}$ (Gartel et al. 2001).

1.3 The MYCN oncoprotein

1.3.1 MYCN vs c-MYC

MYCN identification dates back to 1983, when a gene showing homology with v-myc, but different from c-MYC, was found amplified in neuroblastoma and firstly defined N-Myc (Kohl et al. 1983). MYCN and c-MYC share a high homology concerning both mRNA and protein, which includes all the previously described domain for DNA-binding and protein-protein interaction (Meyer and Penn 2008). Moreover, these two MYC family members show a

substantial, albeit incomplete, functional homology. Knockout mice for c-MYC or MYCN die during embryogenesis (Davis et al. 1993) (Sawai et al. 1993). This evidence suggests that the lethal phenotype cannot be compensated by the endogenous MYCN or c-MYC, respectively. Moreover, in the embryonic neuroepithelium of *MYCN*$^{-/-}$ mice it has been shown an increase of the endogenous c-MYC which is however unable to rescue the *MYCN*$^{-/-}$ lethality (Stanton et al. 1992). Besides indicating a cross-regulated expression of c-MYC and MYCN, this observation confirms a lack of compensation between the two proteins. Nevertheless, homozygous mice for the substitution of the endogenous c-MYC coding sequence with the MYCN coding sequence undergo proper development until adulthood and can reproduce (Malynn et al. 2000). A possible explanation for that could rely on their different spatiotemporal expression. In mice, c-MYC is broadly expressed during development (especially in thymus, spleen and liver) and lasts in many tissues of adult mice. Contrarily, MYCN is mostly expressed during early development stages and in a tissue-specific manner (abundant in forebrain, hindbrain and kidney), then decreases and it is virtually absent in adult tissues (Zimmerman et al. 1986). Consistently, human MYCN is mainly expressed in peripheral and central nervous system, lung, kidney and spleen during embryogenesis. MYCN mRNA is well detectable in immature neural cells of fetal brain primordial cortex, but it drops during differentiation (Grady et al. 1987). It is worth noting that MYCN expression in developing nervous system and its physiological decrease in differentiating cells are highly consistent with the MYCN expression in neural crest cells. Indeed, as previously mentioned NCC show a physiological MYCN expression during their maturation but MYCN level decrease to let these cells differentiate in sympathoadrenal neurons (Zimmerman et al. 1986).

1.3.2 MYCN transcription factor

Like c-MYC, MYCN has an important function as transcriptional activator. To exert this function, it forms heterodimers with MAX and binds E-box sequences (CANNTG) in the promoter of positive regulated target genes. The high conservation of MBI, MBII and BR/HLH/LZ domains between proteins of the MYC family accounts for conserved interactions with co-factors and let MYCN promote cell proliferation and cell cycle progression in a MYC-like manner. In 2012, Valentijn and colleagues identified a specific MYCN signature through the transcriptomic analysis of *MYCN*-amplified neuroblastoma cell line IMR32. Upon MYCN silencing, the expression of 157 selected genes appeared to be strictly regulated by MYCN in IMR32 cells as well as in primary tumours. Interestingly, this signature was shared also by

MYCN-non-amplified tumours. In these tumours, despite the low amount of MYCN mRNA, the nuclear MYCN protein level was high, reinforcing the hypothesis of MYCN protein stabilization as oncogenic event in MYCN-non-amplified neuroblastomas. Unsurprisingly, the majority of the 157 MYCN-regulated genes, is involved in cell cycle progression, G1/S phase transition, DNA replication and repair or small GTPase mediating signal transduction. These genes are both positive and negative MYCN targets. Particularly, 87 out of 157 genes are up regulated by MYCN but only 2% of these 87 genes are expressed in brain. Conversely, even 30% of the 70 down-regulated genes are normally expressed in the nervous system. In IMR32 cell line the MYCN silencing promotes cell differentiation. Therefore, authors envisaged a possible MYCN repression of genes active on neuronal differentiation. (Valentijn et al. 2012).
Over the last years several examples of MYCN-mediated transcriptional repression have been described, highlighting MYCN central role in regulating multiple processes such as cell proliferation, differentiation and mobility.
Like c-Myc, MYCN can bind the transcription factor SP1 and recruit histone deacetylases. In particular, the recruitment of histone deacetylase 1 (HDAC1) by MYCN-SP1 is responsible for transglutaminase 2 (TG2) repression. That leads to arrested neuronal differentiation of neuroblastoma cells accounting, at least in part, for MYCN-induced malignant transformation. Remarkably, the interaction between MYCN and HDAC1 occurs in absence of MAX, suggesting that the MYCN-MAX dimers should not be strictly required in MYCN-mediated repression (Liu et al. 2007). Further evidence of MYCN-induced block of differentiation is the MYCN-dependent repression of Cyclin G2 occurring after MYCN-SP1 interaction and HDAC2 (which is transcriptionally upregulated by MYCN) recruitment at the Cyclin G2 promoter. Differently from other cyclins, Cyclin G2 blocks cell cycle progression, it is expressed by cells undergoing terminal differentiation and its repression contributes to MYCN-mediated increase of cell proliferation in neuroblastoma (Marshall et al. 2010). As mentioned earlier, the differentiation state of neuroblastoma cells has an important prognostic significance. Unsurprisingly, a robust expression of the neurotrophins receptors TrkA and p75NTR predicts a favourable tumour outcome, while low-level of TrkA and p75NTR is associated with highly aggressive neuroblastomas. The ternary complex composed by MYCN, SP1 and MIZ-1 recruits HDAC1 on TrkA and p75NTR promoters leading to TrkA and p75NTR transcriptional repression. The pharmacological inhibition of HDAC1 as well as the silencing of any member of the ternary repressive complex causes the reactivation of TrkA or p75NTR expression in neuroblastoma cell lines and exposes these cells to NGF-mediated apoptosis (Iraci et al. 2011).

TrkA cooperation with p75NTR is essential to trigger NGF-mediated neuronal differentiation which eventually leads to transcriptional activation of the cyclin-dependent kinase inhibitor $p21^{CIP/WAF}$ promoting cell cycle arrest (Diolaiti et al. 2007), inhibited by a c-MYC-SP1-dependent mechanism. Altogether, these lines of evidence suggest a complex scenario in which MYCN oncoprotein might contribute to malignant transformation by both upregulating pro-proliferative genes and downregulating genes involved in cell differentiation or cell cycle exit.

1.4 *Drosophila* MYC

The *Drosophila* MYC gene (hereafter referred as *dMyc*) was firstly described in 1935 by Calvin Bridges before the c-MYC discovery (Vennstrom et al. 1982) thanks to the identification of a hypomorph mutant allele that was named *diminutive* because of the decreased body size of the mutant flies (Bridges CB 1935). In 1996 Gallant demonstrated that this mutant allele corresponds to a hypomorphic mutation of the *Drosophila* MYC homolog (Gallant et al. 1996). In the fruit fly genome, only a single homolog is present for MYC (*dMyc*), MAX (hereafter referred as *dMax*) and MXD (*dMnt*) genes. The lack of gene redundancy in the MYC/MAX/MXD network and the diversified genetic tools available for different experimental approaches make *Drosophila* an excellent model to study MYC function in both physiological and pathological conditions. dMyc is equally similar to all vertebrate paralogs sharing a moderate overall sequence identity of 26%. Nevertheless, except for Myc Box 1 which shows poor sequence conservation, dMyc protein is highly conserved in all the functional domains compared to the vertebrate counterpart. In fact, it is characterized by an N-terminal Myc Box 2, by a central Myc Box named Myc Box 3 or 4 and by a C-terminal basic-helix-loop-helix leucine zipper domain (Gallant 2013). Consistently to a structural similarity, a robust functional conservation has also been demonstrated between the two homologs. dMyc can partially recover the proliferation deficiency caused by the lack of MYC in murine fibroblasts (Trumpp et al. 2001), and human MYC rescues the lethality induced by *dMyc* mutation (Benassayag et al. 2005).

Like MYC, dMyc dimerizes with MAX through the BR/HLH/LZ domain (both the vertebrate and *Drosophila* MAX orthologues) then binds E-boxes and recruits chromatin modifiers to promote transcription of its target genes. As in human, also in *Drosophila* the dMyc-dMax function is antagonized by dMax-dMnt dimers which bind E-boxes and repress transcription through the interaction between dMnt and corepressors like dSin3A/B (*Drosophila* homologues of Sin3A/B). The switch between dMyc-dMax dimers to dMax-dMnt represses cell

proliferation and cellular growth that are positively regulated by dMyc (Loo et al. 2005). Indeed, by stimulating ribosome biogenesis and protein translation dMyc promotes cell size growth (Gallant 2013). While dMyc moderate overexpression leads to increased size of adult body, dMyc hypomorphic mutant alleles result in the opposite effect and the null mutation is lethal (Gallant et al. 1996).

1.5 MAX-independent functions of MYC

MYC association with MAX seems to be strictly required for many MYC-mediated biological functions. A strong evidence for this generally accepted notion comes from experimental approaches based on mutated forms of c-MYC and MAX able to structurally complement and heterodimerize but unable to bind their endogenous counterparts. Indeed, only the simultaneous expression of both these complementing mutants mimic the effect of the endogenous c-MYC on cell proliferation and apoptosis. According to this evidence, c-MYC dimerization with MAX is required for c-MYC binding to E-box-related sequences and consequent induction of S-phase entry and apoptosis (Amati et al. 1993). A more complex scenario is represented by MYC-mediated repression, where the requirement of MAX appears still controversial. c-MYC binding to MAX seems to be necessary for c-MYC presence at non-canonical repressive sites, like GC reach regions, to which c-MYC binds indirectly through the interaction with others DNA binding factors such as SP1 (Mao et al. 2003). Nevertheless, c-MYC-mediated repression of p21 does not seem to require the interaction with MAX (Gartel et al. 2001) as well as the repression of TG2 by MYCN (Liu et al. 2007). Moreover, c-MYC expression inhibits cell differentiation (Vaqué et al. 2008) and causes apoptosis (Wert et al. 2001) in the PC12 pheochromocytoma tumour cell line that lacks a functional MAX protein (Hopewell and Ziff 1995). The ability of c-MYC to induce programmed cell death in absence of MAX has been confirmed by using a c-MYC dominant negative mutant, named Omomyc, which competes with MAX for dimerization with c-MYC. Even though c-MYC-Omomyc dimers cannot activate c-MYC-reporter constructs, they allow the repression of c-MYC negative targets and lead to enhanced apoptosis, suggesting that c-MYC itself might exert inhibitory functions (Soucek et al. 2002). Overall, these observations point out intriguing and still poorly investigated MAX-independent activities of MYC.

1.5.1 The *Drosophila* perspective

Thanks to the MYC/MAX/MXD network conservation and the low redundancy typical of invertebrates, *Drosophila* has provided several lines of evidence highlighting MYC activities that do not require interaction with MAX.

Firstly, *dMyc* null mutants (dm^4) show defective growth and die during the larval stage, while *dMax* null mutants (Max^1) develop until pupal stage, undergo metamorphosis and die as pharate adult, the stage just before the eclosion of the adult fly from the puparium. The milder phenotypic traits shown by Max^1 mutants cannot be explained by either a maternal contribution of dMax RNA (possibly compensating the lack of zygotic dMax) or the loss of dMax-dMnt heterodimers that potentially could compensate the loss of activating dMyc-dMax dimers. Indeed, the half-life of maternally supplied dMax protein is much shorter than the time needed to accomplish larval development and reach pupal stage. Moreover, the dMnt null mutation (Mnt^1) does not fully rescue dm^4 phenotype and dm^4 Mnt^1 double mutants still show evident delayed development and growth defects compared to Max^1 mutant. Interestingly, the decrease of body size and the lethality showed by dm^4 Mnt^1 mutants is more severe than that showed by dm^2 Mnt^1 double mutants. dm^2 refers to a nonsense mutation in the dMyc leucine zipper domain which leads to a truncated dMyc protein unable to dimerize with dMax. Hence, this evidence suggests an, albeit partial, MAX-independent function of dMyc in regulating cell growth and survival.

In *Drosophila*, like in vertebrates (Gomez-Roman et al. 2003), dMyc can promote the expression of RNA polymerase III targets in a MAX-independent manner by direct interaction with the RNA polymerase III cofactors Brf. Notably, dm^2 mutants show a higher number of dMyc targets transcribed by RNA polymerase III compared to dm^4, while dMyc targets transcribed by RNA polymerase II (activated by MYC-MAX dimers) are not significantly different. Therefore, the different phenotypic severity between dm^2 and dm^4 mutants could rely on dMax-independent activation of RNA polymerase III by dMyc.

dMyc-mediated regulation of cell growth is detectable also at cellular level. Indeed, in wing imaginal disc homozygous Max^1 clones are composed by cells showing only a slight size decrease, while dm^4 Mnt^1 cells are much smaller and do not survive to "cell competition" of heterozygous cells surrounding the mutant somatic clones. Furthermore, at physiological dMax level, dMyc overexpression in differentiating eye cells leads to increased cell size and apoptosis resulting in a rough eye (See Section 3.1). The additional *dMax* knockdown causes a small but

rough eye, suggesting that a reduced dMax level can prevent dMyc-mediated overgrowth but not dMyc-mediated apoptosis (Steiger et al. 2008).

Concluding, all these observations let us envisage a possible dMyc activity in absence of dMax, making extremely intriguing the study of cellular processes possibly affected by this poorly explored regulatory mechanism in both physiological and pathological conditions.

AIM

Neuroblastoma is the most common and deadly extracranial solid tumour of childhood. About 22% of neuroblastomas show amplification and/or overexpression of *MYCN* oncogene, which still represents the most reliable prognostic marker of poor tumour outcome (Cohn et al. 2009). Neuroblastoma onset is related to the failure of neural crest cells differentiation (Maris et al. 2007). These cells physiologically express MYCN and the decrease of MYCN level seems to be required to let them exit cell cycle and differentiate in sympathoadrenal neurons (Zimmerman et al. 1986) (Wartiovaara et al. 2002). Consistently, most neuroblastomas are undifferentiated tumours and this significantly contributes to the unfavourable prognosis. MYCN, as the other members of the MYC family, is a BHLHZ transcription factor which dimerizes with MAX and promotes the expression of positive target genes. Much effort has been made to acquire a comprehensive knowledge of MYCN-regulated genes. Besides the transcriptional activation of genes involved in cell growth, cell cycle progression, DNA replication and repair, MYCN seems to retain an important activity as transcriptional repressor (Valentijn et al. 2012). In neuroblastoma MYCN can form repressive complexes with SP1 and MIZ-1 transcriptional factors and recruit chromatin modifiers like HDACs leading to the epigenetic silencing of negative target genes involved in block of proliferation, exit from cell cycle and neuronal differentiation (Liu et al. 2007) (Marshall et al. 2010) (Iraci et al. 2011). Nevertheless, the requirement of MAX in this process is still controversial. Moreover, multiple lines of evidence in human and *Drosophila* highlighted a possible MAX-independent activity of MYC (Soucek et al. 2002) (Steiger et al. 2008).

Therefore, we adopted *Drosophila melanogaster* as gold-standard genetic system to better elucidate *in vivo* the effect of a high MYC to MAX expression ratio caused by an excess of MYC level compared to MAX level. Particularly, we focused our analysis on possible MAX-independent function of MYC in cell proliferation and differentiation to disclose possible deregulated developmental processes.

This will contribute to define the mechanisms underlying MYC-mediated oncogenesis and further elucidate the impact of MYCN amplification in neuroblastoma biology. Moreover, it will provide valuable indications for therapeutic treatments especially in high-risk neuroblastomas which are strongly associated with *MYCN* amplification and characterized by poor tumour prognosis.

RESULTS

3.1 *Drosophila* eye as cellular model

MYC-MAX dimer participates in the regulation of many fundamental aspects of cell biology, such as cell proliferation and growth, apoptosis and metabolisms. To analyse *in vivo* the cellular effects caused by an unbalanced MYC to MAX expression ratio (hereafter MYC/MAX ratio) we chose the *Drosophila* eye as suitable readout. Indeed, it is a non-vital organ, albeit highly differentiated, and a well-established and characterized cellular model for studying processes underlying cell proliferation, cell fate specification, cell differentiation, patterning and morphogenesis.

The adult fly has a compound eye in which approximatively 800 photoreceptive units, named ommatidia, are arranged into an extremely regular array (Kumar 2012) (**Fig. 1 A, B**). The mature organ originates from a small group of cells set apart during embryogenesis and specified by a retinal determination gene network (RDGN). Throughout the larval life, these cells proliferate and generate the eye primordium, called eye imaginal disc, which forms the posterior part of the of the eye-antenna imaginal disc complex (**Fig. 1 C**).

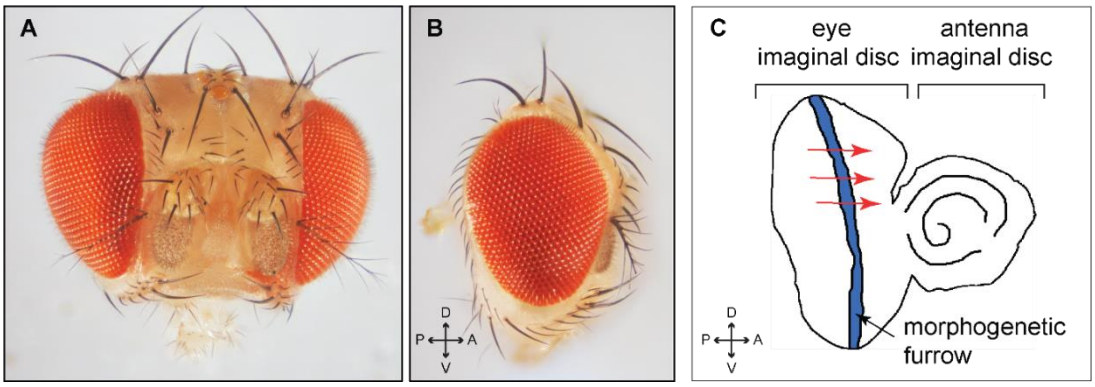

Figure 1 - *Drosophila* eye. Frontal (**A**) and lateral (**B**) view of a wild type adult eye. (**C**) Drawing of the eye-antenna imaginal disc complex at late 3rd larval instar. In the eye imaginal disc cells within the morphogenetic furrow (blue stripe) are committed to terminal differentiation. This differentiative wave extends along the dorso-ventral axis of the eye disc and moves (red arrows) from the posterior to the anterior margin of the disc.

The differentiation of the eye primordium begins during the 3rd larval instar with the formation of a groove, named morphogenetic furrow (MF), at the posterior margin of the eye disc. This cell indentation extends all along the dorso-ventral axis and sweeps progressively across the

eye disc from posterior to anterior (**Fig. 1 C**). Within the furrow final cell fate determination and cell cycle arrest occur. As result, cells anterior to the MF are still uncommitted to terminal differentiation and proliferate asynchronously, whereas cells posterior to the MF are committed and organized into regularly spaced clusters within which eight photoreceptors and several accessory cells differentiate, leading to the development of the highly ordered array of ommatidia (Cagan 2009).

dMyc overexpression in differentiating eye cells (located posteriorly to MF) affects the regular organization of the ommatidia array leading to a so-called "rough" eye phenotype due to increased growth and enlargement of each cell in ommatidia (Secombe et al. 2007) (Steiger et al. 2008). This phenotype seems to be MAX-dependent since *dMax* downregulation suppresses it, highlighting the role of MYC-MAX dimers in cell growth regulation (Steiger et al. 2008). We asked which is the effect of MYC overexpression and/or MAX downregulation, namely increased MYC to MAX expression ratio, in undifferentiated eye cells anterior to the MF. For this purpose, we used the binary system Gal4-UAS (See Section 5.2) to express an RNAi construct targeting *dMax* (*Max-RNAi* transgene) and/or a *UAS-MYC* overexpression construct (*UAS-dMyc* to overexpress the *Drosophila* dMyc or *UAS-hMYCN* to overexpress the human MYCN) under the control of the *eyeless* promoter (*ey-Gal4* driver construct). The *eyeless* gene encodes a transcription factor strictly required for eye development and it is expressed in all proliferating eye disc cells still uncommitted to terminal differentiation (Halder et al. 1998). Efficacy and specificity of the *dMax-RNAi* and *UAS-dMyc* transgenes expression have been tested through quantification of dMax and dMyc transcripts in total RNA extracts from eye imaginal discs of wandering 3rd instar larvae. As expected, eye discs expressing 1 copy of *ey-Gal4* and 1 copy of *Max-RNAi* (number of constructs copies will be hereafter referred as #X i.e. 1X*ey-Gal4,* 1X*Max-RNAi,* respectively) showed a reduced *dMax* expression that further dropped by increasing the number of transgenes copies (2X*ey-Gal4,* 2X*Max-RNAi*) (**Fig. 2** green columns**)**. *dMyc* RNA level was substantially unchanged compared to control expressing the only driver construct. Conversely, *UAS-dMyc* expression (1X*ey-Gal4,* 1X*UAS-dMyc*) was sufficient to double the amount of dMyc RNA present in the negative control, without altering Max RNA quantity (**Fig. 2** blue columns).

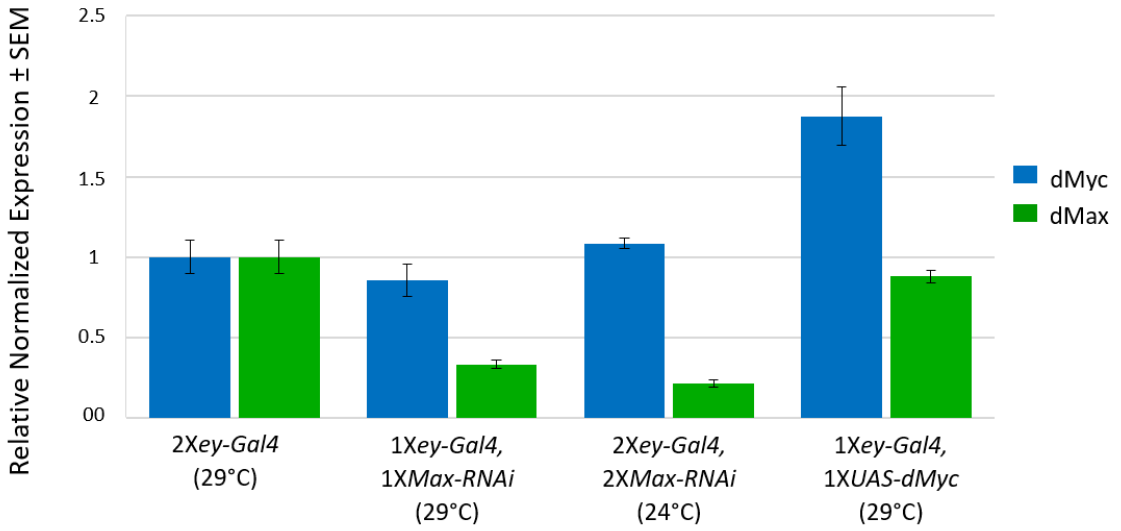

Figure 2 – Efficiency of *dMax* downregulation and dMyc overexpression upon targeted gene expression. The expression of *Max-RNAi* and *UAS-dMyc* constructs in eye progenitor cells leads to a decreased level of dMax transcript and increased level of dMyc transcript in eye disc cells. Genotype and growth temperature are indicated below each column. The 2X*ey-Gal4*, 2X*MaxRNAi* animals have been raised at 24°C due to the extreme phenotype showed at 29°C (See Section 3.2). Total RNA was extracted from eye imaginal discs dissected from wandering 3rd instar larvae. dMax (green columns) and dMyc (blue columns) transcripts were quantified through quantitative Real Time PCR., normalized on the reference genes *Gapdh1* and *RpL32* and represented as relative expression ± SEM (standard error of the mean) compared to the negative control set as 1.

3.2 MAX silencing induces a decreased eye size and eye cell proliferation

First, we increased the MYC/MAX ratio by reducing MAX level without altering the physiological MYC amount. Upon *dMax* silencing we observed a size reduction of the adult eye. This phenotype (MAX phenotype) showed incomplete penetrance and variable expressivity. To quantify it, we established three arbitrary phenotypic classes representing the most recurrent phenotypic traits. Class 0 (**Fig 3 A**) is the mildest class. It includes animals showing wild-type-like eyes (**Fig 1 A, B**) in terms of ommatidia size and array organization. Class 1 (**Fig 3 B**) corresponds to eyes lacking a limited subset of anterior ommatidia (**Fig 3 B** arrow) although the overall eye structure is substantially maintained. The most severe phenotypic class, Class 2 (**Fig 3 C**), includes animals showing a small-size eye closely surrounded by periorbital vibrissae that typically encircle the eye area in the adult head (**Fig 3** arrowheads).

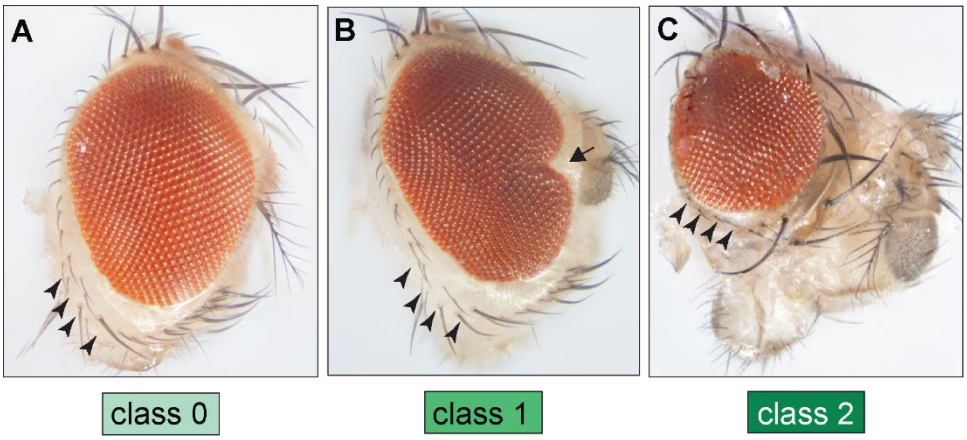

Figure 3 - *dMax* silencing in eye progenitor cells leads to a decreased size of the adult eye. Phenotypic classes representing the most frequent defects observed in adult eyes upon *dMax* downregulation in undifferentiated eye disc cells. (**A**) Class 0: wild-type-like eye. Periorbital vibrissae delimiting the eye field are correctly located at the posterior-ventral eye margin (arrowheads). (**B**) Class 1: mild eye reduction consequent to the loss of few ommatidia mostly at the anterior margin of the eye (arrow). Periorbital vibrissae are correctly distributed (arrowheads). (**C**) Class 2: severe eye reduction with periorbital vibrissae closely surrounding the small eye (arrowheads).

The efficiency of the Gal4-UAS binary system can be improved by increasing the growth temperature (from 24°C to 29°C) and/or the number of transgenes copies carried by the experimental progeny (See Section 5.2). It is worth noting that both conditions exacerbate the described phenotype in terms of phenotype penetrance and severity (**Fig 4 A, B**). Moreover, the phenotype is rescued by adding an extra copy of the genomic *dMax* locus (*Max-rescue*), indicating the dependence of the observed eye defects on dMax dosage (**Fig 4 A** column 13 vs 6**)**. The strongest *dMax* silencing (animals carrying 2X*eyGal4*, 2X*Max-RNAi*, and grown at 29°C) resulted in a fully penetrant lethality (**Fig 4 A** column 12). These animals show a typical MAX phenotype when grown at 24°C (**Fig 4 A** column 11) but when grown at 29°C they undergo metamorphosis and the formed adult animals (called pharate adults at this stage) die inside the puparium. Interestingly, these pharate adults appear completely developed and of normal body size compared to wild type, but they have an extremely reduced head capsule and one or both eyes are often absent (**Fig. 4 C, D**). The ventral portion of the eye imaginal disc contributes to the formation of different sensory organs and head capsule (Park et al. 2015). Therefore, the reduced size of the pharate's head suggests that in the eye imaginal disc of these animals dMax level is below the threshold that let eyes and head capsule properly develop.

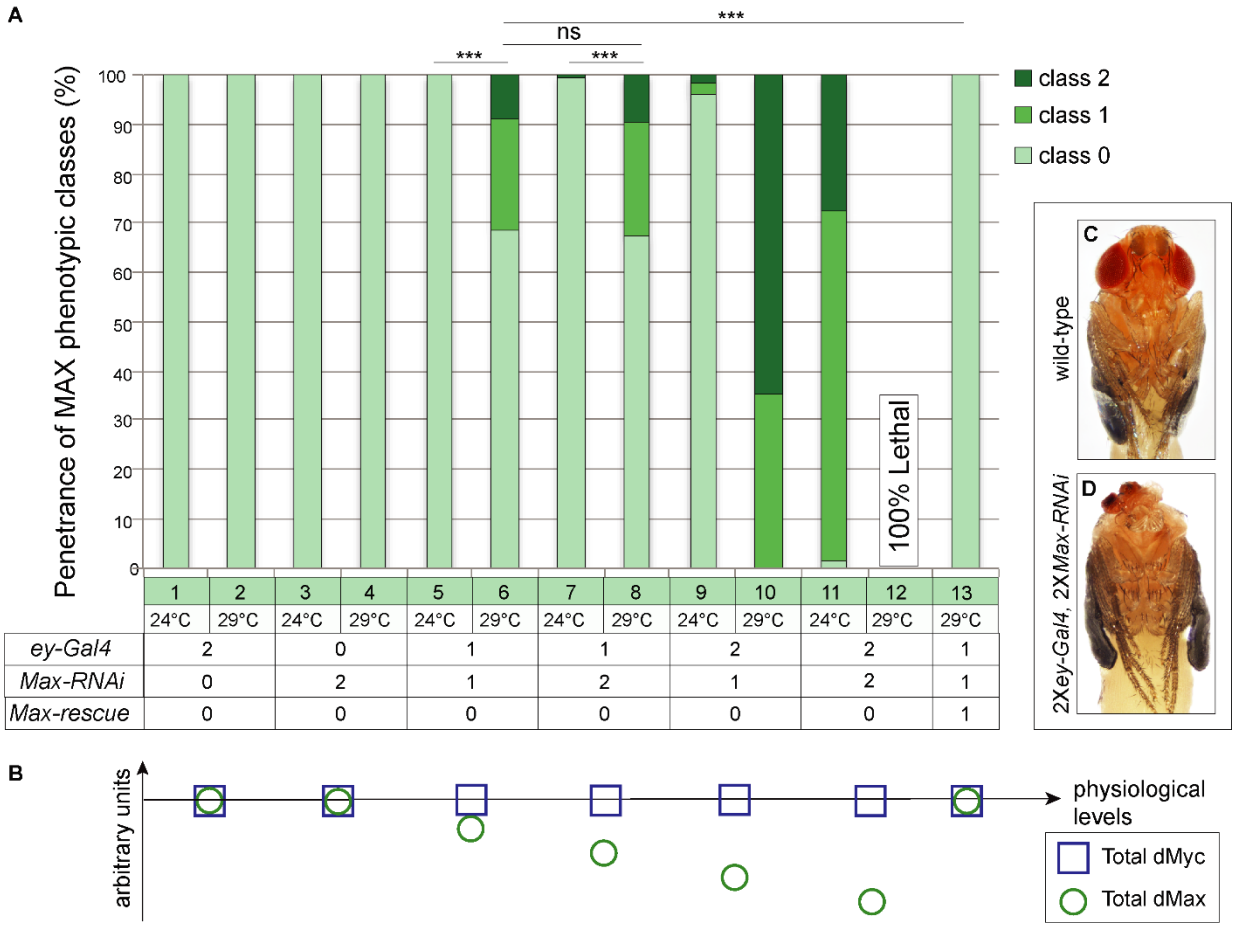

Figure 4 – The severity of the phenotype induced by *dMax* downregulation increases according to the enhanced *dMax* downregulation. (**A**) Stacked column chart showing the frequency of MAX phenotypic classes observed in the analysed progeny upon increase of transgenes copies (copy number of transgenes is reported in table) and temperature (24°C or 29°C). Statistics: Mann-Whitney Wilcoxon test, p<0,001 *** (**B**) Graphical representation of dMax and dMyc levels in the different genotypes. Animals carrying 2X*eyGal4*, 2X*Max-RNAi* and grown at 29°C die as pharate adults (A, column 12) showing a strong reduction of the head capsule and eyes (**D**) compared to a wild type pharate (**C**).

As mentioned before, in most of the eyes showing a Class 2 MAX-phenotype the ommatidia area is closely encircled by periorbital vibrissae which are sensory bristles surrounding and delimiting the eye territory (**Fig. 3 C**). This suggests that the reduced-size eye might originate from a small eye imaginal disc. To test whether this could be due to defects in the proliferation and/or differentiation programs, we analysed the expression of cell proliferation and cell differentiation markers in the eye-antenna imaginal disc of wandering 3rd instar larvae. Upon *dMax* downregulation many eye-antenna complexes are often significantly smaller compared to control (**Fig. 5**). Consistently, the mitotic marker PhosphoH3 (phosphorylated form of the histone H3) is expressed at lower level and in many fewer cells compared to control (**Figure 5**

C, F). Nevertheless, the pattern of Elav (embryonic lethal abnormal vision), a pan-neuronal marker expressed in all differentiating photoreceptors, is substantially unaltered (**Fig. 5 A, D**). We further evaluated the differentiation status of eye disc cells through the immunolabeling of the activated form of Notch receptor (Notch Intracellular Domain, NICD) expressed by cells within the morphogenetic furrow where the Notch pathway regulates the ommatidia spacing (Kumar and Moses 2001) (**Fig. 5 B, E**). Remarkably, the progression of the morphogenetic furrow located at the anterior border of Elav expression and marked by NICD was substantially unchanged (**Fig. 5 A, D, B, E** arrowheads), indicating the absence of any developmental delay. This body of evidence suggests that *dMax* downregulation impairs the organ growth mainly by decreasing the proliferation rate but does not substantially affect eye cells differentiation.

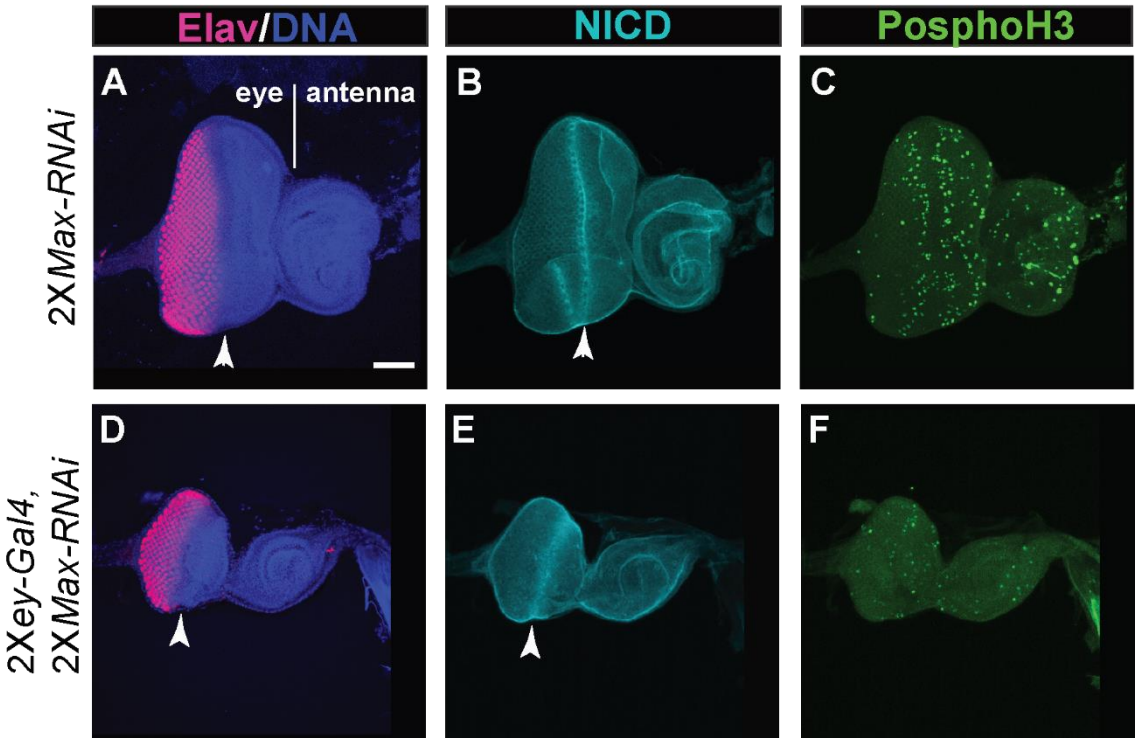

Figure 5 – *dMax* downregulation causes defective proliferation of eye imaginal disc cells without affecting cell differentiation. Eye-antenna imaginal discs dissected from wandering 3rd instar larvae grown at 24°C. Immunolabeling with the differentiation marker Elav in pink (**A,D**), the morphogenetic furrow marker NICD in cyan (**B,E**) and the mitotic marker PhosphoH3 in green (**C,F**). Cell nuclei are labelled by HOECHST. *dMax* downregulation induces disc size reduction and decreased number of proliferating cells (**F**) compared to control (**C**). The differentiation rate and the progression of the morphogenetic furrow (arrowhead) (**D,E**) are not substantially changed compared to control (**A,B**). Scale bar: 15 μm.

Altogether these data suggest that dMax is required for proper proliferation of eye imaginal disc cells and its silencing eventually leads to a reduction of the adult eye size. This is in line with the role of MYC-MAX dimers in the transcriptional activation of genetic programs controlling cell proliferation and organ growth. Moreover, our findings are consistent with the phenotype caused by homozygous loss-of-function *dMax* mutations. These animals survive embryogenesis but show impaired growth at larval and pupal stage and they never eclose (Steiger et al. 2008).

3.3 MYC overexpression inhibits eye cells differentiation

We then analysed the impact on eye development of high MYC/MAX ratio obtained by increasing MYC level in a MAX physiological context. In this experimental set the MYC MAX-dependent functions should be preserved.

For this purpose, we overexpressed dMyc or hMYCN (using *UAS-dMyc* or *UAS-hMYCN* constructs) in eye cells still uncommitted to terminal differentiation (*eyGal4* driver), maintaining the physiological MAX level. Such genetic manipulation does not seem to affect eye size while ommatidia organization is clearly impaired, suggesting a defective cell differentiation. Indeed, ommatidia arrangement in adult eye is so precise that any developmental failure of even a single ommatidium results in disrupted positioning of surrounding eye units and this makes easy to detect also mild phenotypes. To quantify the "MYC phenotype", that is incompletely penetrant and variable, we stratified the observed progeny in four new phenotypic classes set on the basis of the most frequent phenotypic traits. Class 0 animals show a wild-type-like eye (**Fig. 6 A-C**). In Class 1 eyes a limited number of ommatidia in the posterior part of eye are not correctly distributed and the ommatidia array is slightly deformed (**Fig. 6 D, E**). In Class 2 a similar defect involves also ommatidia located in the middle and anterior part of the eye along the dorso ventral midline (**Fig. 6 F, G**). Strikingly, Class 3 animals show a cone-shaped eye, often combined with a widespread alteration of ommatidia organization (**Fig. 6 H-J**).

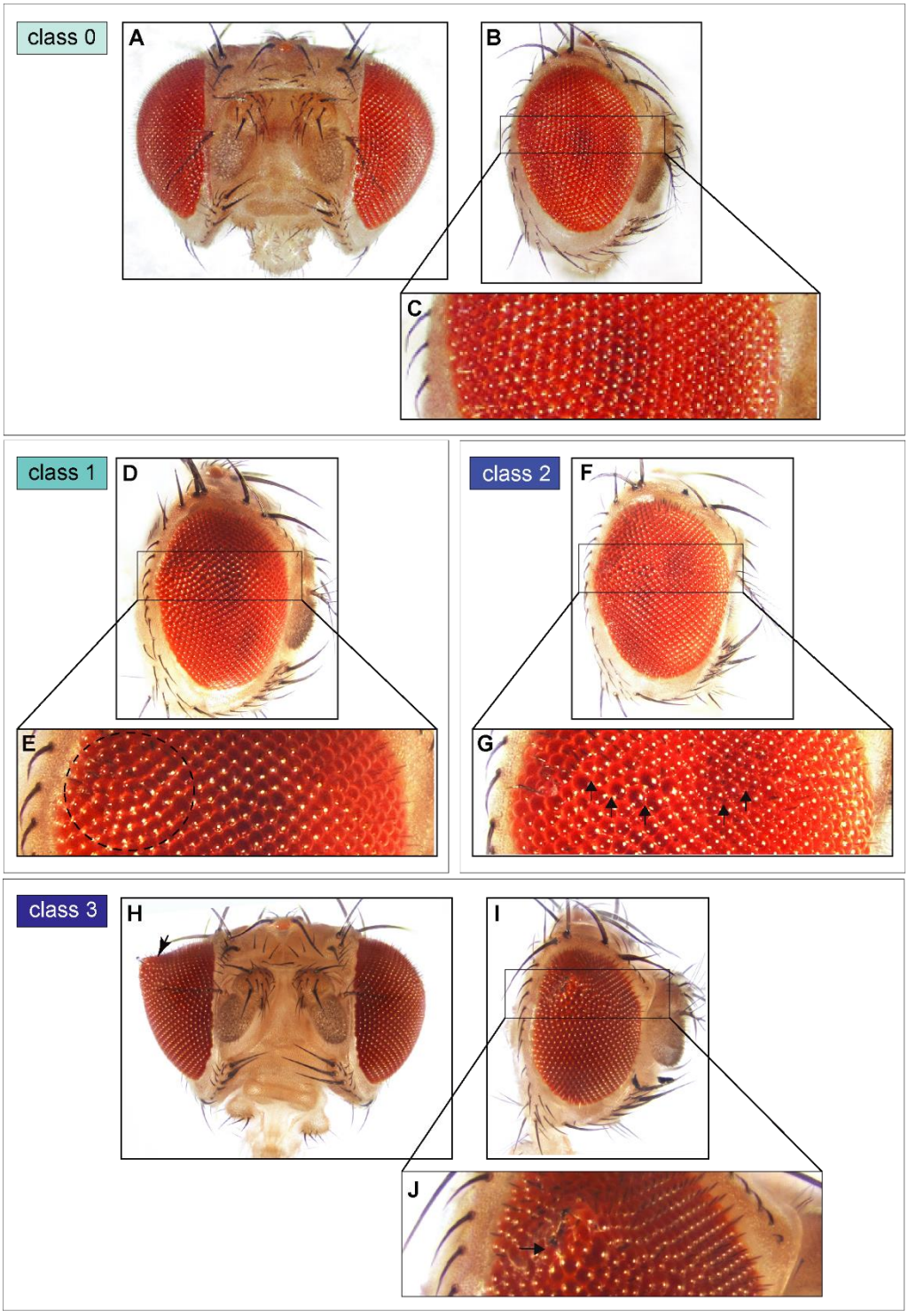

Figure 6 – dMyc or hMYCN overexpression inhibit eye cell differentiation. Phenotypic classes representing the most frequent defects observed in adult eyes upon dMyc or hMYCN overexpression in undifferentiated eye disc cells. (**A-C**) Class 0: wild-type-like eye in frontal view (**A**), lateral view (**B**) and high magnification of the area along the dorso-ventral midline (**C**). (**D-E**) Class 1: the differentiation defect involves a limited number of ommatidia located at the posterior margin of the eye (dashed circle in **E**). (**F-G**) Class 2: the impaired differentiation affects also medial and anterior ommatidia along the midline (arrows in **G**). (**H-J**) Class 3: cone-shaped eye (arrow in **H,J**).

Notably, dMyc or hMYCN overexpression phenotype is partially rescued by halving the *dMyc* gene dosage in animals carrying a *dMyc* heterozygous null mutation (Myc^{G0354}). Indeed, the phenotype severity of 1X*ey-Gal4,* 1X*UAS-dMyc* or 1X*ey-Gal4,* 1X*UAS-hMYCN* decreases in a Myc^{G0354}/+ genetic background (**Fig. 7**). This evidence indicates that the observed eye defects are specifically caused by a higher level of MYC and suggests that both the fruit fly and the human orthologs act on the same mechanism.

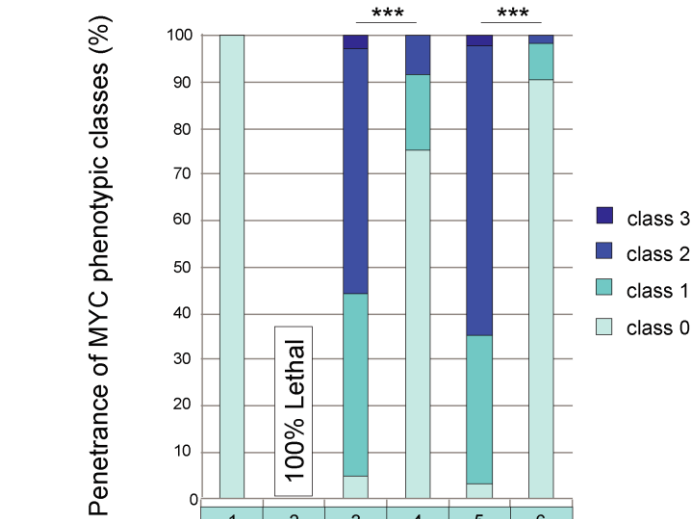

	1	2	3	4	5	6
	29°					
ey-Gal4	0	0	1	1	1	1
UAS-dMyc	0	0	1	1	0	0
UAS-hMYCN	0	0	0	0	1	1
Myc^{GO354}/+	yes	no	no	yes	no	yes
Myc^{GO354}/Myc^{GO354}	no	yes	no	no	no	no

Figure 7 – dMyc or hMYCN overexpression phenotype is rescued by *dMyc* heterozygous null mutation. Stacked column chart showing the frequency of MYC phenotypic classes in different genetic conditions (table). In a Myc^{G0354}/+ genetic background the phenotype caused by dMyc or hMYCN overexpression is partially rescued (column 3 vs 4 and column 5 vs 6). Statistics: Mann-Whitney Wilcoxon test, p<0,001 ***

The dependence of MYC phenotype on dMyc dosage is further confirmed by the enhanced phenotype penetrance and expressivity obtained upon increased growth temperature and number of transgenes copies (**Fig. 8 A, B**). Importantly, dMyc overexpression phenotype is suppressed by adding a genomic *dMax* locus copy (*Max-rescue*) (**Fig. 8 A** column 9 vs 8).This observation indicates that MYC phenotype does not originate from an absolute high dMyc level but from an increased MYC/MAX ratio whose effect can be overcome by a third *dMax* gene copy supposed to increase the dMax level. Moreover, this body of evidence suggests that the "free MYC", presumably not engaged in MYC-MAX dimers, partially inhibits eye cell differentiation possibly in a MAX- independent manner.

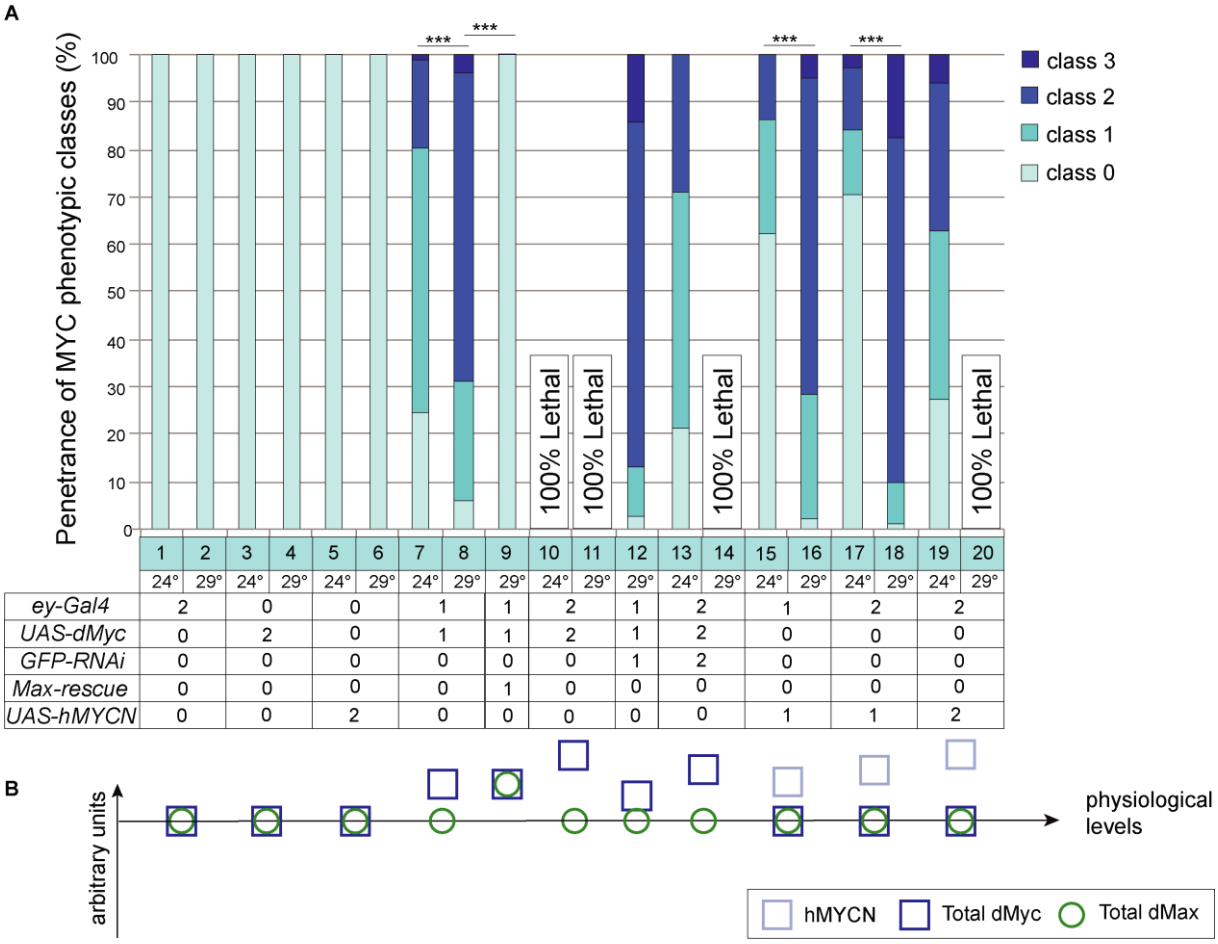

Figure 8 – The severity of MYC phenotype increases accordingly to dMyc or hMYCN overexpression. (**A**) Stacked column chart showing the frequency of MYC phenotypic classes observed in the analysed progeny upon increase of transgenes copies (copy number of transgenes is reported in table) and temperature (24°C or 29°C). Statistics: Mann-Whitney-Wilcoxon test, p<0,001 ***. Remarkably, dMyc overexpression is suppressed by an extra copy of the genomic *dMax* locus (column 8 vs 9). (**B**) Graphical representation of dMax, dMyc and hMYCN levels in the different genotypes.

A further indication of the MAX-independence comes from the unaffected cell proliferation (MAX-dependent function of MYC) showed by eye-antenna imaginal discs overexpressing dMyc. Indeed, *dMax* silencing leads to small-size eye disc with low expression of the mitotic marker PhosphoH3 (**Fig. 5 F**). Conversely, upon dMyc overexpression PhosphoH3 level does not seem to be impaired when compared to a control disc (**Fig. 9 B, D, F**). Nevertheless, Elav expression, labelling differentiated photoreceptors, decreases indicating a reduction of eye disc cells differentiated in post mitotic neurons compared to control (**Fig. 9 A, C**). A more severe phenotype is showed by 1X*ey-Gal4*, 2X*UAS-dMyc* animals whose eye discs are often characterized by a very low number of Elav-positive cells (**Fig. 9 E**). Most likely this could be

related to a delayed development of eye disc suggested by the disc shape and by the backward position of the morphogenetic furrow (**Fig. 9** arrowheads).

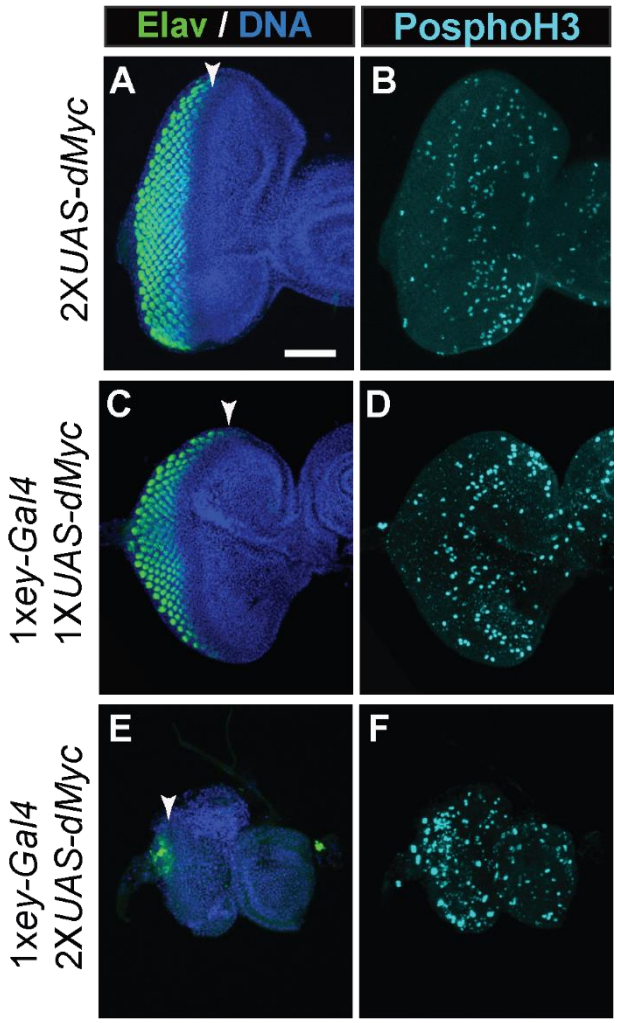

Figure 9 – dMyc overexpression does not affect cell proliferation in the eye imaginal discs. Eye-antenna imaginal discs dissected from wandering 3rd instar larvae grown at 29°C. Immunolabeling with the differentiation marker Elav in green (**A, C, E**) and the mitotic marker PhosphoH3 in cyan (**B, D, F**). Cell nuclei are labelled by HOECHST. dMyc overexpression does not impair PhosphoH3 expression level (**D, F**) compared to a control disc (**B**). A mild dMyc overexpression causes a slight decrease in the number of Elav-positive cells (**C**). The further increase of dMyc level in eye disc cells leads to defective eye disc development as revealed by disc shape and size and by a very low number of Elav-positive cells (**E**). This could be plausibly associated with a developmental delay. Scale bar: 15 µm.

3.4 High MYC/MAX ratio leads to an eye-to-wing homeotic transformation

To better assess whether MAX is required for the MYC-dependent inhibition of ommatidia formation, we further increased the amount of "free Myc" and analysed the impact of such a high MYC/MAX ratio on cell differentiation. To this end, we combined dMyc overexpression with *dMax* downregulation obtaining a stronger unbalance between dMyc and dMax expression levels (animals carrying *ey-Gal4*, *UAS-dMyc*, *Max-RNAi* constructs). Beyond the wild-type-like Class 0 (**Fig. 10 A**), the mildest MYC/MAX phenotypic class, Class 1 (**Fig. 10 B**), seems to recapitulate the previously described MAX phenotype (**Fig.3**) and MYC phenotype (**Fig. 6**). Class 1 eyes are characterized by a moderate lack of ommatidia in the eye anterior part (**Fig. 10 B** arrow) resembling the MAX Class 1 (**Fig. 3 B**). Moreover, these animals show a partial disruption of the regular ommatidia distribution analogous to MYC Class 1 or 2 (**Fig. 6 D-G**). Eye defects in more severe MYC/MAX classes mostly affect cell differentiation and not cell proliferation. Class 2 eyes of the MYC/MAX phenotype (**Fig. 10 C**) show a size decrease of the ommatidia area reminding that described upon *dMax* downregulation (MAX Class 2, **Fig. 3 C**). Interestingly, beyond the similarity we observed an important difference between MAX Class 2 and MYC/MAX Class 2 eyes. In most MAX Class 2 eyes the periorbital vibrissae closely encircle the ommatidia area, suggesting that the small eye develops from a small eye disc. In MYC/MAX Class 2 eyes the periorbital vibrissae delimit a field only partially differentiated in ommatidia (**Fig. 10 C** arrowheads). This could mean that the small eye in this case could develop from a disc of almost normal size that differentiates a smaller ommatidia area. Class 3 eyes (**Fig. 10 D**) closely resemble Class 2 eyes but they show an additional greyish overgrowth of apparently undifferentiated tissue in the ventral part of the eye area which lacks ommatidia. Surprisingly, in Class 4 eyes (**Fig. 10 E-G**) the ventral part of the eye territory differentiates a structure very similar to a wing bud surrounded by ommatidia. This ectopic wing often shows a structure strongly resembling the triple row of wing sensory bristles (**Fig. 10 E-G** arrows). This sensory organ is normally located at the anterior wing margin and develops from sensory organ precursor cells which are recruited from the wing disc epithelia at the border between the dorsal and the ventral compartments (Ripoll et al.).

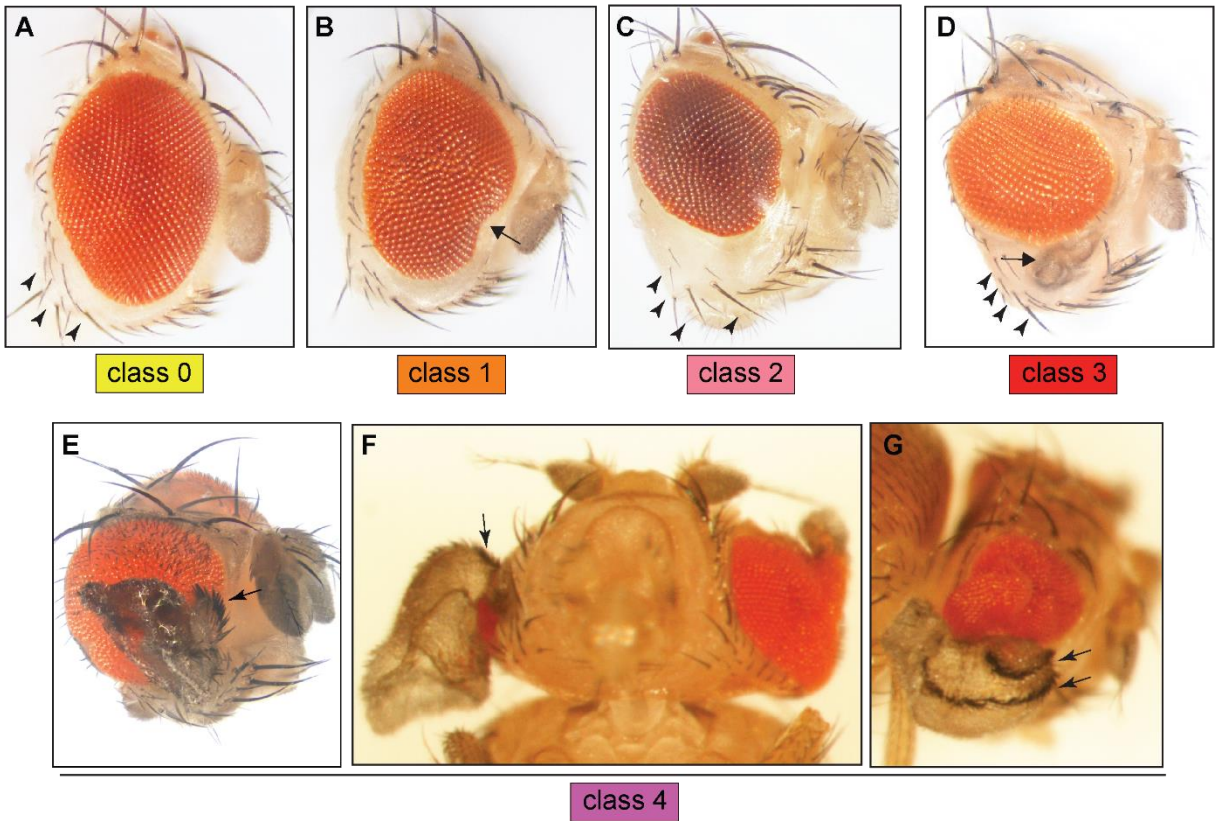

Figure 10 – dMyc overexpression and *dMax* downregulation mostly affect eye differentiation leading to an eye-to-wing homeotic transformation. Phenotypic classes representing the most recurrent defects observed in adult eyes upon simultaneous dMyc overexpression and *dMax* downregulation in undifferentiated eye disc cells. (**A**) Class 0: wild-type-like eye (**B**) Class 1: the lack of anterior ommatidia (arrow) is combined with a widespread disorganization of the ommatidia array. (**C**) Class 2: only a small area of the eye field delimited by periorbital vibrissae (arrowheads) has correctly differentiated ommatidia, while the ventral region appears similar to the cuticle of the head capsule and does not show any eye cells. (**D**) Class 3: a greyish overgrowth of presumably undifferentiated tissue (arrow) can be observed in the ventral part of the eye field. (**E-G**) Class 4 animals in lateral (**E, G**) and ventral view (**F**) showing a wing bud differentiating from the eye. Arrows point a structure very similar to the triple row of sensory organs normally located at the wing anterior margin.

Penetrance and expressivity of MYC/MAX classes increase following the growth temperature and the copy number of *ey-Gal4*, *UAS-dMyc* and *Max-RNAi* transgenes (**Fig. 11 A, B**) indicating that the higher is MYC/MAX ratio the more severe is the phenotype due to high MYC function. This suggests that MYC effect on cell differentiation should not require MAX. It is worth noting that, even at dMyc physiological level, a strong but viable *dMax* downregulation is able *per se* to generate a mild MYC/MAX phenotype (**Fig. 11 A** column 19). At 29°C a mild *dMax* downregulation (1X*ey-Gal4*,1X*Max-RNAi*) leads to defective

proliferation and results in MAX phenotypic classes (**Fig. 4 A** column 6). We can suppose that this level of *dMax* silencing is sufficient to impair MAX-dependent functions of MYC on cell proliferation but not enough to generate an amount of "free MYC" able to affect cell differentiation. Conversely, a significant increase of transgenes copies (2X*ey-Gal4,*2X*Max-RNAi*) causes an excessive *dMax* downregulation which strongly impairs cell proliferation and leads to death pharate adults which often show a reduced head capsule and lack of eyes (**Fig. 6 A** column 12). We have generated an intermediate condition represented by animals carrying 1X*ey-Gal4,*1X*Max-RNAi* and heterozygous for a *dMax* null allele (Max^1) that halves the *dMax* gene dosage. Adult flies with such genotype are viable and their eyes show Class1 and Class2 MYC/MAX phenotype, despite the MYC physiological amount (**Fig. 11 A** column 19). Moreover, Max^1 null allele enhances the phenotypic effect observed in 1X*ey-Gal4,*1X*UAS-dMyc*,1X*Max-RNAi* animals (**Fig. 11 A** column 7 vs 20 and 8 vs 21). Consistently, the MYC/MAX phenotype induced by 1X*ey-Gal4,*1X*UAS-dMyc*,1X*Max-RNAi* is suppressed by an increased dMax expression obtained by adding one copy of the genomic *dMax* locus (*Max-rescue*) (**Fig. 11 A** column 8 vs 22). Overall, these data confirm that the MYC/MAX ratio, and not the MYC absolute level, is responsible for MYC-dependent but MAX-independent partial inhibition of cell differentiation, which can result in an eye-to-wing homeotic transformation.

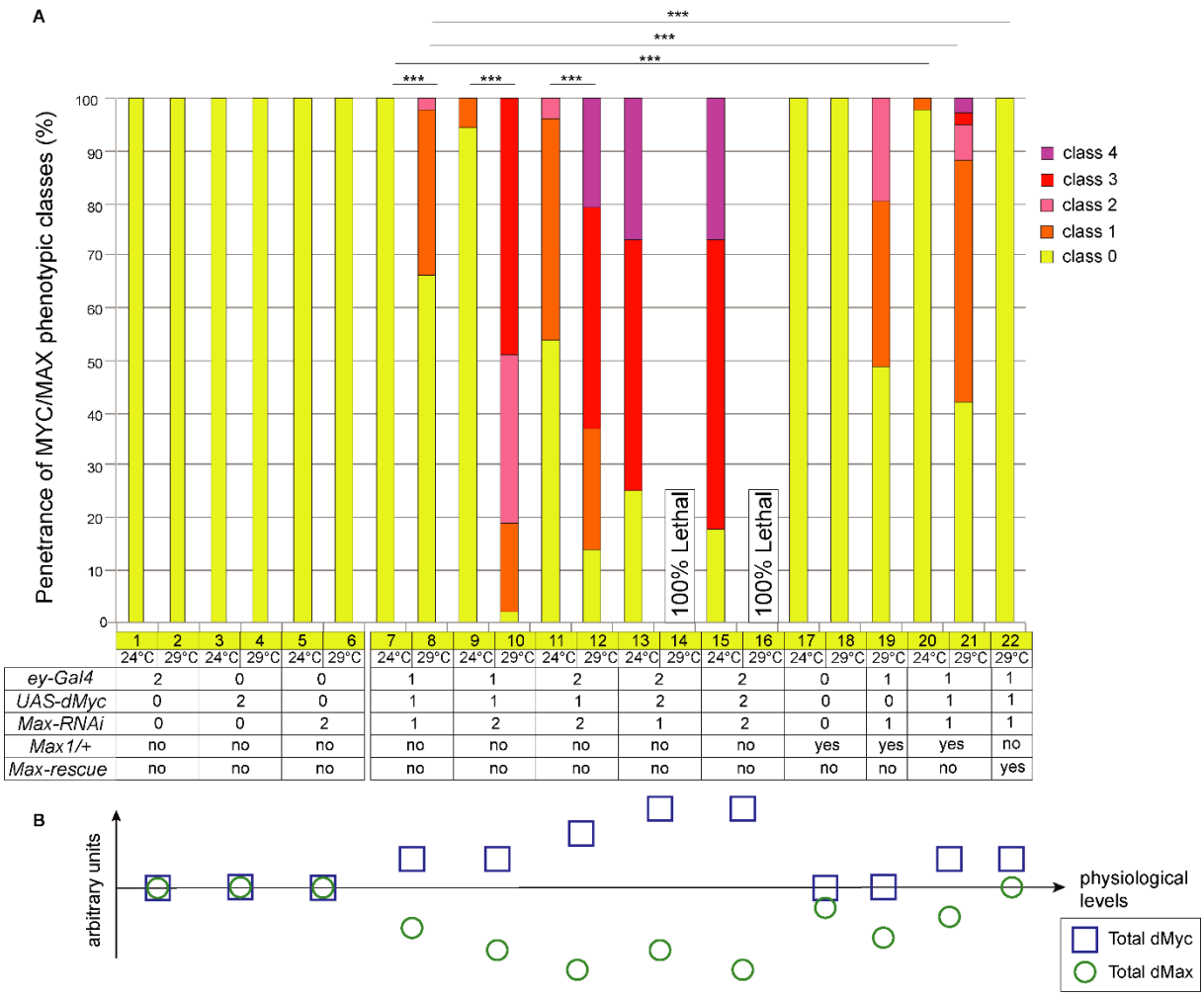

	1	2	3	4	5	6	7	8	9	10	11	12	13	14	15	16	17	18	19	20	21	22
	24°C	29°C	24°C	29°C	24°C	29°C	24°C	29°C	24°C	29°C	24°C	29°C	24°C	29°C	24°C	29°C	24°C	29°C	29°C	24°C	29°C	29°C
ey-Gal4	2		0		0		1		1		2		2		2		0		1	1		1
UAS-dMyc	0		2		0		1		1		1		2		2		0		0	1		1
Max-RNAi	0		0		2		1		2		2		1		2		0		1	1		1
Max1/+	no		no		no		no		no		no		no		no		yes		yes	yes		no
Max-rescue	no		no		no		no		no		no		no		no		no		no	no		yes

Figure 11 – The severity of MYC/MAX phenotype increases according to the increase of MYC to MAX expression ratio. (**A**) Stacked column chart showing the frequency of MYC/MAX phenotypic classes observed in the analysed progeny upon increase of transgenes copies (copy number of transgenes is reported in table) and growth temperature (24°C or 29°C). Statistics: Mann-Whitney-Wilcoxon test, p<0,001 ***. Importantly, a strong but viable *dMax* downregulation leads to MYC/MAX phenotypic traits. Moreover, the phenotypic severity caused by 1X*ey-Gal4*,1X*UAS-dMyc*,1X*Max-RNAi* is enhanced by a further decrease of dMax level (column 7 vs 20 and 8 vs 21) and suppressed by increased dMax level (column 8 vs 22). (**B**) Graphical representation of dMax and dMyc levels in the analysed genotypes.

3.5 High MYC/MAX ratio causes the ectopic expression of the wing Hox gene *Antennapedia*

A homeotic transformation is normally the phenotypic trait due to mutations in homeotic genes (Hox genes). Hox genes regulate the organization of the body plan by specifically dictating the differentiation pattern of tissues and organs composing each singular metamere.

During *Drosophila* early development, the sequential activity of gene networks establishes a segmental organization along the anterior-posterior axis of the fly embryo. These signals regulate the spatiotemporal expression of Hox genes which, in turn, activate pathways responsible for organs formation in each specific body segment (Beira and Paro 2016). Together with the second pair of legs, wing is the appendage of the second thoracic segment (T2), whose specification is strictly controlled by the expression of the Hox gene *Antennapedia* (*Antp*). When ectopically expressed in the head, Antp converts head structures into appendages of the second thoracic segment (e.g. homeotic transformation of antenna in T2 leg) (Gibson and Gehring 1988). The Antp protein has been detected in the thoracic imaginal discs of leg, wing and haltere but it is absent in eye-antenna imaginal disc (Wirz et al. 1986). Plaza and colleagues demonstrated that the ectopic expression of Antp in eye progenitor cells (located anteriorly to morphogenetic furrow) inhibits eye development by interacting with the protein product of the eye selector gene *eyeless* thus disrupting the *eyeless* regulatory cascade. Moreover, the simultaneous expression of Eyeless and Antennapedia causes a massive cell death (Plaza et al. 2001). Nevertheless, when a constitutively active Notch receptor prevents apoptosis, Antp ectopic expression is sufficient to transform part of the eye in wing (Kurata et al. 2000).

The highest MYC/MAX ratio that we can generate in viable flies leads to a similar phenotype: the formation of a wing bud protruding from the adult eye. Therefore, we asked whether in presence of high MYC/MAX ratio Antp was expressed in the eye disc indicating a possible involvement of this Hox gene in the observed phenotype. We analysed by immunolabeling the expression of Antp in eye-antenna imaginal discs dissected from wandering 3rd instar larvae with high MYC/MAX ratio. While Antp is not detectable in control eye discs carrying the only *UAS-dMyc* construct (**Fig. 12 B**), upon dMyc or hMYCN overexpression some Antp positive cells are clearly visible (**Fig. 12 F, J, N**). Interestingly the same cells co-express the proliferation marker PhosphoH3, indicating that they are dividing (**Fig. 12 H, L, P**), although the general proliferation pattern does not seem to be affected (**Fig. 12 G, K, O**). As previously shown, a high dMyc overexpression (1X*ey-Gal4*,2X*UAS-dMyc*) causes also a delay of the eye imaginal disc development, as suggested by the backward position of the morphogenetic furrow and the reduced number of Elav-positive photoreceptors (**Fig. 9 E-F** and **Fig. 12 I**). The differentiation of Elav-positive photoreceptors does not seem to be visibly affected in 1X*eyGal4*,1X*UAS-hMYCN* eye disc (**Fig. 12 M**), however eyes of the same genotype show a moderate MYC phenotype (**Fig. 8 A** column 16). Altogether, these observations suggest that a mild increase of MYC/MAX ratio causes the ectopic expression of Antp in scattered and

proliferating eye disc cells, supporting the idea that the eye-to-wing transformation due to high MYC/MAX ratio should require Antp.

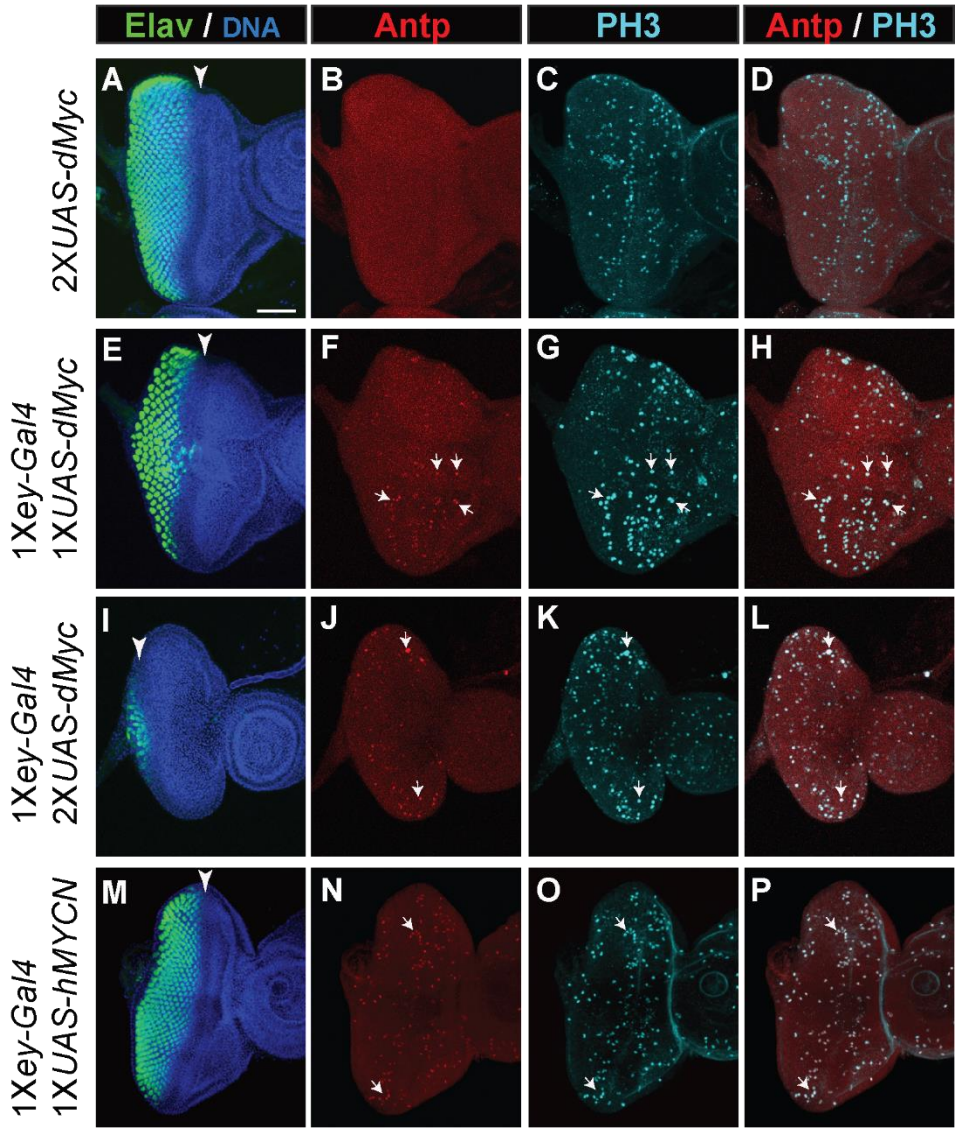

Figure 12 – dMyc or hMYCN overexpression leads to the ectopic expression of the Hox gene *Antennapedia* in eye disc cells. Eye-antenna imaginal discs dissected from wandering 3rd instar larvae grown at 29°C. Immunolabeling with the differentiation marker Elav in green (**A,E,I,M**), the mitotic marker PhosphoH3 (PH3) in cyan (**C,G,K,O**) and the anti-Antennapedia antibody (**B,F,J,N**). Cell nuclei are labelled by HOECHST. Antennapedia protein is absent in the control disc (**B**) while it is ectopically expressed in eye discs overexpressing dMyc (**F,J**) and hMYCN (**N**) and it co-localizes with the PH3 labelling (**H,L,P**) (arrows point exemplificative cells). dMyc overexpression causes a slight (**E**) or severe (**I**) delay in morphogenetic furrow progression (arrowheads) and a decreased number of Elav-positive differentiated cells, which are not substantially affected by hMYCN overexpression (**M**). Cell proliferation does not seem to be altered by dMyc (**G,K**) or hMYCN overexpression (**O**). Scale bar: 15 μm.

The further increase of MYC/MAX ratio leads to a similar phenotype. Indeed, eye discs with a strong but viable *dMax* downregulation (*Max*^{1}/+ mutants carrying 1X*ey-Gal4*,1X*Max-RNAi*) show Antp ectopic expression in proliferating cells and a slight size decrease when compared to a *Max*^{1}/+ mutant control disc (**Fig. 13 E-H**). This last shows normal size, normal morphology of the Elav-positive clusters of photoreceptors and any detectable Antp expression (**Fig. 13 A-D**). Among the eye discs with the highest MYC/MAX ratio (2X*ey-Gal4,2XUAS-dMyc*,2X*Max-RNAi*) we occasionally observed a more severe phenotype. As shown in **Fig. 13 I,J**, the expression patter of Elav is completely disrupted, indicating that both morphology and localization of photoreceptors are strongly affected. Moreover, Antp is ectopically expressed in clustered cells and not in single scuttered cells.

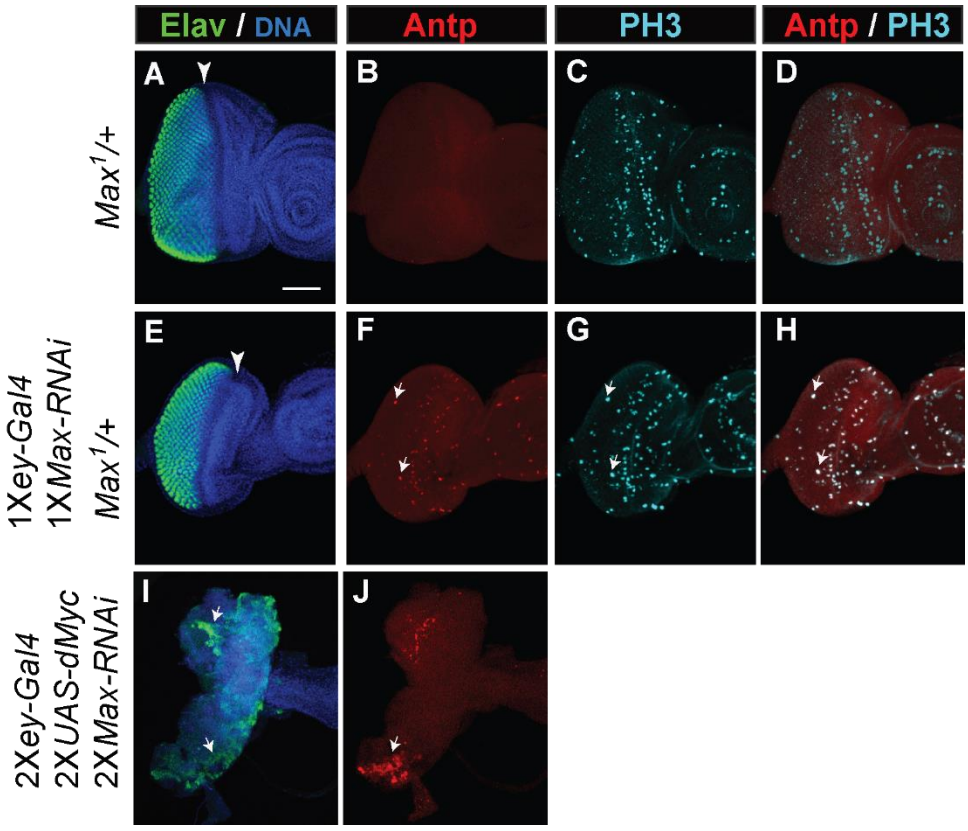

Figure 13 – Increased MYC/MAX expression ratio can result in a strong ectopic expression of *Antennapedia* and severe impairment of eye cell differentiation. Eye-antenna imaginal discs dissected from wandering 3rd instar larvae grown at 29°C (**A-H**) or 24°C (**I-J**). Immunolabeling with the differentiation marker Elav in green (**A,E,I**), the mitotic marker PhosphoH3 (PH3) in cyan (**C,G**) and the anti-Antennapedia antibody (**B,F,J**). Cell nuclei are labelled by HOECHST. Antennapedia protein is absent in *Max*^{1}/- control disc (**B**) while it is ectopically expressed in eye discs with a stronger but viable *dMax* downregulation (**F**) where co-localize with the PH3 labelling (**H**) (arrows point exemplificative cells). The further increase of MYC/MAX ratio leads to Antp expression in clustered cells (**J**) and disruption of Elav expression pattern (**I**). Scale bar: 15 μm.

It is worth reminding that adults carrying 2X*ey-Gal4,2XUAS-dMyc*,2X*Max-RNAi* can undergo eye-to-wing transformation. This might suggest that Antp expression in clustered eye cells could be required to burst the homeotic transformation, while Antp expression in scattered cells could lead to defective cell differentiation accounting for ommatidia disorganization or MYC/MAX mild phenotypes. Altogether these data support the notion that high MYC to MAX expression ratio affects cell differentiation. An increased amount of "free MYC" seems to negatively modulate this process in the developing eye likely through the ectopic activation of the *Antennapedia* Hox gene in proliferating cells.

3.6 MYC inhibition of cell differentiation requires dHDAC1 and Smrter co-repressors

Our findings suggest that MYC-mediated inhibition of cell differentiation relies on a MAX-independent mechanism. The transcriptional activation of MYC target genes strictly requires the binding of MYC-MAX dimers to specific E-box sequences in the target promoter (Amati et al. 1993). Conversely, over the last years it has been demonstrated that MYC can also negatively regulate gene transcription and this mechanism does not seem to be necessarily dependent on MYC/MAX heterodimerization (Gartel et al. 2001) (Liu et al. 2007). For example, in neuroblastoma MYCN binds TRKA and p75NTR promoters through the interaction with the transcription factors SP1 and MIZ-1 and recruits the chromatin modifier HDAC1 to repress transcription (Iraci et al. 2011). Hence, we envisaged that MYC-induced phenotype could rely on a mechanism based on MYC-mediated transcriptional repression. To explore this hypothesis, we assessed whether low level of the co-repressors dHDAC1 or Smrter (Smr) would be able to modify the dMyc overexpression phenotype. The first is the *Drosophila* homolog of human histone deacetylase 1 (HDAC1) which removes acetyl group from histone lysine residues promoting chromatin condensation and the epigenetic inhibition of gene transcription. The latter is a protein required to stabilize the HDACs recruitment into complexes that repress transcription and is the homolog of human NCoR/SMRT (Mottis et al. 2013). Interestingly, dMyc overexpression phenotype (1X*ey-Gal4*,1X*UAS-dMyc*) is partially suppressed in animals heterozygous for null mutations of *dHDAC1* (*HDAC1*^{04556}) or *Smrter* (*Smr*^{G0060}) (**Fig. 14 A, B** column 1-3), suggesting a genetic interaction between dMyc and the two repressors. We confirmed this result downregulating *dHDAC1* or *Smrter* through RNAi. Indeed, animals carrying 1X*ey-Gal4*,1X*UAS-dMyc*,1X*HDAC-RNAi* or 1X*ey-Gal4*,1X*UAS-dMyc*,1X*Smr-RNAi* showed a weakened phenotype compared to control flies (1X*ey-*

Gal4,1X*UAS-dMyc*,1X*GFP-RNAi*) (**Fig. 14 A, B** column 6, 7). The only *dHDAC1* or *Smr* downregulation does not lead to any evident phenotype (**Fig. 14 A, B** column 4, 5).

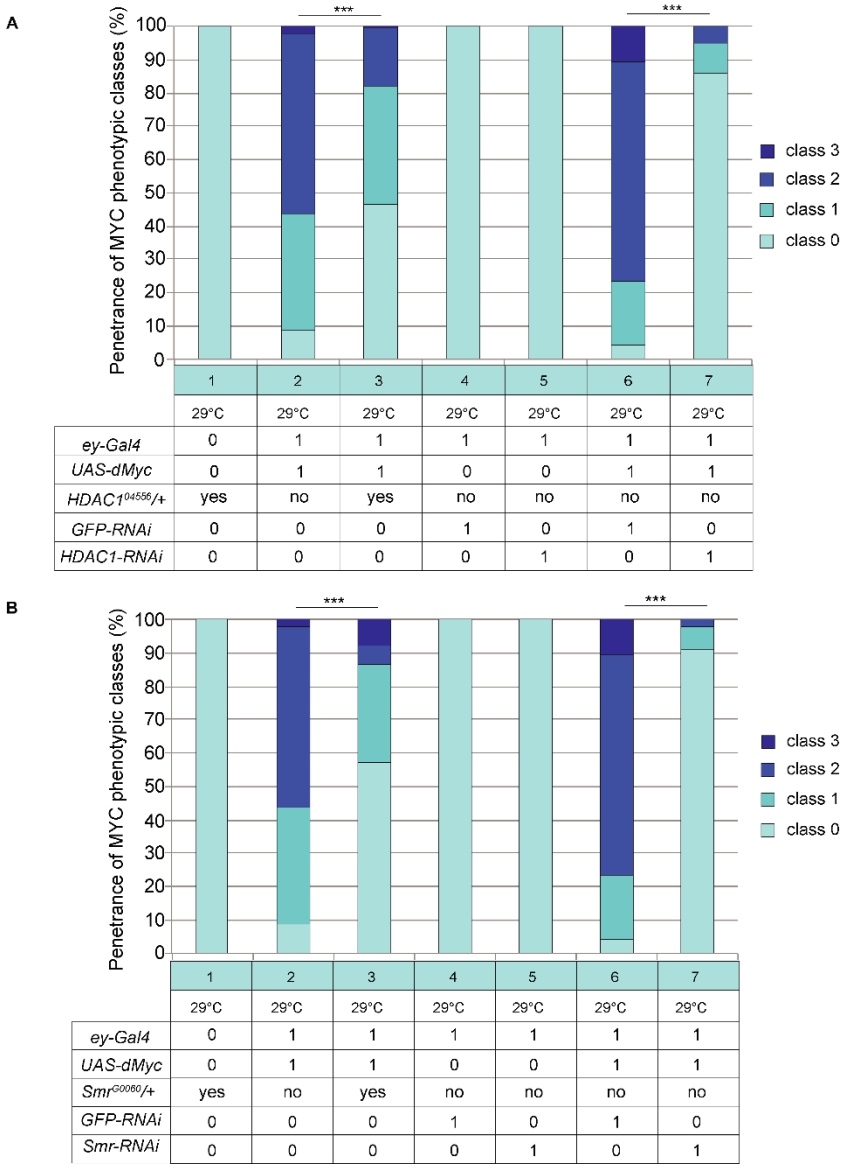

	1	2	3	4	5	6	7
	29°C	29°C	29°C	29°C	29°C	29°C	29°C
ey-Gal4	0	1	1	1	1	1	1
UAS-dMyc	0	1	1	0	0	1	1
HDAC1^{04556}/+	yes	no	yes	no	no	no	no
GFP-RNAi	0	0	0	1	0	1	0
HDAC1-RNAi	0	0	0	0	1	0	1

	1	2	3	4	5	6	7
	29°C	29°C	29°C	29°C	29°C	29°C	29°C
ey-Gal4	0	1	1	1	1	1	1
UAS-dMyc	0	1	1	0	0	1	1
Smr^{G0060}/+	yes	no	yes	no	no	no	no
GFP-RNAi	0	0	0	1	0	1	0
Smr-RNAi	0	0	0	0	1	0	1

Figure 14 – dMyc-induced phenotype is partially suppressed by low levels of dHDAC1 or Smrter co-repressors. Stacked column chart showing the frequency of MYC phenotypic classes observed upon decreased level of dHDAC1 (**A**) or Smrter (**B**). Carried transgenes and mutations are reported in table. Statistics: Mann-Whitney-Wilcoxon test, p<0,001 ***.

This evidence strongly suggests that the MYC-mediated impairment of eye cell differentiation might rely on transcriptional repressive mechanisms and could require the activity of transcriptional co-repressor proteins.

3.7 Downregulation of the Hox gene *Deformed* recapitulates the MYC overexpression phenotype

The MYC-dependent regulation of cell differentiation seems to be based on repressive mechanisms and it is associated with the ectopic expression of the Hox gene *Antennapedia*

Specific Hox genes act in specific segments to regulate cell identity and organ determination, hence their expression is sharply regulated in time and space through multiple mechanisms. Among others, a transcriptional regulation program is established during embryogenesis and it leads to a highly defined expression pattern of Hox genes. The activity of Polycomb (PcG) and trithorax (trxG) protein families properly maintains the above-mentioned pattern by repressing or activating Hox genes, respectively. Besides, important cross-regulations among the Hox genes themselves occur (reviewed in Mallo & Alonso, 2013). All together these regulatory inputs eventually result in the expression of each Hox gene in a specific segment along the antero-posterior axis. The order of the Hox genes expression from anterior to posterior corresponds to the order of the genes in the two Hox genes complexes (Antennapedia Complex and Bithorax Complex) of the fruit fly genome. Loss or gain of function of Hox genes in a segment can cause the ectopic expression of Hox proteins normally active in neighbouring segments, leading to cell identity changes (Lamka et al. 1992) (Miller et al. 2001) (Rusch and Kaufman 2000). Accordingly, we envisaged that a MYC-dependent inhibition of Hox genes normally expressed in eye primordium could provoke the ectopic activation of *Antennapedia* in the same cells.

The eye primordium originates from the neuroectodermal placode located in the embryonic head. Its development depends on the activity of a network of transcription factors that commits cells to originate the larval eye imaginal disc (Daniel et al. 1999). The Hox gene *Deformed* (*Dfd*) is expressed the eye-antenna imaginal disc complex and in the embryonic region where the eye field is specified (Diederich et al. 1991). To date, the function of Dfd in the eye development has not been well assessed. *Dfd* loss of function due to hypomorphic viable alleles induces lack of part of the head or partial transformation of the head capsule in thoracic structure suggesting that the loss of this anterior Hox gene could let posterior Hox genes expand their expression field (Merrill et al. 1987).

We expressed a *Dfd-RNAi* construct in all eye progenitor cells to assess whether *Dfd* silencing could affect eye formation. Interestingly, we observed a defective ommatidia organization very similar to that induced by dMyc or hMYCN overexpression. We then analysed *Dfd* downregulation phenotype using the same phenotypic classes adopted for MYC overexpression

phenotype (**Fig. 15 A-F**). The penetrance and severity of these classes increase accordingly to raising growth temperature and transgenes copy number (**Fig. 15 G**).

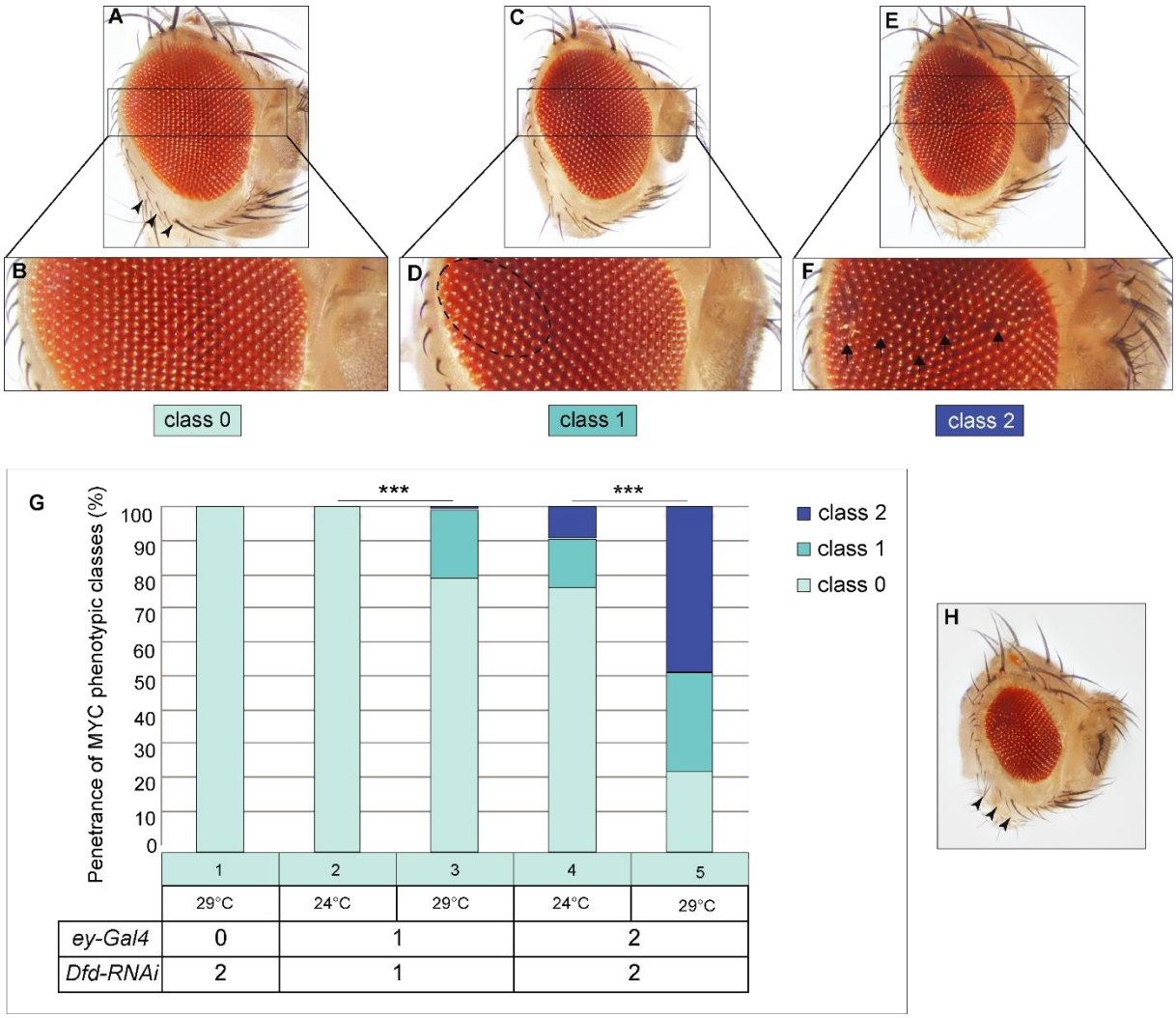

Figure 15 – *Dfd* downregulation results in the same eye defects than dMyc overexpression. (A - F) Most frequent phenotypic classes observed upon *Dfd* silencing. (**A, B**) Class 0: wild-type-like eye in frontal view (**A**) and high magnification of the area along the dorso-ventral midline (**B**). (**C, D**) Class 1: the differentiation deficit involves a limited number of ommatidia located at the posterior margin of the eye (dashed circle in **D**). (**E, F**) Class 2: the impaired differentiation affects also medial and anterior ommatidia along the midline (arrows in **F**). (**G**) Stacked column chart showing the frequency of MYC phenotypic classes observed upon *Dfd* silencing with increasing copy number of transgenes (reported in table) and growth temperature (24°C or 29°C). Statistics: Mann-Whitney-Wilcoxon test, p<0,001 ***. (**H**) Phenotype shown by few 2X*ey-Gal4*,2X*Dfd-RNAi* animals grown at 29°C strongly resembling a MYC/MAX Class 2 eye.

Remarkably, among the progeny carrying 2X*ey-Gal4*,2X*Dfd-RNAi* and grown at 29°C we observed few animals characterized by periorbital vibrissae delimiting an eye field only

partially differentiated in ommatidia (**Fig. 15 H**), reminding a mild MYC/MAX Class 2 (**Fig.10 C**). Moreover, in eye-antenna imaginal discs of the same genotype we detected ectopic *Antennapedia* expression in scattered cells (**Fig. 16 F**). Hence, we asked whether dMyc overexpression and *Dfd* downregulation could genetically interact. For this purpose, we generated animals carrying *ey-Gal4,UAS-dMyc,RNAi-Dfd* and *ey-Gal4,UAS-dMyc,RNAi-GFP* as control. Unfortunately, we did not observe any worsening of the MYC phenotype in the adult eye, despite the maximization of transgenes expression (data not shown). Nevertheless, we found few eye discs dissected from 2X*ey-Gal4*,1X*UAS-dMyc*,1X*RNAi-Dfd* larvae showing a completely disrupted organization of Elav-positive cells and Antp expression in many clustered cells that did not express PhosphoH3 (**Fig. 16 M-P**). This severe phenotype is very similar to that occasionally observed in 2X*ey-Gal4*,2X*UAS-dMyc*,2X*RNAi-Max* eye discs (**Fig. 13 I,J**) and it has never been observed upon comparable dMyc overexpression in 2X*ey-Gal4*,2X*UAS-dMyc*,2X*RNAi-GFP* control eye discs (**Fig. 16 I-L**). As expected, the strong dMyc overexpression in 2X*ey-Gal4*,2X*UAS-dMyc*,2X*RNAi-GFP* leads to the already described developmental delay indicated by eye disc size and shape together with the highly delayed progression of morphogenetic furrow. Nevertheless, the few differentiating Elav-positive photoreceptors do not seem to be altered in morphology and localization (**Fig. 16 I**) and Antennapedia is ectopically expressed only in scattered proliferating PH3 positive cells (**Fig. 16 J-L**). As previously shown, dMyc overexpression is sufficient to cause the activation of Antennapedia in eye disc cells (**Fig. 12 E-L**). Nevertheless, only when we combined dMyc overexpression with *dMax* (**Fig. 13 I,J**) or *Dfd* downregulation (**Fig. 16 M,N**), we observed, albeit occasionally, group of eye disc cells expressing high Antp level in clustered cells and showing a severe disruption of differentiated photoreceptors. This last observation suggests a weak genetic interaction, at least in the tested experimental set, between dMyc overexpression and *Dfd* downregulation which sporadically leads to a phenotype similar to that induced by high MYC/MAX ratio.

Altogether these data sustain the hypothesis that an increased level of "free MYC" might inhibit *Deformed* expression leading to ectopic expression of Antennapedia in eye disc cells. This would cause impaired eye cell differentiation and would result eventually in an eye-to-wing homeotic transformation.

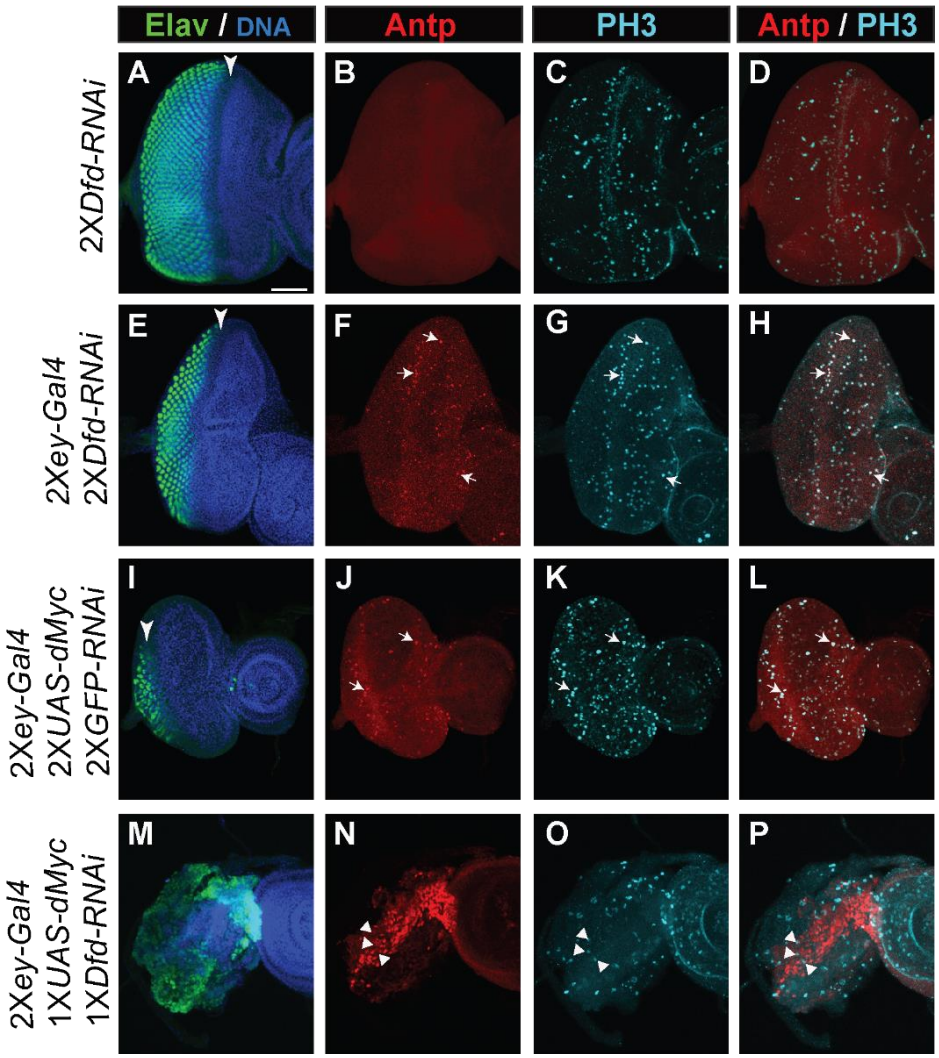

Figure 16 – *Dfd* downregulation induces Antennapedia ectopic expression in eye imaginal disc and mildly genetically interact with dMyc overexpression. Eye-antenna imaginal discs dissected from wandering 3rd instar larvae grown at 29°C (**A-H**) and 24°C (**I-P**). Immunolabeling with the differentiation marker Elav in green (**A,E,I,M**), the mitotic marker PhosphoH3 (PH3) in cyan (**C,G,K,O**) and the anti-Antennapedia antibody (**B,F,J,N**). Cell nuclei are labelled by HOECHST. Antennapedia protein is absent in 2X*Dfd-RNAi* control disc (**B**) while it is ectopically expressed in eye discs upon *Dfd* silencing (**F**) where it co-localizes with the PH3 labelling (**H**) (arrows point exemplificative cells). The simultaneous dMyc overexpression and *Dfd* downregulation sporadically leads to the disruption of Elav expression pattern (**M**) and a high expression of Antp (**N**) in PH3-negative cells (**P,P**) (triangles). This phenotype is not shown by discs with comparable dMyc overexpression even though we can observe a delayed progression of the morphogenetic furrow (**I**) (arrowheads) and a scattered Ant expression (**J**) in PH3-positive cells (**K-L**). Scale bar: 15 μm.

3.8 MYC associates to the *Deformed* promoter in putative transcriptional repressive sites

To better define the putative transcriptional repressive function of MYC on the Hox gene *Deformed*, we tested the ability of MYC to bind the *Dfd* promoter using a dual cross-linking chromatin immunoprecipitation (ChIP) approach.

Reliability and efficiency of the antibody used for immunoprecipitation represent a strong limitation in such experiments. Therefore, we decided to use an already tested and ChIP grade anti human MYCN antibody to immunoprecipitate the associated chromatin from eye disc cells overexpressing hMYCN. Our approach is based on the assumption that dMyc and hMYCN binding profiles would overlap at least partially. A robust basis for this assumption is provided by several analogies between dMyc and hMYCN overexpression phenotypes. In both cases we observed similar phenotypic traits in adult eyes due to inhibited ommatidia differentiation. Moreover, dMyc- and hMYCN-mediated phenotypes are suppressed by a heterozygous *dMyc* null allele, suggesting a conserved activity and mechanism of the two orthologs. Finally, both dMyc and hMYCN overexpression are sufficient to induce ectopic expression of Antennapedia in scattered eye disc cells. To extend the functional similarity between dMyc and hMYCN and to set positive controls for the ChIP assay, we assessed the ability of hMYCN to bind the promoter of two known dMyc positive target genes: *Cyclin-dependent kinase 4 (Cdk4*) and *pitchoune* (*pit*). The protein-serine kinase Cdk4 is a well-known target of human c-MYC, which binds E-box sequences on *Cdk4* promoter and induces *CDK4* transcription (Hermeking et al. 2000). Consistently, it has been demonstrated that dMyc binds the *Drosophila Cdk4* promoter region (Orian et al. 2003) and upregulates *Cdk4* transcription (Duman-Scheel et al. 2004). The fruit fly gene *pit* encodes a DEAD-box RNA helicase largely co-expressed with dMyc and involved in cell growth regulation (Zaffran et al. 1998). Ectopic expression of dMyc drives an ectopic expression of *pit* (Zaffran et al. 1998) and, conversely, *pit* expression is strongly reduced in $dMyc^{PG45}$ or $dMyc^{PL35}$ loss of function mutants (Benassayag et al. 2005a). Human c-Myc expression in the wing imaginal disc leads to *pit* mRNA increase (Benassayag et al. 2005). Moreover, the *pit* human homologue MrDb is transcriptionally activated by the binding of MYC-MAX dimers to the promoter region (Grandori et al. 1996).

We assessed the association of hMYCN to the promoter of these genes in the proximity of the transcription start site (TSS), were hMYCN usually localizes (+/- 500 pb from TSS). Both *Cdk4* and *pit* present multiple transcript isoforms. Therefore, for each positive target we decided to test the association of hMYCN in the proximity of two alternative TSSs (i.e. *Cdk4* BS3 and

BS4 and *pit* BS2 and BS3) and to a distal region far from TSSs as negative control (i.e. *Cdk4* BS2 and *pit* BS1). Notably, we found that hMYCN associates to the promoter of both dMyc positive targets at *Cdk4* BS4 and *pit* BS3 sites, respectively (**Fig. 17 A, B**). While *pit* BS3 is a canonical E-box (CACGTG), *Cdk4* BS4 is a TATCGATA sequence which has been found close to E-boxes bound by dMyc-dMax dimers *in Drosophila* (Orian et al. 2003). Remarkably, an E-box related sequence CAGCTG localizes 49 pb downstream the TATCGATA sequence in the *Cdk4* promoter. This result indicates that hMYCN protein can associate *in vivo* to the promoter of dMyc target genes and validates our ChIP approach.

Multiple lines of evidence so far described let us envisage a possible MYC-dependent inhibition of the Hox gene *Deformed*. As already mentioned, MYC associates to the promoter of its negative targets interacting with other transcription factors which mediate the binding to DNA. Therefore, we adopted a dual cross-linking chromatin immunoprecipitation to efficiently stabilize both protein-protein and protein-chromatin interactions. In neuroblastoma, transcription factors such as SP1 and MIZ-1 are known to be involved in the MYCN-dependent inhibition of genes such as p75NTR, TrkA, TG2, Cyclin G2 (Iraci et al. 2011) (Liu et al. 2007) (Marshall et al. 2010). A fruit fly homolog of human MIZ-1 has not been identified, yet (Wiese et al. 2013). Differently, human SP1 is a member of the SP1/KLF (Sp1-like proteins and Krüppel-like factors) zinc-finger protein family, which is present also in *Drosophila*. The fruit fly SP1/KLF family accounts for 10 SP1/KLF zinc finger proteins that bind a GC-rich consensus sequence as their human counterpart (Kaczynski et al. 2003) (Nagaoka et al. 2001) (Brown et al. 2005). Most of the molecularly characterized Polycomb Response Element (PREs), mainly involved in maintenance of chromatin repressive state of Hox gene regulatory regions, contain sequences bound by SP1/KLF, suggesting that one or more SP1/KLF family members play a role in PRE function in *Drosophila* (Brown and Kassis 2010). In the *Deformed* promoter, two close partial binding sites for *Drosophila* SP1/KLF factors are present in the proximity of the TSS (*Dfd* BS3 - GGGTGT and GGCGT), while a consensus sequence for the human SP1 (*Dfd* BS2 - TGGGCGGAGT) is located upstream. A canonical E-box is around 2000 pb upstream the TSS (*Dfd* BS1 - CACGTG). We assessed the association of hMYCN to all the three binding sites and we found enrichment only of the BS3 which includes two partial binding sites for *Drosophila* SP1/KLF proteins (**Fig. 17 C**).

This evidence supports the idea that overexpressed hMYCN could bind the *Deformed* regulatory region and possibly mediate *Dfd* transcriptional repression in eye imaginal disc cells.

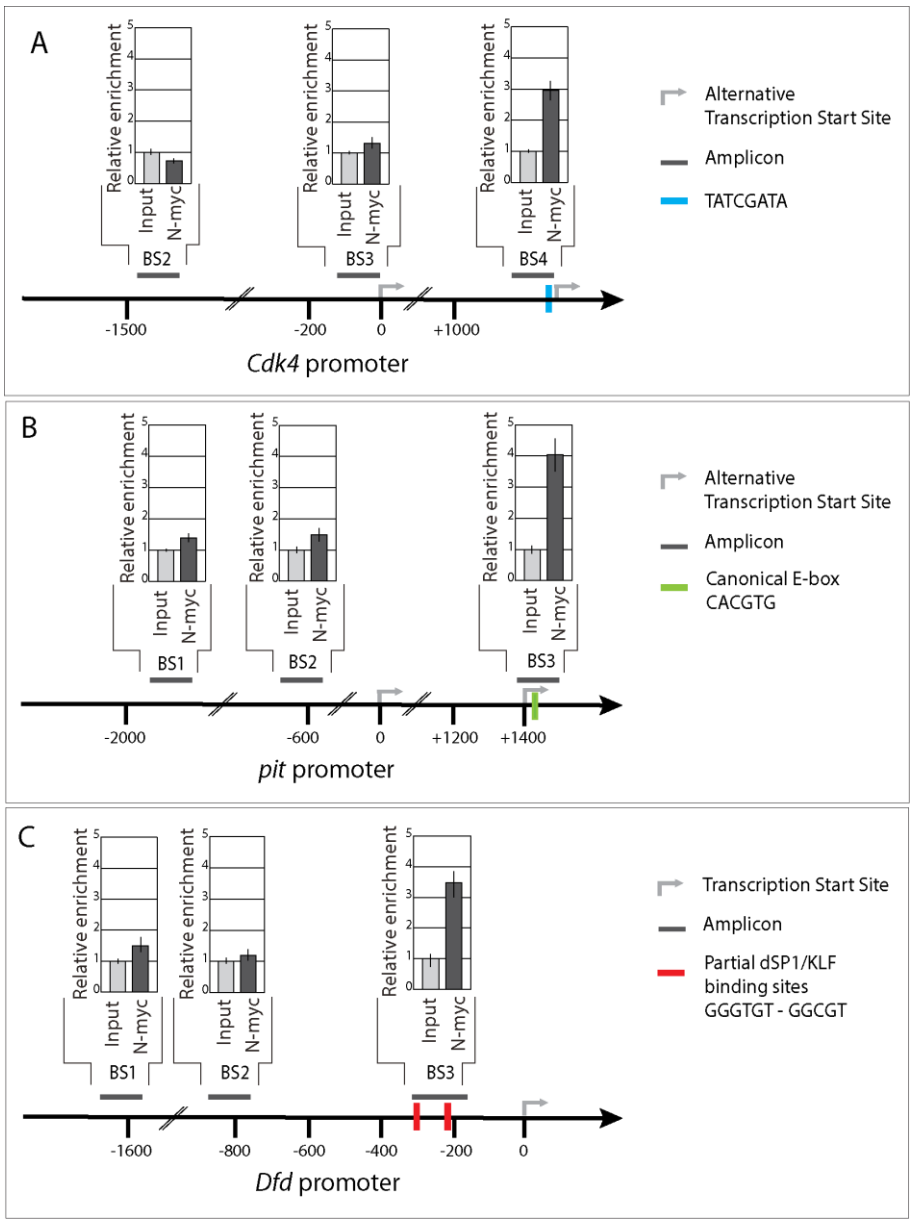

Figure 17 – hMYCN associates to the transcription start site on the promoter of positive MYC/dMyc targets and in the proximity of *Drosophila* SP1/KLF binding sites in the *Deformed* promoter. Dual cross-linking chromatin immunoprecipitation with anti-hMYCN antibody performed on chromatin extracted from eye imaginal discs of 2X*ey-Gal4*, 2X*UAS-hMYCN* wandering 3rd instar larvae grown at 24°C. The enrichment analysis has been performed through quantitative Real Time PCR. (**A,B**) The c-MYC and dMyc positive targets *Cdk4* and *pit* have been tested in two candidate binding sites (BS) close to two alternative transcription start sites (TSS) (*Cdk4* BS3 and BS4, *pit* BS2 and BS3) and on a site largely upstream the TSS (*Cdk4* BS4 and *pit* BS1). (**C**) The *Deformed* promoter has been tested in regions containing either canonical E-box (*Dfd* BS1) or a binding site for human SP1 (*Dfd* BS2) or two partial binding sites for *Drosophila* dSP1/KLF factors (*Dfd* BS3).

DISCUSSION

Genes belonging to the MYC family (i.e. c-MYC, MYCN and L-MYC) are among the most studied oncogenes in cancer research. An increased amount of MYC oncoproteins characterizes several human tumours and strongly contribute to tumour onset and progression. Over the past years, it has been demonstrated that MYC oncoproteins participate to the regulation of different aspects of tumour cell biology. This ability mainly relies on the large number of genes whose expression is modulated by MYC transcription factors. Most of MYC targets are involved in cell cycle regulation, cell adhesion, apoptosis, cellular metabolism, ribosome biogenesis, protein synthesis, and mitochondrial function. MYC is known to drive cell proliferation promoting cell cycle progression and repressing cell cycle arrest and differentiation. Moreover, MYC stimulates cell growth, vasculogenesis and loss of cell adhesion predisposing to metastasis formation and spreading (Adhikary and Eilers 2005).

Among the tumours in which MYC proto-oncogenes are activated there is the neural crest-derived cancer neuroblastoma. Neuroblastoma is the most common and deadly extracranial solid tumour of the early infancy. To date, the most robust prognostic marker has been the genomic amplification of the *MYCN* gene and/or the increase of MYCN protein level. MYCN is a member of MYC family and shares with c-MYC many structural and functional features. Through its BR/HLH/LZ domain MYCN interacts with the MYC associated factor X MAX and MYC-MAX dimers bind E-box-related DNA sequences harboured by the promoter of target genes. Once the binding occurred, MYCN recruits co-activators and promote the transcription of genes involved in cell cycle progression, cell growth, protein translation and apoptosis. Besides that, recent findings highlighted a MYCN activity as transcriptional repressor relying on the MYCN interaction with co-factors like SP1 and MIZ-1 at DNA sites different from E-boxes. Within these complexes MYCN does not directly bind DNA but it recruits chromatin modifiers, such as histone deacetylases (HDACs), whose activity results in chromatin condensation and transcriptional repression. Such mechanisms underlie the MYCN-mediated inhibition of Cyclin G2 known to arrest cell cycle progression (Marshall et al. 2010), of TrkA and p75NTR neurotrophin receptors (Iraci et al. 2011) and of the transglutaminase TG2 required for neuritic differentiation (Liu et al. 2007). Therefore, a high MYCN level in neuroblastoma cells might result in both the transcriptional activation of cell cycle promoting factors and in the repression of anti-proliferative and pro-differentiative genes, overall contributing to the acquisition of selective advantages and possibly triggering the malignant

transformation. To date, the role of MAX in MYCN repressive complexes is still not clear. The dimerization with MAX is known to be essential for MYC binding to E-box sequences. Since MYCN-mediated repression does not involve E-boxes recognition, the formation of a MYCN-MAX dimers could not be necessary. Evidence of that is the MAX-independent repression of TG2 (Liu et al. 2007). The existence of MAX-independent functions of MYC has been strongly suggested by many observations in *Drosophila*. While the homozygous *dMyc* null mutation strongly affects body size and results in larval lethality, *dMax* null mutants undergo metamorphosis and die later during development as pharate adults unable to eclose from the puparium. The different severity of these mutant phenotypes suggests a, albeit partial, MAX-independent function of dMyc in the regulation of cell proliferation, growth and survival (Steiger et al. 2008). In this scenario, not only the intracellular amount of MYC but also the MAX protein level could be crucial to modulate the balance between the MYC-MAX-dependent transcriptional activation and the putative MYC-dependent but MAX-independent transcriptional repression. Eventually, both these MYC-mediated transcriptional activities result in a fine tuning of cell proliferation and differentiation whose alteration plays a pivotal role in tumour onset and progression.

Therefore, we focused our analysis on investigating *in vivo* the effect of a high MYC to MAX expression ratio choosing the *Drosophila* eye as powerful cellular readout. Firstly, we analysed the effect of *dMax* downregulation using an interfering RNA targeting *dMax* mRNA in eye progenitor cells. Although these cells are determined to differentiate the adult eye, they are still proliferating and not yet committed to terminal differentiation. Upon *dMax* silencing, adult eyes lack part of the anterior ommatidia or, in more severe cases, show an evident size reduction. Consistently with previously described phenotypes (Steiger et al. 2008), a strong *dMax* downregulation is lethal. These flies reach the pharate adult stage but show a striking reduction of the head capsule and never eclose from the puparium. To define the cause of these phenotypes we analysed cell proliferation and differentiation in the eye larval primordium. Upon *dMax* silencing, eye imaginal discs showed an evident size reduction and a strong decrease of dividing cells (PhosphoH3-positive cells). However, cell differentiation did not seem to be affected as demonstrated by a wild-type-like pattern of the Elav marker expressed in all post-mitotic neuron, including the eye photoreceptors. Moreover, we observed a proper progression of the morphogenetic furrow (characterized by the expression of the activated form of the Notch receptor) that marks the border between the anterior eye cells still uncommitted to terminal differentiation and the posterior already committed eye cells. These lines of evidence

suggest that *dMax* downregulation in dividing eye cell progenitors impairs cell proliferation without substantially affecting cell differentiation. Notably, the small eye observed upon *dMax* silencing is in most cases closely encircled by periorbital vibrissae, normally delimiting the eye territory. This could further indicate that all the cells of the imaginal disc differentiate properly but, being less than normal, they result in an adult eye of reduced size. Such observation appears to be consistent with a dMax-dependent role of dMyc on cell proliferation.

Differently, the overexpression of dMyc or hMYCN affects eye cell differentiation leading to a mildly defective organization of the ommatidia array in the adult eye. In most severe cases, a high dMyc or hMYCN level can result in a cone shaped eye, possibly suggesting that eye cells attempt to grow in a proximal-distal direction. This feature is not typical of the eye but characterizes, for instance, the thoracic lateral appendages as wing and legs. Interestingly, a higher MYC/MAX ratio, obtained by the simultaneous *dMax* downregulation and dMyc overexpression, mainly affect cell differentiation with a dose-dependent severity. Indeed, although some animals show a small eye, this phenotype is likely due to loss of differentiation and not to loss of proliferation. In most of these flies periorbital vibrissae encircle an area including few differentiated ommatidia and a region lacking eye units. The latter one is similar to the surrounding cuticle of the head capsule and possibly indicates that a portion of the eye field did not properly differentiate ommatidia. In more severe cases, in this region we observed a grey tissue overgrowth or, at the highest and viable MYC/MAX ratio that we could generate, a wing bud protruding from the eye. This wing bud shows a differentiated structure resembling the triple row of sensory bristles located at the wing anterior margin. Interestingly, the differentiation of these sensory organs relies on the establishment of a dorso-ventral border in the anterior compartment of the wing imaginal disc (Ripoll et al. 1988). This observation suggests that the ectopic wing bud could acquire antero-posterior and dorso-ventral polarization and follow the wing differentiation pathway.

The eye-to-wing homeotic transformation let us infer that a high MYC/MAX expression ratio is sufficient to change the cell fate determination of eye progenitor cells. Several lines of evidence indicate that in this mechanism the main player is the MYC to MAX expression ratio, rather than the absolute MYC or MAX levels. While 2X*ey-Gal4*, 2X*UAS-dMyc*, 2X*Max-RNAi* animals show the MYC/MAX phenotype including homeotic transformation in a dose-dependent manner, 2X*ey-Gal4*, 2X*UAS-dMyc*, 2X*GFP-RNAi* flies exhibit typical MYC phenotypic classes. This indicates that a high MYC/MAX ratio induced by dMyc overexpression weakly inhibits cell differentiation, while a higher MYC/MAX ratio obtained

by dMyc overexpression and *dMax* silencing has a more severe impact. Indeed, in some cases the differentiation program is completely subverted and cells of the eye imaginal disc organize to give a wing bud. Importantly, the phenotypic traits induced by dMyc overexpression and *dMax* downregulation are suppressed by increasing the MAX level through an additional copy of the *dMax* locus (*Max-rescue*). Conversely, they are exacerbated by *dMax* heterozygous null mutation (Max^1/+). Furthermore, the strong but viable *dMax* downregulation (1X*ey-Gal4*, 1X*Max-RNAi*, Max^1/+) induces mild MYC/MAX phenotypic classes despite the dMyc physiological level. Overall, our observations strongly suggest that the modulation of dMax level is able to suppress both the MYC and the MYC/MAX phenotypic traits indicating that all these effects depend on a MYC/MAX ratio higher than wild type. Moreover, we could trace a sort of dose dependence of the phenotype due to partial loss of dMax function. A weak *dMax* silencing mainly affects eye cell proliferation and growth, a strong but viable *dMax* silencing impairs cell differentiation and the strongest *dMax* downregulation is lethal. These data suggest that when the loss of dMax function is below a viable threshold that allows cell proliferation and tissue formation, *dMax* silencing is able *per se* to unbalance MYC/MAX ratio leading to a weak MYC/MAX phenotype despite the physiological level of dMyc. We are tempted to speculate that a high MYC to MAX expression ratio could result in a certain amount of "free MYC" that should not be engaged in MYC-MAX dimers and that seems to play a role in the negative modulation of cell differentiation and cell identity. This body of evidence well correlates with what we have shown in a previous work concerning cohorts of patients affected by *MYCN*-non-amplified neuroblastoma. Indeed, at physiological MYCN level, the low expression of MAX clearly correlates with an unfavourable tumour prognosis. Moreover, in *MYCN*-non-amplified neuroblastoma cell lines *MAX* silencing leads to increased cell proliferation and motility, while the forced MAX overexpression has the opposite effects (Ferrucci et al. 2018). These observations might support the idea of possible pro-oncogenic activities exerted by MYCN in absence of MAX that could significantly contribute to the tumour progression.

To deeply understand the cellular basis of the eye-to-wing transformation, we assessed whether the increased MYC/MAX ratio induces the expression of the wing Hox gene *Antennapedia* in the eye progenitors. In fact, the ectopic expression of Antp in eye cells still uncommitted to terminal differentiation is known to inhibit ommatidia differentiation (Plaza et al. 2001) and to transform part of the eye in wing (Kurata et al. 2000). Multiple immunolabeling experiments revealed that dMyc or hMYCN overexpression are sufficient to trigger the ectopic activation

of Antp in few scattered eye disc cells, a slightly decreased number of Elav-positive cells and a bona fide normal number of dividing cells. The limited expression of Antp is consistent with the mild phenotype affecting cell differentiation observed upon dMyc/hMYCN overexpression. Possibly, in these conditions the high dMyc/hMYCN level inefficiently contrasts the action of chromatin regulating complexes including proteins of the Polycomb and Thritorax families which robustly maintain the Hox gene expression profile once cell fate identity has been established during embryogenesis (Schuettengruber et al. 2017). Interestingly, we obtained a very similar result mildly increasing the MYC/MAX ratio by a strong but viable *dMax* downregulation. Indeed, 1X*ey-Gal4,* 1X*Max-RNAi*, Max^{1}/+ eye imaginal discs express ectopic Antp, confirming that the differentiation is affected whenever the MYC/MAX ratio goes beyond a critic threshold that can be obtained also at dMyc physiological level. The further increase of MYC/MAX ratio induces many more eye cells to express Antp and causes a delayed progression of the morphogenetic furrow, likely suggesting that the whole development program of the eye primordium has been delayed. Moreover, we occasionally observed eye imaginal discs with *dMax* downregulation and dMyc overexpression showing a very severe phenotype. The expression pattern of Elav appeared completely disrupted, the morphology of the Elav-positive cells was completely altered and clusters of cells expressing high Antp level were evident, suggesting a strong impairment of photoreceptor differentiation possibly compatible with the eye-to-wing homeotic transformation.

To elucidate the mechanism underlying the ectopic expression of Antp in eye progenitors, we investigated the involvement of a MYC repressive activity. The MYC/MAX phenotypes worsen according to high MYC level and low MAX level, indicating that MYC-MAX dimers are unlikely to be required. While MYC-mediated transcriptional activation is strictly correlated to MYC/MAX dimers formation and binding to E-box sequences, MYC-mediated repression seems to occur also in absence of MAX and through the recruitment of co-repressors like histone deacetylases and other scaffold proteins (Liu et al. 2007). Interestingly, we found that the dMyc overexpression phenotype requires the co-repressor dHDAC1 and the scaffold protein Smrtr. The decreased expression of either dHDAC1 or Smrtr in heterozygous null mutants, or in animals expressing a specific RNAi, genetically interact with dMyc overexpression leading to a partially suppressed MYC phenotype. This suggests that the MYC phenotype, and conceivably also the MYC/MAX phenotype, could depend on dMyc repressive function and could involve the formation of complexes containing dMyc/hMYCN and corepressors like dHDAC1 and Smrtr.

Interestingly, we showed that the downregulation of the Hox gene *Deformed*, normally expressed in the eye imaginal disc, causes the same phenotype as MYC overexpression, including the ectopic activation of Antennapedia in eye disc cells. The contribution of one or more head Hox genes to eye development is still not well defined. Our findings suggest that *Dfd* is expressed and required during eye cells differentiation and could have a role in MYC-mediated inhibition of ommatidia differentiation. The simultaneous dMyc overexpression and *Dfd* silencing did not enhance the MYC-phenotype in adult eyes. Nevertheless, eye imaginal discs expressing high dMyc and low Dfd, showed, albeit occasionally, a strong Antp expression and a severe alteration of Elav-positive cell morphology. These eye discs were very similar to those expressing high dMyc and low dMax, suggesting a weak genetic interaction between dMyc overexpression and *Dfd* silencing.

These observations pointed at Deformed as a possible target of a dMyc-mediated and dMax-independent transcriptional repression. To date, many mechanisms of cross regulation between Hox genes have been already described as essential for the maintenance of the proper Hox pattern along the anterior-posterior axis. According to that, the deregulation of Hox factors in a segment can cause the ectopic activation of Hox proteins normally expressed and required in neighbouring segments leading to cell identity changes (Mallo and Alonso 2013). Therefore, we could envisage that the dMyc-mediated inhibition of Dfd in eye progenitor cells could, in turn, lead to the ectopic activation of Antp in the eye disc, eventually causing the eye-to-wing homeotic transformation. Through chromatin immunoprecipitation we assessed that, in hMYCN overexpressing eye disc cells, hMYCN associates to the promoter of two known positive targets of human and *Drosophila* MYC: *Cdk4* (Hermeking et al. 2000) (Orian et al. 2003) and *pitchoune* (Zaffran et al. 1998) (Benassayag et al. 2005a) (Grandori et al. 1996). This evidence contributes to the reliability of the detected association of hMYCN to the *Dfd* promoter in proximity to a putative binding site for *Drosophila* dSP1/KLF factors. On this basis, we are tempted to infer that dMyc, like hMYCN, could bind the *Deformed* promoter and likely repress the head Hox gene. Besides the high functional conservation between human and *Drosophila* MYC, many of our findings highlight an evident overlap between hMYCN and dMyc overexpression effects. In both cases we observed similar phenotypic traits in adult eyes and in eye imaginal discs, including the ectopic expression of Antp. Moreover, phenotypes depending on dMyc and hMYCN overexpression are both rescued by *dMyc* heterozygous null mutations (Myc^{G0534}). Therefore, at least a partial overlap in dMyc and hMYCN binding profile

should not be surprising and it would explain the molecular basis of the MYC-mediated and MAX-independent inhibition of cell differentiation in *Drosophila* eye progenitor cells.

Notably, our results well correlate with inhibitory activities of hMYCN on cell differentiation already described in neuroblastoma cell lines (Iraci et al. 2011) (Liu et al. 2007). Moreover, a MAX-independent and repressive function of MYC has been demonstrated also in other tumours, such as pheochromocytoma (PCC). PCC is a neural crest tumour characterized by *MAX* loss of function mutations (Comino-Méndez et al. 2011). In the rat PCC cell line PC12 no functional MAX protein can be detected and MYC overexpression in PC12 cells causes block of Ras-mediated differentiation, suggesting that MYC can act on cell differentiation independently from MAX binding (Vaqué et al. 2008).

Concluding, we showed an *in vivo* analysis of MYC effects on cell proliferation and differentiation using the *Drosophila* eye as reliable and efficient cellular readout. We provided a further confirmation of the MAX-dependent role of MYC on cell proliferation and cell growth. On the other hand, we demonstrated that MYC can inhibit eye cell differentiation through deregulation of Hox genes in a MAX-independent manner. Indeed, the high MYC to MAX expression ratio likely allow MYC to repress the Hox gene *Deformed* normally expressed in the eye primordium. The extreme consequence is the ectopic activation of the posterior Hox gene *Antennapedia*. When the ectopic expression of Antennapedia exceeds a critical threshold and probably affects more clustered cells, the result is not only the prevention of eye cell differentiation, but also a change of cell identity from Antp-negative eye cells to Antp positive-cells. This eventually leads to a homeotic transformation from eye to wing and the development of a wing bud protruding from the adult eye.

In our model, the expression of human MYCN recapitulates many effects of high dMyc. This let us envisage that a similar mechanism might occur in high-risk neuroblastoma, characterized by *MYCN* amplification and extremely low differentiation status. In this scenario, the high MYCN level could mis-regulate the physiological and Hox-dependent differentiation program, thus profoundly affecting cell differentiation and supporting a malignant transformation. If confirmed, this novel MYCN-mediated oncogenic mechanism would greatly contribute to elucidate the impact of high MYCN level in neuroblastoma biology. Moreover, especially in the most aggressive neuroblastomas, it will provide a valuable starting point to establish new therapeutic approaches focused on the reactivation of cell differentiation.

MATERIALS AND METHODS

5.1 *Drosophila* strains

Flies were raised on standard corn-yeast medium and maintained at 22°C. Flies carrying genotypes of interest were generated from original lines or suitable intermediate stocks and raised at specific temperatures (24°C or 29°C) on corn-yeast medium (for adult's analyses) or on agar medium (for larvae analyses). The lines used are listed below.
ey-Gal4 (*P{GAL4-ey.H}SS5*, FlyBase ID:FBti0012711) *UAS-dMyc* (*P{5X UAS-Myc.Z}132*, BL # 9674), *Max-RNAi* (*10XUAS-Max-RNAi*, BL # 29328), *Dfd-RNAi* (*10XUAS-Dfd-RNAi*, BL # 50792), *HDAC1-RNAi* (*10XUAS-HDAC1-RNAi*, BL # 33725), *Smr-RNAi* (*10XUAS-Smr-RNAi*, BL # 27068), *GFP-RNAi* (*10XUAS-GFP-RNAi*, BL # 41553), Myc^{G0354} (*P{lacW}*Myc^{G0354}, BL# 11981), Max^{1} (*Max*^{1}, FlyBase ID: FBal0230159 (Steiger et al. 2008)), $HDAC1^{04556}$ (*P{PZ}HDAC1*^{04556}, BL# 11633), Smr^{G0060} (*P{lacW}*Smr^{G0060}, BL# 11653), *Max-rescue* (*P{*$Max^{+t2.788}$*}*, FlyBase ID: FBal0230161 (Steiger et al. 2008)). Strains were obtained from the Bloomington Stock Center (BDSC, https://bdsc.indiana.edu) and they are described at FlyBase (https://flybase.org). *UAS-hMYCN* was generously donated by Daniela Grifoni (unpublished, daniela.grifoni@unibo.it), while Max^{1} and *Max-rescue* were generously donated by Peter Gallant.

5.2 Genetic manipulation

Gene overexpression and downregulation have been carried out using the system Gal4-UAS. This genetic tool has been developed at early 1990s and has provided incredible advances in *Drosophila* genetic manipulation, allowing a targeted gene expression finely regulated in space and time. It is a binary system consisting of two genetic elements of *S. cerevisiae*: the Gal4 trans-activator and its binding sequence UAS (upstream activating sequence). Based on those, a driver and a responder element can be generated. The first refers to the Gal4 factor expressed under the control of a desired promoter allowing a tissue specific expression of Gal4. The latter consists in UAS repeats placed upstream to a target sequence e.g. an RNAi construct or a gene coding sequence. Once Gal4 binds the UAS repeats, the transcription of the UAS downstream sequence is specifically promoted in those cells where Gal4 is expressed and can result in gene silencing or protein overexpression (Brand and Perrimon 1993). The efficiency of the Gal4-UAS system can be modulated by increasing the number of driver and responder constructs

which results in an increased production of the Gal4 trans-activator and of the UAS-controlled sequence (Brand and Perrimon 1993). Moreover, Gal4 activity can be enhanced by raising temperature. According to the minimum impact of growth temperature on fertility and viability, Gal4 has a minimal activity at 16°C ad a maximal activity at 29°C in *Drosophila* (Duffy 2002). Overall, acting on copy numbers and temperature we can widely modulate the targeted gene expression thanks to a very simple, efficient and flexible genetic tool.

5.3 Phenotypic analysis of adult eyes

Eyes of adult animals were analysed using conventional stereomicroscope and classified on the basis of the established phenotypic classes. For each genotype of interest at a specific temperature a minimum of 4 replicates were performed, with 50 up to 100 flies analysed per replica.

The penetrance of the phenotypic classes shown by genotypes of interest was compared with that of the control genotype using the Mann-Whitney Wilcoxon test to evaluate the statistical significance. *p*-values are as follows: $p \leq 0.05$=*, $p \leq 0.01$=**, $p \leq 0.001$=***.

Images of adult eyes were acquired in bright field using a Nikon Eclypse T90i microscope with 10X magnification. To reach a better definition, images were captured through a z-stack acquisition and converted to focused images using the Enhanced Deep Focus (EDF) module of the NIS Elements AR 3.10 software (Nikon).

5.4 Phenotypic analysis of eye imaginal discs

5.4.1 Fluorescence immunolabeling

Wandering 3rd instar larvae (wL3) were selected after 120 hours (when raised at 24°C) or 91 hours (when raised at 29°C) after egg laying as very mobile larvae that had left the medium and did not show everted spiracles. Larvae were cut in half to separate the anterior and posterior part of the larval body. The anterior potion was fold inside out to expose the imaginal discs to the following steps. Larvae were fixed in 4% paraformaldehyde in 1X PBS for 20 minutes, permeabilized in 0.3% Triton X-100 in 1X PBS (hereafter referred as 0.3% PBT) for 1 hour and incubated in a blocking solution (4% Normal Goat Serum in 0.3% PBT) for 20 minutes. The appropriate mix of primary antibodies diluted in blocking solution was added and let stand overnight at 4°C. The following primary antibodies were used: monoclonal rat anti-Elav (1:200; 7E8A10 - DSHB), monoclonal mouse anti-Antp (1:400; 4C3 - DSHB), monoclonal

mouse anti-Notch Intracellular Domain (1:1000, C17.9C6 - DSHB), rabbit anti-Phospho Histone H3 (1:100, Upstate Biotechnology). Larvae were washed in 0.3% PBT, incubated in blocking solution for 20 minutes and finally incubated in the specific mix of fluorescent-dye conjugated secondary antibodies properly diluted in blocking solution. The following secondary antibodies were used: Cy3 anti-mouse (1:400, Jackson Immunoresearch), FITC anti-rat (1:400, Jackson Immunoresearch), Cy5 anti-rabbit (1:400, Jackson Immunoresearch). All the secondary antibodies were subtracted against the other hosts species to avoid cross-reactions. Cell nuclei were labelled through the incubation in HOECHST (Sigma-Aldrich) 2 μg/ml in 1X PBS for 5 minutes. After washes in 0.3% PBT, eye-antenna imaginal complexes were dissected from the larvae and mounted on microscope slides using Fluoromount-G (Electron Microscopy Sciences). Slides were let stand overnight at room temperature (RT) to allow the mounting medium to polymerize then were stored at -20°C.

5.4.2 Imaging

Immunolabelled imaginal discs were analysed at 20X magnification with a Nikon A1R confocal scanning microscope equipped with a Nikon PlanApo and captured using the NIS Elements AR 3.10 software (Nikon). The whole thickness of the imaginal discs was acquired in all the emitted wavelengths and total projections of maximal intensity of the Z-stack in all the acquired channels were produced with the NIS Element AR 3.10 (Nikon) or the ImageJ (NIH) software.

5.5 Quantification of genes transcripts

5.5.1 RNA extraction and purification

A minimum of 30 eye imaginal discs were dissected from wL3 male larvae (See Section 5.4.1 for larval staging) and transferred in 300 μl of TRI Reagent® (Sigma-Aldrich). Each sample was processed as follows: 60 μl of chloroform were added, the mixture was vortexed and let stand for 10 minutes at RT, then it was centrifuged at 12,000 x g for 15 minutes at 4°C. The aqueous phase containing RNA was transferred into a fresh tube and 150 μl of isopropanol were added. The sample was vortexed, let stand for 10 minutes at RT and it was centrifuged at 12,000 x g for 30 minutes at 4°C. After supernatant removal, 1 ml of 75% EtOH was added to the pellet, the sample was vortexed and centrifuged at 12,000 x g for 5 minutes at 4°C. Three washes in 75% EtOH were performed. Finally, the supernatant was removed, the pellet was dried and resuspended in 15 μl of RNase free water.

To avoid genomic contamination, the extracted RNA was treated with the DNA-*free*™ Kit (Ambion-Life Technologies). A DNA digestion mixture was assembled in a total volume of 20 µl adding 1 µl of rDNase I and 10X DNase I buffer to the extracted RNA. The solution was incubated for 30 minutes at 37°C. The 10X DNase inactivation reagent was added, then the sample was mixed, let stand 2 minutes at RT and centrifuged at 10,000 x g for 1.5 minutes. The supernatant containing the DNA-free RNA was transferred into a fresh tube.

5.5.2 cDNA synthesis

Reverse transcription of RNA was performed using iScript™ Reverse Transcription Supermix for RT-qPCR (Bio-Rad). The cDNA synthesis reaction was assembled in a total volume of 20 µl containing RNA template and 5X iScript reverse transcription supermix consisting of iScript MMLV-RT ($RNaseH^+$), RNase inhibitor, dNTPs, oligo (dT), random primers, buffer, $MgCl_2$ and stabilizers. The mix was incubated in a thermal cycler using the following protocol: 5 minutes at 25°C for a priming phase, 30 minutes at 42°C for the reverse transcription and 5 minutes at 85°C for RT inactivation.

5.5.3 Quantitative Real Time PCR

Gene expression was quantified by Real Time quantitative PCR using Sso Advanced™ SYBR® Green supermix (Bio-Rad) and the CFX96 real-time PCR detection system (Bio-Rad) for SYBR® Green assay. The reaction mix was assembled in a total volume of 15 µl containing 15 ng of cDNA template, 250 nM forward primer, 250 nM reverse primer and 2X Sso Advanced™ SYBR® Green supermix. The Sso Advanced™ SYBR® Green supermix is a ready to use reaction cocktail consisting of 2X reaction buffer with hot start Sso7d-fusion polymerase, SYBR® Green dye, dNTPs, $MgCl_2$, enhancers and stabilizers. The amplification was carried out through the following steps: 1 initial step for enzyme activation and initial DNA denaturation (30 seconds at 95°C), 30 cycles of denaturation phase (5 seconds at 95°C) and annealing/extension phase (30 seconds at 60°C) and 1 final step for melt curve analysis in which temperature raises from 68°C to 95°C in steps of 3 seconds each one characterized by a temperature increment of +0.5 °C. Melting curve analysis was performed at the end of the amplification cycles to evaluate the specificity of the PCR products. This method relies on the dissociation between the two DNA strands of the amplicons upon raising temperature and consequent decrease of fluorescent signal emitted by SYBR® Green (non-specific fluorescent dye binding the minor grove of DNA). Each amplification product is characterized by a specific

melting curve (fluorescence emission during increasing temperature) related to its nucleotide sequence. Therefore, melting curve analysis allows the identification of primer-dimers and other non-specific PCR products ensuring a high-quality control of amplicon specificity.

Primers for quantitative Real Time PCR were designed using Primer 3 (http://bioinfo.ut.ee/primer3-0.4.0/primer3/) on sequences retrieved from the UCSC genome Browser (dm6 assembly) (https://genome.ucsc.edu/). The parameters for primer design are as follows: Product Size Range = 90-140 pb; Primer Size Range =18-27 pb (optimum 20 pb); Primer CG% = 40-50 %, Melting temperature = 57-63 °C (optimum 60°C). Primers used for quantitative PCR are listed in table 1.

	Primer sequence	Product size	RefSeq
RpL32	*Forward* 5'- TGCTAAGCTGTCGCACAAATGG -3' *Reverse* 5'- TTCGATCCGTAACCGATGTTGG -3'	105 pb	NM_079843.4
Gapdh1	*Forward* 5'- AATCAAGGCTAAGGTCGAGGAG -3' *Reverse* 5'- AATGGGTGTCGCTGAAGAAGTC -3'	104 pb	NM_080369.3
dMyc	*Forward* 5'- AACGATATGGTGGACGATGGTC -3' *Reverse* 5'- GGGATTTGTGGGTAGCTTCTTG -3'	102 pb	NM_080323.4
dMax	*Forward* 5'- GCGGAAGATCAGTGAAAACCAG -3' *Reverse* 5'- TCCCCATTTGAACTCTCCAGTG -3'	99 pb	NM_140840.4

Table 1 – Primers and reference mRNA sequences used to quantify through Real Time quantitative PCR the level of dMyc, dMax, RpL32 and Gapdh1.

The detection of PCR products relies on the quantification of the fluorescent signal emitted by SYBR® Green during the exponential phase. In this phase the amount of PCR product is supposed to be proportional to the quantity of input template. The expression of genes of interest (GOI) was evaluated using the comparative Ct method (ΔΔCt method – see formulea below). Ct (threshold cycle) indicates the first cycle during the amplification in which the fluorescence of a specific PCR product rises appreciably above the background fluorescence and it is proportional to the template quantity. The amount of GOI transcripts (dMyc and dMax) is normalized on the expression of reference genes (RG) (*RpL32* and *Gapdh1*) which levels should not be affected by the targeted gene expression (dMyc overexpression and *dMax*

downregulation). Variation in GOI transcript in the genotype of interest (*ey-Gal4,UAS-dMyc* or *ey-Gal4,Max-RNAi*) is expressed as relative fold change compared to a control genotype (*ey-Gal4*) set as 1.

ΔCt experimental genotype = $Ct_{GOI} - Ct_{RG}$
ΔCt control genotype = $Ct_{GOI} - Ct_{RG}$
$\Delta\Delta Ct = \Delta Ct$ experimental genotype - ΔCt control genotype
Ratio = $2^{-\Delta\Delta Ct}$

5.6 Dual cross-linking chromatin immunoprecipitation (dual ChIP)

Dual ChIP was carried out using the True MicroChIP Kit (Diagenode) developed to efficiently work on a 10,000 to 100,000 cells range. 2Xey-*Gal4*, 2X*UAS-MYCN* wL3 male larvae raised at 24°C (See Section 5.4.1 for larval staging) were cut in half to separate the anterior and posterior part of the larval body. The anterior portion was fold inside out to expose the imaginal discs to a dual step cross-linking. First, larvae were incubated in Disuccinimidyl glutarate (DSG) 2 mM in 1X PBS for 45 minutes. Then, larvae were washed in 1X PSB and exposed to the second cross-linking agent: 1% paraformaldehyde in 1X PBS for 10 minutes. Glycine was added to stop fixation (115 µl of Glycine per 1 ml of sample). 30 eye imaginal discs were dissected and collected in 1X PBS. The sample was centrifuged at 300 x g for 10 minutes at 4°C and pellet was resuspended in 1 ml of 1X protease inhibitor cocktail (PIC) diluted in Hank's balanced salt solution (HBSS) and centrifuged at 300 x g for 10 minutes at 4°C. After supernatant removal, 150 µl of lysis buffer containing 1X PIC were added, sample was vigorously agitated and let stand for 5 minutes on ice to ensure complete lysis. 450 µl of 1X PIC in HBSS were added. The sample was split in 6 parts each one containing an amount of chromatin that had been previously tested to be efficiently sonicated. The 6 sub-samples were sonicated in parallel using a Bioruptor® apparatus with 3 runs of 10 cycles of [30 seconds ON / 30 seconds OFF]. The optimized sonication conditions allow chromatin shearing and formation of 200-400 bp fragments. The 6 sub-samples were centrifuged at 14,000 x g for 10 minutes at 4°C then supernatants were pooled together to obtain a homogeneous sample which was then diluted 1:2 by adding 1X PIC in ChIP Buffer tC1. Part of this sample was stored at -20°C and used as negative control (INPUT). The remaining sample (IP) was incubated with 0.25 µg mouse anti MYCN antibody (B8.4B - sc-53993, Santa Cruz Biotechnology) for 16

hours at 4°C on a rotating wheel. The magnetic immunoprecipitation was performed by adding 10 µl of pre-washed Protein A-coated magnetic beads to the IP sample and it was incubated for 2 hours at 4°C on a rotating wheel. The sample was placed on a magnetic rack, supernatant was removed, 100 µl of Wash Buffer tW1 were added and the sample was incubated for 4 minutes at 4°C on a rotating wheel. The described wash was repeated using Buffer tW2, tW3, tW4. After last buffer removal, DNA decrosslinking was performed by adding 200 µl of Elution Buffer tE1 and the sample was incubated for 30 minutes at RT. The supernatant was transferred in a fresh tube and 8 µl of Elution Buffer tE2 were added. 180 µl of Elution Buffer tE1 and 8 µl of Elution Buffer tE2 were added to the INPUT sample and both samples were incubated for 4 hours in a thermomixer at 1300 rpm at 65°C.

5.6.1 DNA purification

DNA purification was performed using MinElute PCRPurification Kit (QUIAGEN). 5 volumes of Buffer PBI were added to the IP and INPUT samples. The samples were applied to a QIAquick spin column and centrifuged for 60 seconds. After the flow-through discard, 0.75 ml of Buffer PE were applied to QIAquick column and the samples were centrifuged for 60 seconds. Flow-through was discarded and a new centrifugation was performed for 2 minutes to remove residual Buffer PE. QIAquick column was placed in a clean tube and DNA was eluted by adding 12 µl of water and centrifuging for 1 minute.

5.6.2 Enrichment analysis

The binding of MYCN to different promoter regions has been investigated evaluating the enrichment of these regions in the IP sample compared to the INPUT sample (set at 1) after a normalization to a not bound genomic region (*Gapdh1* exon). 3 putative MYCN binding sites were tested in a range of +/- 2000 nucleotides from transcription start site in the promoter of two known c-MYC/dMyc targets (*Cdk4* BS2, BS3, BS4 and *pit* BS1, BS2; BS3) and in the promoter of the *Deformed* gene (*Dfd* BS1, BS2, BS3).
For this purpose, a quantitative Real Time PCR was performed using Sso Advanced™ SYBR® Green Supermix (Bio-Rad) and the CFX96 real-time PCR detection system (Bio-Rad). The ΔΔCt method was used to evaluate the enrichment of *Cdk4*, *pit* and *Dfd* promoter regions in the IP sample (See Section 5.5.3). Primers for quantitative Real Time PCR were designed using Primer 3 (http://bioinfo.ut.ee/primer3-0.4.0/primer3/) on sequences retrieved from the UCSC genome Browser (dm6 assembly) (https://genome.ucsc.edu/). The parameters for primer design are

as follows: Product Size Range = 80-130 pb; Primer Size Range =18-22 pb (optimum 20 pb); Primer CG% = 40-50 %, Melting temperature = 57-63 °C (optimum 60°C). Primers used for quantitative PCR are listed in Table 2.

	Primer sequence	Product size	Amplified region
Gapdh1	*Forward* 5'- AATCAAGGCTAAGGTCGAGGAG -3' *Reverse* 5'- AATGGGTGTCGCTGAAGAAGTC -3'	104 pb	chr2R:7,792,256-7,792,359
Cdk4 BS2	*Forward* 5'- TTAAATGGCTAATCCGTTGG -3' *Reverse* 5'- TCTGGGTATCATAATCGGCTTT -3'	84 pb	chr2R:16,578,081-16,578,164
Cdk4 BS3	*Forward* 5'- CTAACAGCGGGCGATAACAG -3' *Reverse* 5'- TTTTGTTGTTGGCACAGCTC -3'	85 pb	chr2R:16,579,419-16,579,503
Cdk4 BS4	*Forward* 5'- ACTCGCACTCTCCCTCTCAC -3' *Reverse* 5'- CGTCTGCATGTCACGTATCG -3'	84 pb	chr2R:16,580,721-16,580,804
pit BS1	*Forward* 5'- CGTAGCCAGAGACCATGTGA -3' *Reverse* 5'- GCCTGCCAGTCGTTAGACA -3'	103 pb	chr3R:22,032,435-22,032,537
pit BS2	*Forward* 5'- GGTCACCCACAAAAGACTGG -3' *Reverse* 5'- ACGTAGAGAAGGCCCACATC -3'	126 pb	chr3R:22,033,622-22,033,747
pit BS3	*Forward* 5'- GGTCACACCTTTTGCATTGA -3' *Reverse* 5'- CGTGTTGCTAACCATTCACC -3'	96 pb	chr3R:22,035,665-22,035,760
Dfd BS1	*Forward* 5'- GCCCCTATACCGCTCACATA -3' *Reverse* 5'- TTGCCGAATAATTGGACCTC -3'	116 pb	chr3R:6,790,158-6,790,273
Dfd BS2	*Forward* 5'- TGGTGTGCTCCATATCCACA -3' *Reverse* 5'- ACGCTCGAAAATTGAACTCG -3'	115 pb	chr3R:6,790,987-6,791,101
Dfd BS3	*Forward* 5'- TCAAAATGGGTGTGACCAAA -3' *Reverse* 5'- GCCATGTCTGTTCACCTTTTC -3'	140	chr3R:6,791,522-6,791,661

Table 2 – Primers used to quantify through Real Time quantitative PCR the enrichment of *Cdk4*, *pitchoune* and *Deformed* promoter regions normalized on *Gapdh1* reference gene.

PART II – Analysis of unexplored functions of *ABCC1* possibly contributing to neurodevelopmental deficits

INTRODUCTION

6.1 The genomic region 16p13.11 is a hotspot for pathogenic copy number variants

6.1.1 Copy number variants

Different genetic alterations contribute to genomic variability between individuals such as single nucleotide polymorphisms (SNPs), variable number of tandem repeats (VNTRs), transposable elements or structural variants (e.g. duplications, deletions, inversions, translocations).

An important component of the intermediate-size structural variations is represented by copy number variants (CNVs). CNVs are duplication or deletion events involving 1 Kb -5 Mb genomic segments which may vary in copy number between different genomes (Freeman et al. 2006). CNVs can have a simple structure, such as a tandem duplication, or they can consist of bi- tri- or multi-allelic variants or complex series of gains or losses at different genomic sites (Redon et al. 2006). Genomic rearrangements have been extensively studied as important causative events for several human disorders. However, CNVs are normally present in the genome of healthy population (Iafrate et al. 2004) (Sebat et al. 2004) (Mills et al. 2011). Indeed, the variation of the diploid status caused by CNVs is associated to a continuous spectrum of effects ranging from the absence of any obvious phenotype to developmental lethality (Hurles et al. 2008). Non-pathogenic CNVs represent a significant source of genetic variability thus providing adaptive potential. Although SNPs have long been considered the main origin of interindividual diversity, CNVs have been demonstrated to encompass a higher number of variant bases compared to SNPs (Redon et al. 2006). On the other hand, CNVs can involve very large genomic tracts including coding sequences and regulatory elements. Moreover, CNVs can indirectly affect gene expression by position effects or predispose to genetic rearrangements (Feuk et al. 2006). Unsurprisingly, a phenotype associated with an unbalanced rearrangement has been described for a number of CNVs. In 1936 Calvin Blackman Bridges identified the duplication of the *Bar* gene on *Drosophila* X chromosome which generates a defective eye

development leading to the so-called Bar phenotype. To date, CNVs have been demonstrated to be associated with different classes of human diseases such as rheumatoid arthritis (Wellcome Trust Case Control Consortium et al. 2010), type 1 diabetes (Wellcome Trust Case Control Consortium et al. 2010), obesity (Jacquemont et al. 2011) and neuropsychiatric conditions like schizophrenia (Stefansson et al. 2008) and autism spectrum disorders (ASD) (recently reviewed in Velinov 2019). Pathogenic CNVs may occur via *de novo* genomic rearrangements or they may be inherited variants. They can be characterized by incomplete penetrance and/or variable expressivity which is influenced and modulated by the genomic context. Moreover, CNVs can cause pleiotropic effects leading to a wide spectrum of phenotypic traits sometimes overlapping between different pathological conditions (Tropeano et al. 2013). The high heterogeneity of the CNVs features, especially in complex genetic diseases, and the presence of benign CNVs in the healthy population still represent a challenge for the detection of disease-associated CNVs.

6.1.2 CNVs encompassing the genomic region 16p13.11 can exert pathologic effects

The Database of Genomic Variants (DGV) provides a publicly available report of structural variants, including CNVs, detected in the genome of worldwide healthy populations. According to DVG, Zarrei and colleagues created a CNV map describing CNV distribution and frequency. They showed that at least 4.8% of human genome is composed by CNVs which are not uniformly distributed along genome and within chromosomes. Chromosomes 9,15,16 and 22 are preferentially characterized by duplications while chromosome 19,22 by deletions (Zarrei et al. 2015). The short arm of chromosome 16 is a known copy number variable region enriched in low-copy repeats (LCRs) (Martin et al. 2004). LCRs are repeated DNA sequences sharing a high homology, thus often implicated in non-allelic homologous recombination (NAHR): one of the principal mechanisms underlying chromosomal rearrangements. Within 16p region, a known hotspot for CNV occurrence is the 16p13.11 locus. Although 16p13.11 CNVs can be carried by healthy population, different authors demonstrated the association between 16p13.11 CNVs and neurodevelopmental pathologic conditions showing a partial overlap in genetic aetiology and phenotypic manifestations (Tropeano et al. 2013). Duplications and/or deletions have been found associated to epilepsy (de Kovel et al. 2010), cognitive impairment (Hannes et al. 2009), ASD (Ullmann et al. 2007) and schizophrenia (Ingason et al. 2011).

6.1.3 The 16p13.11 genomic locus

The large genomic region 16p13.11 can be subdivided in three intervals (namely interval I, II and III) each one characterized by flanking LCR. Interval II is a 0.83 Mb region reported as a preferential site for unbalanced rearrangements (Tropeano et al. 2013). It includes nine protein coding genes: *MPV17L*, *C16orf45*, *MARF1/KIAA0430*, *NDE1*, *MIR484*, *MYH11*, *FOPNL*, *ABCC1* e *ABCC6*. Interestingly, *NDE1*, *MYH11*, *ABCC1* and *ABCC6* are ohnologous genes: paralogs derived from a whole genome duplication (WGD) (Tropeano et al. 2013). Early in vertebrate evolution two WGD events occurred and they are thought to have laid the foundations for the evolution of the complexity characterizing vertebrate genome (Dehal and Boore 2005). While the majority of duplicates were lost, about 20-30% of the protein coding genes retained their ohnologs. Over 60% of duplicate genes are not affected by CNVs and correspond to human disease-associated genes (Makino and McLysaght 2010). Therefore, they have been supposed to be dosage-sensitive genes, whose copy number variation might lead to pathological phenotypes.

MYH11 encodes the heavy chain of the β myosin isoform expressed by smooth muscle fibres. Due to its biological function, it is the most plausible candidate gene belonging to the 16p13.11 locus to explain the risk conferred by 16p13.1 duplication for thoracic aneurysm and dissection occurrence (Kuang et al. 2011). *NDE1* encodes the centrosomal nudE protein. During the nervous system development, nudE is involved in neuron mitosis and microtubule organization, regulating the formation of encephalon and cerebral cortex (Bakircioglu et al. 2011). Therefore, *NDE1* can be referred as a promising candidate gene for the neurodevelopmental deficiency related with 16p13.11 CNV. Finally, the core region of interval II includes the two ABC genes *ABCC1* and *ABCC6*, whose possible involvement in nervous system development has not been investigated, yet.

6.1.4 Preliminary analysis detected the duplication of 16p13.11 locus in an ASD sample

Professor Maestrini's team recently performed a genetic association analysis of CNVs in ASD-affected probands recruited from Stella Maris Scientific Institute for Research Hospitalization and Health Care (Pisa, Italy). The sample consists of 127 Italian ASD-affected families: 126 simplex families (1 ASD-affected individual) and 1 multiplex (2 ASD-affected siblings). All probands were diagnosed on the basis of ADI-R (Lord et al. 1994) and ADOS-G (Lord et al. 2000) tests. The accurate clinical evaluation excluded the presence of comorbidities often associated with ASD. The control sample includes 365 healthy unrelated Italian individuals

recruited from 3 different centres for smoking cessation in Emilia Romagna. CNV analysis has been performed on a total of 731 individuals (128 probands, 238 parents and 365 controls) through a SNPs-array technology (Illumina Infinium® PsychArray) enriched in probes targeting rare variants associated with neuropsychiatric conditions such as schizophrenia, ASD, ADHD, Tourette syndrome and bipolar disorder. After the robust quality control of the data obtained from the genotyping array (Guo et al. 2014), more than 1700 CNVs have been identified through bioinformatic analysis. After filtering for rare CNVs (frequency <1% within the analysed sample) 5 different CNV regions were identified as clinically relevant, namely previously associated to neuropsychiatric conditions. Among these, they found the 16p13.11 duplication affecting 1/128 probands and 1/365 controls. Interestingly, this duplication involves all the genes belonging to the interval II, including *ABCC1*.

Even though the function of ABCC1 in neurons is largely unknown, multiple observations have pointed out its expression in nervous system. The Multidrug Resistance associated Protein 1 (MRP1), encoded by *ABCC1* gene, has been detected in different types of neurons such as pyramidal cells and in the Purkinje cell layer of cerebellum in the developing brain (Daood et al. 2008). In adults, it has been observed in cortical areas, hypothalamic nuclei, *substantia nigra*, *Locus caeruleus*, Purkinje and Golgi cells of cerebellum (Bernstein et al. 2014). Besides the neuronal expression, MRP1 also localizes in the luminal (blood-facing) and abluminal (brain-facing) membranes of brain capillary endothelial cells forming the blood-brain barrier, in pericytes and in astrocytes composing the neurovascular unit and in the choroid plexus epithelia and ventricular ependyma involved in the cerebrospinal fluid production (Bernstein et al. 2014) (Nies et al. 2004). These lines of evidence lay the basis for a possible function of *ABCC1* in neurodevelopment and for its involvement in the pathogenic outcome of 16p13.11 duplication.

6.2 The ABC gene superfamily

ABC transporters are extremely conserved membrane proteins present in prokaryotes and eukaryotes. They use the energy released by ATP hydrolysis to move specific substrates in or out cellular and intracellular membranes. In the human genome 49 ABC genes are arranged in seven subfamilies, designated from A to G. ABC proteins transport a number of substrates, including ions, peptides, amino acids, sugars, cholesterol, metabolites and several drugs. Liver, intestine, kidney and blood-brain barrier are some of the main expression territories of mammalian ABC pumps (Vasiliou et al. 2009).

Despite the great heterogeneity in such a large protein family, ABC pumps are characterized by common and highly conserved structural features. They contain two nucleotide-binding domain (NBD) and two transmembrane domain (TMD). The first account for the ATP binding and hydrolysis, while the latter are responsible for substrate recognition and translocation.
To date, mutations in at least 11 ABC genes are known to be involved in a variety of human inherited diseases, including cystic fibrosis (*ABCC7*), the liver disorder Dubin-Johnson syndrome (*ABCC2*), intrahepatic cholestasis (*ABCB11*), the peroxisome biogenesis disorder Zellweger syndrome (*ABCD3*, *ABCD2*), retinitis pigmentosa (*ABCA4*) and the Tangier disease associated with peripheral neuropathy (*ABCA1*) (Vasiliou et al. 2009). Several genes belonging to A, B, C and G subfamilies (*ABCA2*, *ABCB1*, *ABCB11*, *ABCG2* and members of the C subfamily) are able to export drugs out of the cell. Particularly, MDR1 (encoded by *ABCB1* gene) and MRP1 proteins have long been associated with multidrug resistance (MDR) of cancer cells (Gottesman et al. 2002). This phenomenon refers to the ability of a tumour cell to be unaffected (resistant) by a drug or class of drugs. This cell is positively selected and can develop a cross-resistance to pharmaceutical compounds showing a structural or functional similarity. An important mechanism underlying MDR is the increased expression or activity of membrane proteins transporters, like ABC proteins, that actively pump anticancer drugs out of tumour cell (Gottesman et al. 2002). The resistance of cancer cells to different drugs strongly contributes to the failure of many current chemotherapeutic treatments and partially explains the efficacy of antitumoral therapies combining different agents.

6.3 The *ABCC1* gene

6.3.1 *ABCC1* involvement in multidrug resistance

The ATP-binding cassette transporter MRP1 was firstly identified in a multidrug resistant cell line of small-cell lung carcinoma (Cole et al. 1992). Like other members of the ABCC genes subfamily, MRP1 confers resistance to several chemotherapeutics (doxorubicin, epirubicin, etoposide, vincristine and methotrexate) by actively pumping these compounds out of the cell as glutathione conjugates (Gottesman et al. 2002). High expression of *ABCC1* has been reported in leukaemias, oesophageal carcinomas and non-small-cell lung cancers (Nooter et al. 1995). In the childhood cancer neuroblastoma ABCC1 increased level is associated with a poor tumour outcome. *ABCC1* expression positively correlates with that of the neuroblastoma prognostic marker MYCN (Haber et al. 2006) and has been demonstrated that MYCN binds the *ABCC1*

promoter and activates *ABCC1* transcription, eventually leading to an enhanced efflux activity (Porro et al. 2010).

6.3.2 Evidence of *ABCC1* functions beyond multidrug resistance

MRPs proteins encoded by *ABCC* genes have been extensively studied over the past decades in association with MDR of cancer cells. Nevertheless, the function of MRPs in physiological conditions is still elusive. A known MRP1 physiological substrate is leukotriene C4 (LTC_4). LTC4 is produced through the conjugation of glutathione with the arachidonic acid derivate leukotriene A4 (LTA4). LTC4 is the parental compound of cysteinyl leukotrienes and represents an important pro-inflammatory signalling molecule. Robbiani and colleagues demonstrated that, upon antigen exposition, the migration of dendritic cells from epidermis to lymphatic vessels is defective in *ABCC1* $^{-/-}$ mice, suggesting an important role of MRP1 in mediating immune response (Robbiani et al. 2000)

Intriguingly, the prognostic significance of MRP1 high expression in neuroblastoma persists beyond MDR. Indeed, ABCC1 overexpression is associated with a poor tumour outcome even in absence of chemotherapy. Patients who never received chemotherapy, but with high expression of ABCC1, show rapidly progressive disease. Consistently, in neuroblastoma murine model the pharmacological or genetic inhibition of *ABCC1* leads to a delayed tumour progression in absence of any chemotherapeutic treatments (Henderson et al. 2011). This body of evidence suggests that ABCC1 might contribute to tumour outcome through functions other than its role in resistance to cytotoxic drugs. Interestingly, ABCC1 depletion in neuroblastoma cell lines reduces cell motility and colony-forming ability, while ABCC1 overexpression leads to the opposite. The impact of ABCC1 overexpression on cell mobility is abrogated in cells overexpressing a mutated form of ABCC1 unable to bind ATP (Henderson et al. 2011), demonstrating that ABCC1 function on cell motility relies on the ability of MRP1 protein to serve as an active transporter.

Overall, these findings suggest that *ABCC1* might contribute to the regulation of cell motility in immune system and in a tumour context. More generally, they point out the existence of still unknown functions of *ABCC1*which are unrelated to MDR. Among these unexplored roles we cannot exclude the involvement of *ABCC1* in cell motility or other aspects of neurodevelopment.

6.4 *Drosophila* model system

6.4.1 *Drosophila* as model organism to study complex genetic diseases

Despite the evolutionary distance between *Drosophila* and human, the fly genome shows orthologues of several human genes involved in different neuropsychiatric disorders (e.g. ASD, Fragile X syndrome, Angelman syndrome). Sophisticated genetic approaches and efficient tools for cellular and molecular biology make *Drosophila* an outstanding model for neurodevelopmental and behavioural studies in controlled genetic backgrounds and environmental conditions (Gatto and Broadie 2011). Moreover, the low gene redundancy characterizing the *Drosophila* genome provides a valuable advantage to validate *in vivo* the functions of predicted disease-associated genes and to perform gene interaction analyses. These latter are crucial to unravel the cooperation between heterogeneous and incomplete penetrant risk variants associated with complex neurodevelopmental disorders.

6.4.2 *dMRP*: the *Drosophila* ortholog of human *ABCC1*

In the fruit fly genome 56 different ABC genes have been identified over the past years, with at least one representative for each of the known mammalian subfamilies. Among these, dMRP (multidrug-resistance protein 1) has been referred as the ortholog of the human MRP1 protein. dMRP and MRP1 share 48% identity (percentage of identical amino acids) and 65% similarity (percentage that includes similar amino acids derived from conservative substitutions). Similarly to its human counterpart, dMRP has been predicted to consist of three transmembrane domains and two nucleotide binding domains connected by a linker region (Grailles et al. 2003). The good level of sequence conservation is supported by the ability of dMRP to transport the known MRP1 substrate LTC_4 across the membrane of Sf9 cells. This transport is ATP-dependent and it is blocked in presence of the ABC transporter inhibitor vanadate (Tarnay et al. 2004). *dMRP* transcript has been detected in *Drosophila* embryos with a pick during the early embryogenesis (0-2 hours embryos). In situ hybridization experiments revealed a ubiquitous expression of *dMRP* until gastrulation. At later developmental stages, *dMRP* has been shown to be preferentially expressed in larval and adult brain, this would be consistent with a possible role of dMRP in neurodevelopment (Tarnay et al. 2004).

AIM

Copy number variants of the genomic locus 16p13.11 have long been associated with several neurodevelopmental disorders such as ASD, cognitive impairment and schizophrenia (Tropeano et al. 2013) (Hannes et al. 2009) (Ingason et al. 2011). Consistently, in our laboratory the duplication of the 16p13. 11 has been observed in an ASD-affected sample (unpublished data). The pathogenetic core of 16p13.11 region involves nine protein coding genes. Among those, *NDE1* is a promising candidate gene to account for the 16p.13.11 CNV phenotypic effect, due to its involvement in nervous system development (Bakircioglu et al. 2011). The 16p13.11 locus also includes two members of the ABC gene family: *ABCC1* and *ABCC6*. These genes encode the ATP-binding cassette transporters MRP1 and MRP6 which actively export different substrates out of the plasma membrane. MRP proteins have been found overexpressed in multiple human tumours and they are known to promote the efflux of many chemotherapeutic compounds out of cancer cells, contributing to multidrug resistance development. In the childhood tumour neuroblastoma, high-level ABCC1 is associated with unfavourable prognosis. Interestingly, this association persists regardless of the administration of any chemotherapeutic agents. Moreover, ABCC1 overexpression in neuroblastoma cell lines leads to improved cell motility and colony forming ability, suggesting a drug-independent contribution of ABCC1 to poor tumour outcome. To date, the function of MRP1 in physiological conditions has been poorly studied but it seems to promote the mobilization of immune cells after antigen exposure. Although the role of *ABCC1* in nervous system has not been investigated yet, these observations make *ABCC1* an extremely intriguing gene possibly involved in fundamental cellular processes and its duplication might contribute to the phenotypic manifestations associated with 16p13.11 CNV. Indeed, complex diseases like ASD show a very intricated genetic architecture characterized by rare high-risk variants buffered by common low-risk variants. Hence, interactions between ASD-associated genes is often critical to the onset of the pathological condition.

Therefore, our aim is to elucidate the physiological function of *ABCC1* and to assess its role in nervous system development in order to disclose a possible contribution of high-level ABCC1 to the pathogenicity of 16p13.11 duplication. This might also shed some light on *ABCC1* involvement in the modulation of neuroblastoma outcome.

For this purpose, we adopted *Drosophila* as powerful genetic model to study biological processes underlying neurodevelopment.

RESULTS

8.1 *dMRP* downregulation might affect integrin function in *Drosophila* wing

Loss-of-function analysis (LOF) is an extensively used approach to elucidate the physiological role of genes. Over the years, many LOF methods have been developed. They basically rely on the impairment or fully ablation of gene function targeting DNA, RNA or protein followed by phenotypic analysis (Housden et al. 2017).

According to that, we started investigating the physiological function of *ABCC1* downregulating the *Drosophila* ortholog, *dMRP*, through the binary system Gal4-UAS (See Section 5.2). First, we expressed an interfering RNA construct targeting dMRP transcript (*dMRP-RNAi* transgene) under the control of the *engrailed* promoter (*en-Gal4* transgene). Since the earliest development stages, a segmental organization characterizes *Drosophila* body along the anterior-posterior axis and lays the foundation for the patterning of adult structures. The establishment of this segmental organization is governed by a well-defined genetic cascade. During embryogenesis, the sequential expression of specific gene sets eventually leads to the formation of segments, each one composed by an anterior and a posterior compartment. The segment-polarity gene *engrailed* is expressed in all posterior compartments of body segments and it is required to set a posterior cell identity in each organ and tissue (Alberts et al. 2002). Consequently, the *en-Gal4* transgene activates the expression of *dMRP-RNAi* in the posterior part of each body structure. This allowed us to analyse possible phenotypes in an unbiased manner using the anterior compartment of each organ as internal negative control. Interestingly, the most striking phenotype that we observed upon *dMRP* silencing is the formation of a blister in the posterior compartment of the adult wing (**Fig. 18**).

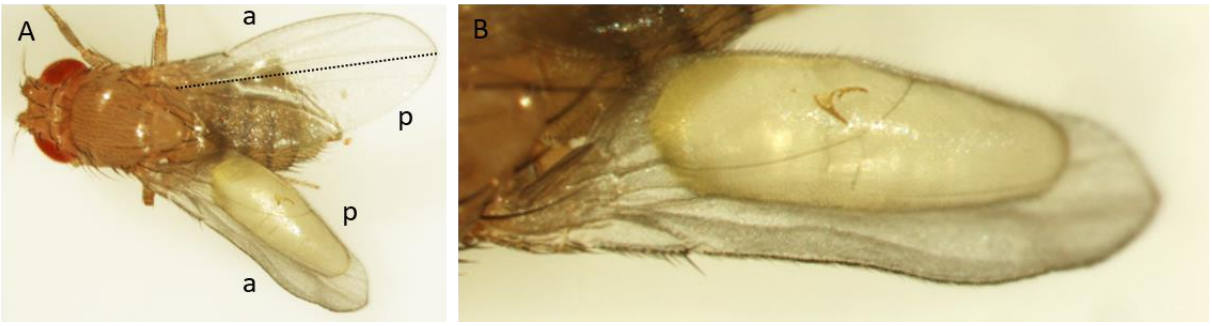

Figure 18 – *dMRP* silencing in the posterior compartment of body segments leads to the formation of a blistered wing. (**A**) Dorsal view of an adult fly expressing *dMRP-RNAi* under the control of *en-Gal4* (**B**) High magnification of the left wing showing a blister in the posterior compartment. Anterior (a) Posterior (p).

This phenotype involves only the posterior compartment of the wing and that is consistent with the activation of the *engrailed* promoter in the posterior part of the larval wing primordium, the wing imaginal disc (Brower 1986) (Nienhaus et al. 2012) (**Fig. 19**), where the Engrailed function is required for establishment and maintenance of the antero-posterior border (Morata and Lawrence 1975) (Tabata et al. 1995).

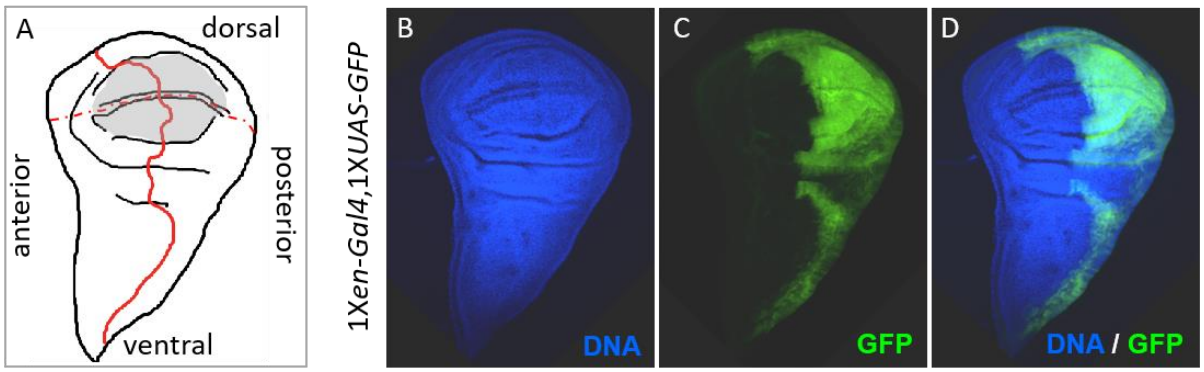

Figure 19 – The *engrailed* promoter is active in the posterior compartment of the wing imaginal disc. (**A**) Drawing of a wing disc at late 3rd larval instar. Antero-posterior border (red line), dorso-ventral border (dashed red line) and winch pouch (grey area) are indicated. (**B-D**) Wing imaginal disc dissected from wandering 3rd instar larva carrying 1X*en-Gal4*, 1X*UAS-GFP*. The expression of the GFP reporter transgene (**C**) is restricted to the posterior compartment of the wing imaginal disc (**D**).

We confirmed the specificity of the observed phenotype by expressing the *dMRP-RNAi* under the control of the *nubbin* promoter targeting the wing proximal part (*nub-Gal4* driver) or under the control of the *tubulin* promoter (*tub-Gal4* driver) which leads to the ubiquitous *dMRP* silencing (Cifuentes and García-Bellido 1997). In both cases *dMRP* downregulation causes the

formation of a wing blister which is located proximally (*nub-Gal4*) or in a random position in the wing blade (*tub-Gal4*) (**Fig. 20**).

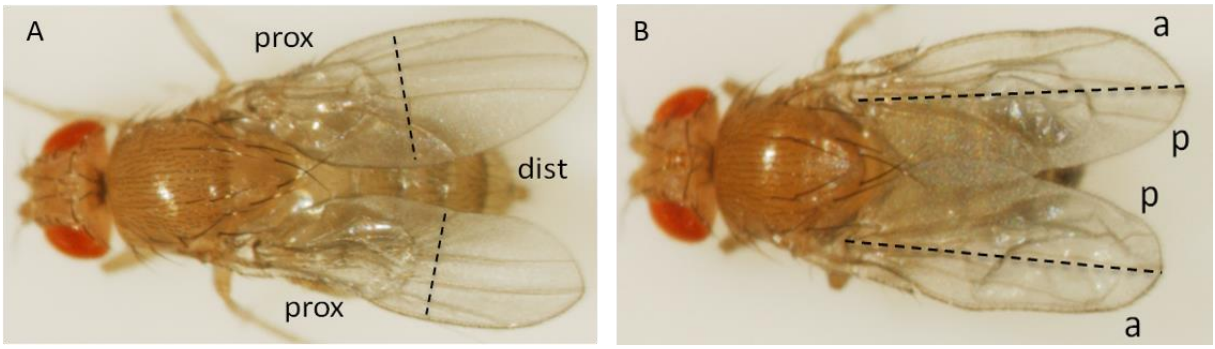

Figure 20 – The location of the wing blisters specifically depends on the targeted *dMRP* silencing. (**A**) Animals carrying 1X*nub-Gal4*, 1X*dMRP-RNAi* show wing blisters located in the proximal part of the blade while (**B**) blisters occupy random positions in the wing of animals carrying 1X*tub-Gal4*, 1X*dMRP-RNAi*. Proximal (prox) Distal (dist) Anterior (a) Posterior (p).

A wing blister is known to be due to the detachment of the dorsal and ventral wing epithelia that compose the wing blade. These pseudostratified columnar epithelia originate during metamorphosis from a specific area of the wing disc, named wing pouch (**Fig. 19 A**). Initially they are coplanar, then they undergo well defined morphogenetic movements and rearrangements hereafter described. As first step, the monolayered epithelium of the larval wing disc telescopes out generating a bilayered wing blade. During blade eversion and elongation, the dorsal and ventral epithelia approach and the juxtaposition of their basal sides occurs. A basal lamina consisting in a specialised form of extracellular matrix (ECM) separates the two basal surfaces. Epithelial cells are anchored to the interposed ECM through a transalar apparatus and this allows the adhesion between the two wing layers. Particularly, an intracellular array of microtubules and microfilaments is projected from the cells' basal surfaces. These cytoplasmic processes extend towards the cavity separating the two wing epithelia and they anchor the ECM through basal junctions. These junctions mostly rely on transmembrane integrin dimers connecting the intracellular cytoskeleton to the basal lamina (**Fig. 21**). This first adhesion is unstable, and it is reverted during pupation when an influx of hemolymph (fluid analogous to the vertebrate blood) forces the dorsal and ventral layers apart. The disruption of epithelia adhesion seems to be required to allow wing cells to accomplish final mitosis. Then, a second round of apposition and adhesion occurs as above described. Finally, after the wing blade expansion (wing blade area increases of 2-3 fold), a slight separation between the apposed

surfaces terminate the wing morphogenesis (Fristrom et al. 1993). Specific cells, named vein cells, do not differentiate any transalar cytoskeleton and are not connected with the facing epithelium. They form wing veins: narrow chitinous channels providing structural support and allowing passage of tracheae and nerves. Five longitudinal veins populate the wing blade. They are designated from L1 to L5 along the antero-posterior axis, with the anterior-posterior border located between L3 and L4 (Tabata et al. 1995) (position of the antero-posterior border indicated in **Fig. 18 A**).

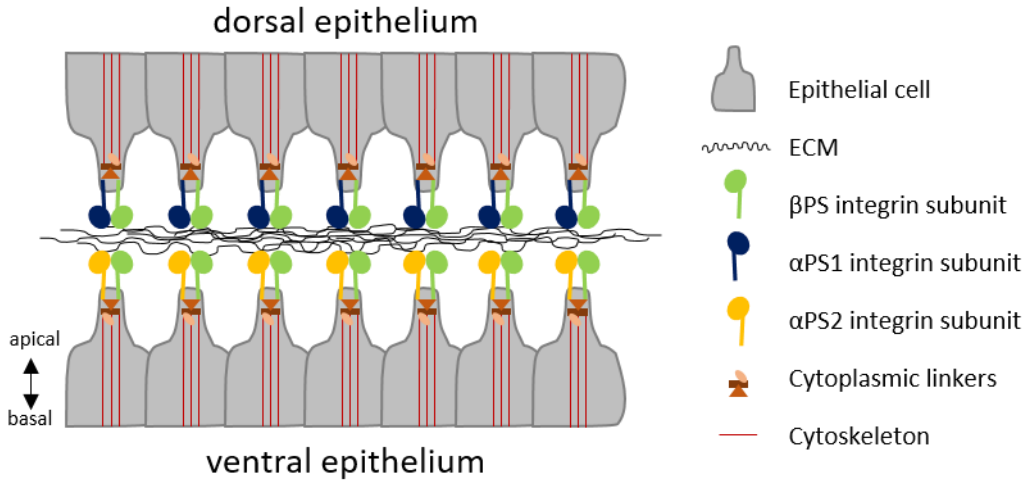

Figure 21 – Schematic representation of a cross section of the mature *Drosophila* wing. The dorsal and ventral epithelia composing the wing blade adhere through integrin-mediated basal junctions mediating the connection between ECM and the intracellular cytoskeleton.

The formation of a wing blister upon *dMRP* silencing suggests a failure of adhesion between the two layers, followed by infiltration of extracellular fluid. This blister eventually collapses leaving a scar in the wing blade. To better analyse this intriguing phenotype, we focused our attention on the effect caused by the expression of *dMRP-RNAi* promoted by *en-Gal4* in the posterior wing compartment. The penetrance of this phenotype is incomplete, moreover we observed blisters of different sizes indicating a variable expressivity. Therefore, we established four phenotypic classes of increasing severity reflecting the most recurrent phenotypic traits. Class 0 includes animals with unaffected wings (**Fig. 22 A**). Class1 animals are characterized by a small blister covering roughly a quarter of the posterior compartment (**Fig. 22 B**). In Class 2 animals the blister involves a half of the posterior compartment (**Fig. 22 C**). Finally, all the posterior compartment is blistered in Class 3 animals (**Fig. 22 D**).

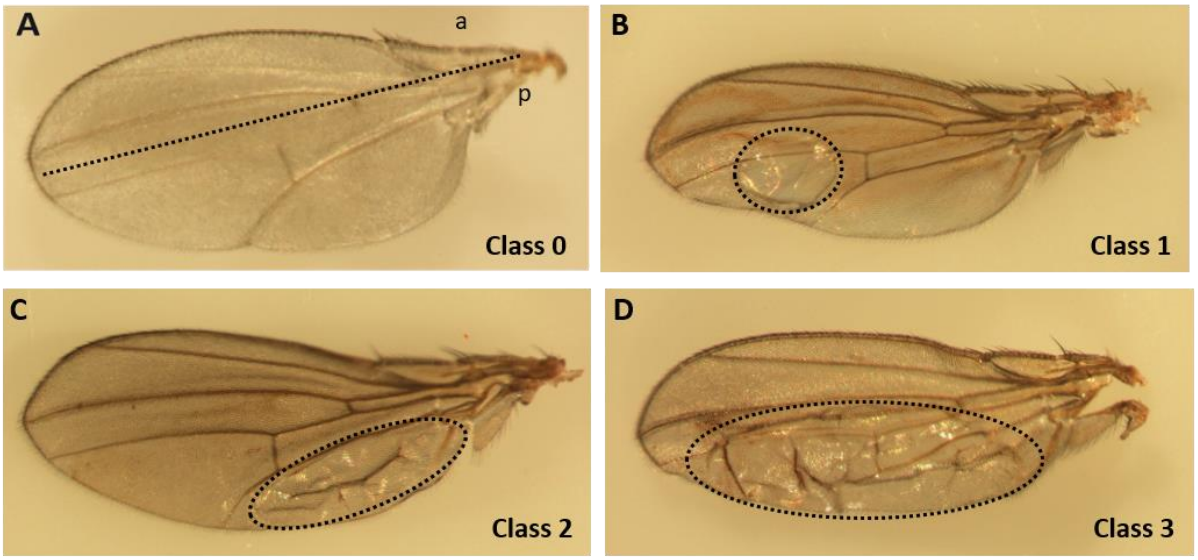

Figure 22 – The phenotype induced by *dMRP* downregulation in the wing is characterized by a variable expressivity. Phenotypic classes representing the most recurrent defects observed in adult wings of animals carrying 1X*en-Gal4*, 1X*dMrp-RNAi*. (**A**) Class 0: wild-type-like wing. In (**B**) Class 1, (**C**) Class 2 and (**D**) Class 3 the blister (dashed circle) involves a quarter, a half or the entire wing posterior compartment, respectively. The dashed line indicates the antero-posterior border. Anterior (a) Posterior (p)

While in control flies expressing a neutral *UAS-GFP* transgene, we do not observe any blistered wing, *dMRP* silencing causes the formation of wing blisters in more than 80% of the analysed progeny at 24°C (**Fig. 23**). Notably, the enhanced efficacy of Gal4-UAS system obtained raising the growth temperature from 24°C to 29°C worsens the *dMRP* downregulation phenotype. Besides the increased phenotype penetrance (nearly 100%), most wings show a Class 3 phenotype, with blisters occupying the entire posterior compartment (**Fig. 23**).

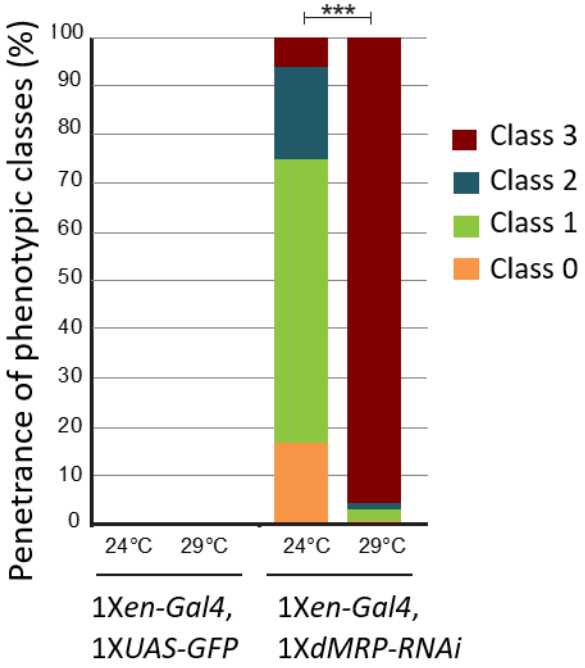

Figure 23 – The severity of the phenotype caused by *dMRP* downregulation increases according to the enhanced *dMRP* silencing. Stacked column chart showing the frequency of the phenotypic classes observed upon *dMRP* downregulation (1X*en-Gal4*, 1X*dMRP-RNAi*) or in control progeny (1X*en-Gal4*, 1X*UAS-GFP*) at 24°C or 29°C. Statistics: Mann-Whitney Wilcoxon test, p<0,001 ***

As previously mentioned, the adhesion between the dorsal and ventral wing epithelia largely rely on integrin receptors. Integrins function as heterodimers composed by an α and a β subunits. In *Drosophila*, the spectrum of integrin subunits consist of 2 β subunits (βPS and βν) and five α subunits (αPS1 – αPS5), where PS refers to the position specific distribution of the first discovered integrin subunit in wing imaginal disc (Wilcox et al. 1981). In the fruit fly wing, βPS is the unique β subunit expressed in both wing epithelia and forms dimers with αPS1, expressed by the dorsal compartment, and αPS2, expressed by the ventral compartment (Brower et al. 1985). These subunits are encoded by the genes *myospheroid* (*mys* - βPS), *multiple edematous wing* (*mew* - αPS1) and *inflated* (*if* - αPS2). All of them map on the sex-linked X chromosome. While animals homozygous for null alleles of one of these genes do not survive, homozygous somatic clones of wing cells are known to causes the failure of the wing layers adhesion and eventually result in a wing blister very similar to that observed upon *dMRP* downregulation (Brower and Jaffe 1989) (Brower et al. 1995) (Brabant and Brower 1993). Interestingly, at least for αPS1 and αPS2, it has been demonstrated that also the overexpression leads to the same effect, highlighting the importance of the integrin balance for proper wing development (Brabant et al. 1996)

To assess whether a low dMRP level could somehow be related to integrin function, we tested the genetic interaction between *dMRP* silencing phenotype and the loss-of-function of different integrin subunits. For this purpose, we generated animals carrying 1X*en-Gal4*, 1X*dMRP-RNAi* and heterozygous null alleles for either *mys* or *if* or *mew* (mys^{1}/+, if^{B2}/+ or mew^{M6}/+, respectively) which do not lead *per se* to any wing blister phenotype (data not shown). Notably, we found that the halved gene dosage of integrin subunits partially suppresses *dMRP* downregulation phenotype (**Fig. 24**). At 24°C we can observe a robust decrease of the phenotypic penetrance, especially in a mys^{1}/+ genetic background. At 29°C the number of animals belonging to severe phenotypic classes is reduced compared to controls and, concerning mys^{1} and if^{B2} mutations, there is also a reduction of the phenotype penetrance.

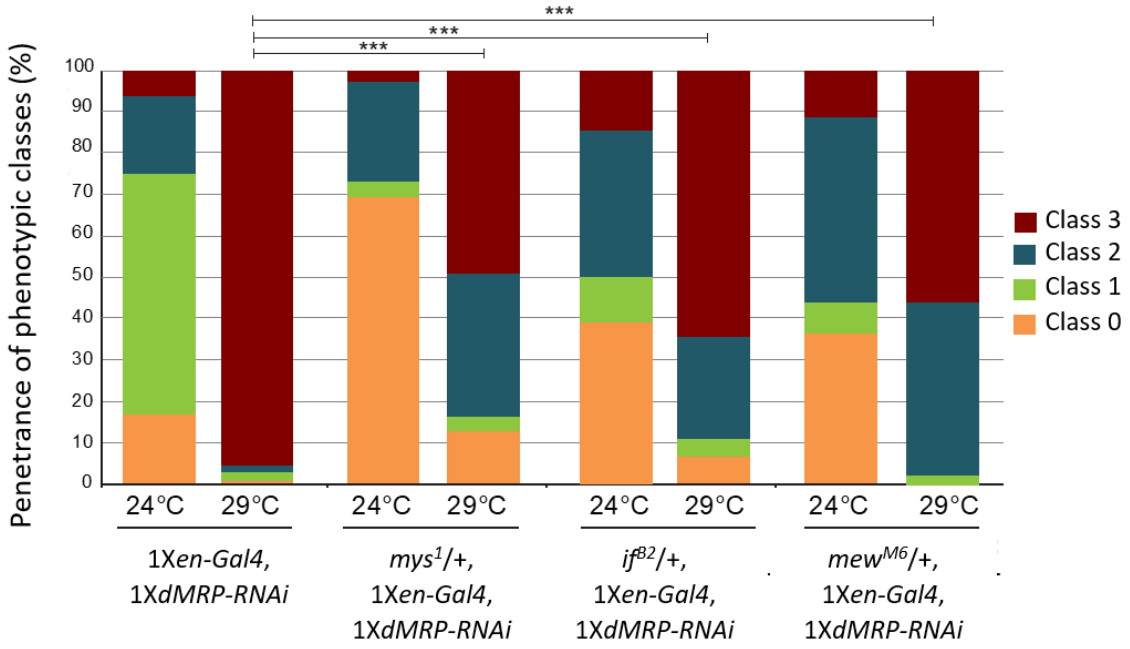

Figure 24 – Heterozygous null mutations in integrin subunits partially suppress the phenotype induced by *dMRP* downregulation. Stacked column chart showing the frequency of the phenotypic classes observed at 24°C or 29°C upon *dMRP* downregulation (1X*en-Gal4*, 1X*dMRP,RNAi*) alone or in presence of heterozygous null mutations in the genes encoding the βPS (mys^{1}/+) αPS1 (mew^{M6}/+) or αPS2 (if^{B2}/+) integrin subunits. Remarkably, integrin loss-of-function partially suppress the *dMRP* downregulation phenotype. Statistics: Mann-Whitney Wilcoxon test, p<0,001 ***.

These results suggest that *dMRP* downregulation might cause a hyperactivation of the integrin function and they prompt us to infer a possible role of dMRP as negative modulator of integrins in *Drosophila* wing formation.

Integrins are known to be involved in the regulation of several processes during development and adult life in physiological (e.g. immune responses and haemostasis) and pathological contexts (e.g. cancer, genetic disorders and autoimmune diseases). Serving as transmembrane receptors, they regulate cell-cell adhesion, cell-matrix adhesion and cell migration. Through adaptor proteins, they connect ECM to the intracellular cytoskeleton mediating the transduction of mechanical stimuli between the inner and the outer of the cell and vice versa. Moreover, their activation can result in the stimulation of many signal transduction pathways, modulating different cellular processes such as cell proliferation, differentiation and apoptosis (Hynes 2002). Particularly, integrins play important functions during nervous system development, whose alterations are known to be associated with neuropsychiatric disorders (Lin et al. 2016). Unexpectedly, our preliminary findings suggest that, at least in *Drosophila* wing, integrin function might be somehow inhibited by the ATP-binding cassette transporter dMRP which has been reported to be expressed in larval and adult brain (Tarnay et al. 2004). Therefore, we could speculate a still unexplored physiological role of dMRP in nervous system development. This would be consistent with a possible contribution of the *ABCC1* duplication to the pathogenicity of 16p13.11 copy number variant.

8.2 Non-physiological dMRP/MRP1 levels result in defective embryonic nervous system development

To assess a potential role of dMRP in nervous system development, we adopted the *Drosophila* embryo as well-characterized and efficient readout. This attractive model provides several advantages for investigating mechanisms underlying neuronal development. Among others, are worthy of mention the relative simplicity, the stereotyped organization and the number of available molecular and genetic tools for the genetic manipulation of either neurons or glial cells and for the labelling of neuronal cell bodies and projections. The embryonic central nervous system (CNS) consists of two brain lobes and a ventral nerve cord (VNC), analogous to the brain and the spinal cord of vertebrates (**Fig. 25**). Both these structures derive from the ventral neuroectoderm specified during the early neurogenesis. Through the activity of proneural genes, neuroblasts are selected within neuroectoderm, they delaminate internally and eventually generate the neuromeres of the VNC. Differently, the procephalic neuroectoderm located in the embryonic head originates the brain hemispheres (Hartenstein and Wodarz 2013). An interesting feature of VNC is its segmental organization along the antero-posterior axis in repeated neuromeres. Each abdominal hemisegment (right and left) is composed by a set of

around 300 neurons, out of which 36 are motor neurons and the remaining are interneurons (Landgraf et al. 2003) (Rickert et al. 2011). Some of the axonal projections extended by these neurons remain ipsilateral connecting different neuromeres along the antero-posterior axis. Others cross the midline within the anterior or posterior commissure present in each neuromere and innervate contralateral targets. As result, thoracic and abdominal CNS axons form a ladder-like structure consisting of two longitudinal nerves, called connectives, and many crossing nerves, called commissural nerves. This structure can be efficiently visualized after immunolabelling with BP102 antibody.

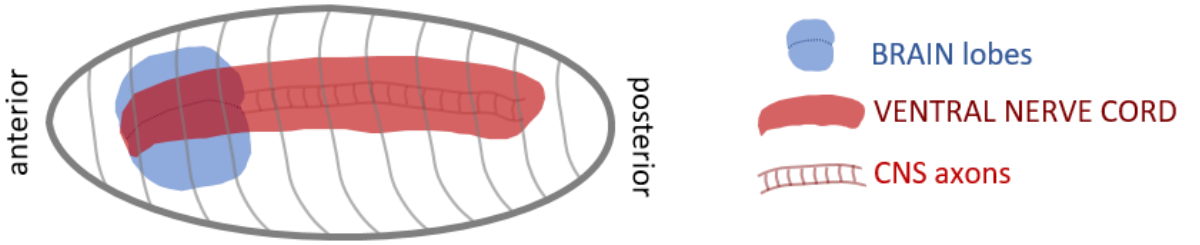

Figure 25 – Schematic representation of the central nervous system of a *Drosophila* embryo (ventral view, stage 16). The segmental organization of the embryo is marked by the grey longitudinal lines delimiting the body segments along the antero-posterior axis.

To evaluate the impact of altered dMRP levels in the development of embryonic CNS, we downregulated the endogenous *dMRP* (*dMRP-RNAi*) or overexpressed the human ABCC1 (*UAS-hABCC1*) under the control of the *elav-Gal4* driver promoting the expression of the above-mentioned constructs in all post-mitotic neurons. The efficiency of the *elav-Gal4* driver is demonstrated by the perfect overlap between the expression of a *UAS-GFP* reporter transgene and the expression of the endogenous Elav protein revealed with an anti-Elav antibody (**Fig. 26**). That indicates that the driver construct is active in all the Elav-positive neurons.

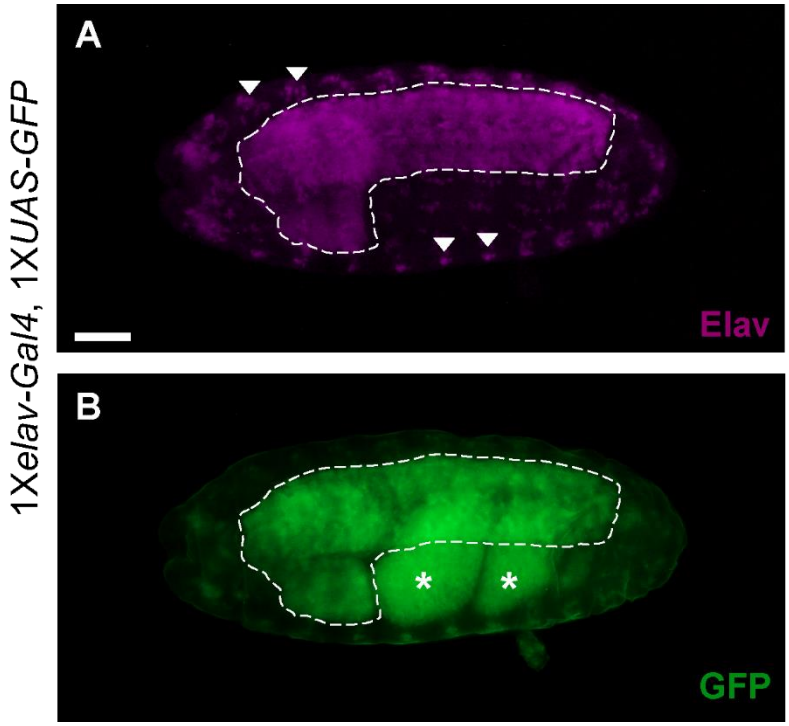

Figure 26 – The *elav* promoter activates the expression of a *UAS-GFP* reporter transgene in all embryonic post-mitotic neurons. Immunolabeling of a 1X*elav-Gal4*, 1X*UAS-GFP* stage 16 embryo (ventro-lateral view). The expression pattern of the pan-neural marker Elav revealed with the anti-Elav antibody (**A**) and the GFP expression promoted by the *elav-Gal4* driver (**B**) completely overlap. Triangles in (**A**) point out representative sensory organs of the peripheral nervous system where Elav is normally expressed. Asterisks in (**B**) indicate autofluorescence of the gut. Dashed line encloses the embryonic CNS. Scale bar: 25 μm

Upon dMRP silencing or hABCC1 overexpression we observed a defective development of embryonic VNC, as revealed by the CNS axons marker BP102 and the neuronal cell body marker Elav. Besides an incomplete penetrance, this phenotype shows a variable expressivity ranging from mild defects in axon bundles to VNC disruption. Therefore, we grouped the most frequent phenotypic traits in three classes. Class 0 includes wild-type-like embryos (**Fig. 27 A-C**). Class 1 consists of embryos showing mild defects in nerve fasciculation such as an extreme thinning or a gap in longitudinal connectives or disorganization of commissural nerve projections (**Fig. 27 E, F, H, I**). Nevertheless, the global structure of VNC is substantially preserved (**Fig. 27 D, G**). In Class 2 we included embryos showing severe alterations in VNC structure consisting in the detachment of the right and the left sides, VNC interruptions and/or neuron mis-localization strongly compromising the VNC integrity (**Fig. 27 J, M**). Not surprisingly, these embryos showed also strong nerve fasciculation defects including extended gaps in connectives, loss of commissural nerves, or completely disorganized projections (**Fig. 27 K, L, N, O**).

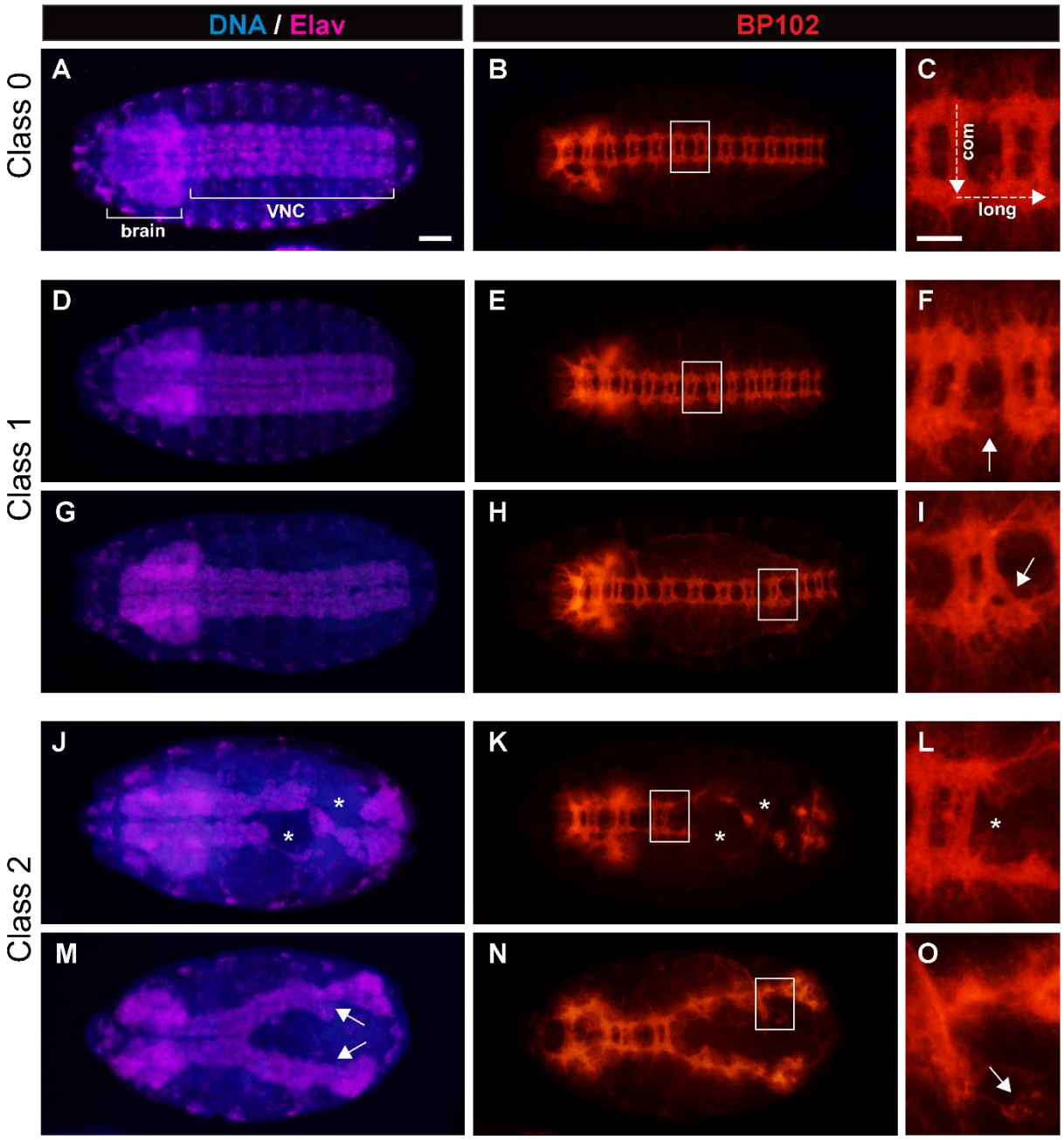

Figure 27 – Altered dMRP/MRP1 level affect embryonic CNS development with a variable expressivity. Ventral view of stage 15-16 embryos immunolabeled with the anti-Elav (**A,D,G,J,M**) and the BP102 antibody (**B**,**C**,**E**,**F**,**H**,**I**,**K**,**L**,**N**,**O**). In **C**,**F**,**I**,**L**,**O** is shown the high magnification of the area indicated by the white square in the corresponding low magnification image. The panel shows the phenotypic classes representing the most frequent defects observed upon the pan-neural *dMRP* silencing or hABCC1 overexpression. (**A-C**) Class 0: wild-type-like embryo. (**D-I**) Class 1: fasciculation deficits consisting in gaps in longitudinal nerves (long) (**E,F** arrow) or disorganized projections of commissural nerve (com) (**H-I** arrow). The VNC does not seem to be affected (**D,G**). (**J-M**) Class 2: disruption of the VNC consisting in VNC gaps (asterisks in **J**) or separation between the right and left sides (**M** arrows). These defects are followed by impaired nerve fasciculation, namely absence of tracts of longitudinal nerves (**K** asterisks) and commissural nerves (**L** asterisk) or disorganized projections (arrow in **O**). Scale bar in A,B,D,E,G,H,J,K,M,N: 25 µm. Scale bar in C,F,I,L,O 10 µm

Interestingly the described phenotypic alterations can be caused by both *dMRP* downregulation and hABCC1 overexpression, even though hABCC1 overexpression seems to have a more severe impact on phenotypic penetrance and expressivity (**Fig. 28**). This observation suggests that the dMRP/MRP1 expression level might play an important role in CNS development and any alteration in post-mitotic neurons could impair their ability to form proper nervous structures. Moreover, the overexpression a hABCC1 allele mutated in the ATP-binding site (*UAS-hABCC1mut*) causes a weaker phenotype than hABCC1 overexpression (**Fig. 28**). This observation might indicate that the possible function of ABCC1 on CNV development could not be totally dependent on its activity as efflux pump.

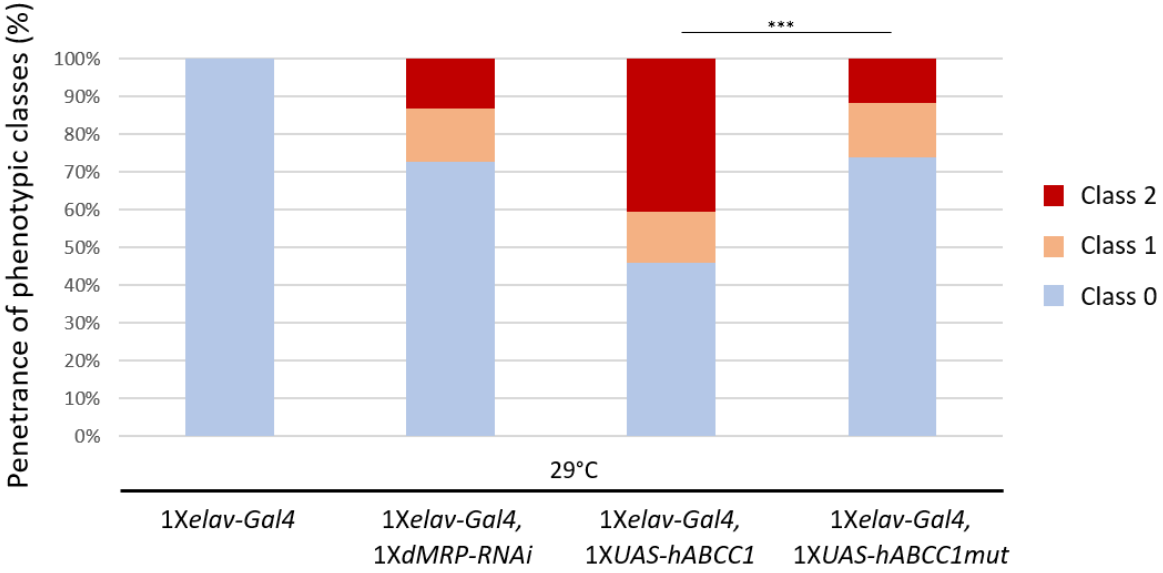

Figure 28 – *dMRP* downregulation and hABCC1 overexpression affect CNS development. Stacked column chart showing the frequency of the phenotypic classes observed in embryos grown at 29°C and carrying the indicated transgenes. *dMRP* downregulation (1X*elav-Gal4*, 1X*dMRP-RNAi*) cause CNS defects in around 30% of the analysed progeny while the phenotypic penetrance exceeds 50% upon hABCC1 overexpression (1X*elav-Gal4*, 1X*UAS-hABCC1*). Notably, the phenotype caused by a mutated hABCC1 overexpression (1X*elav-Gal4*, 1X*UAS-hABCC1mut*) leads to a less penetrant phenotype than wild type hABCC1. Statistics: Mann-Whitney Wilcoxon test, p<0,001 ***.

Notably, the immune labelling with an antibody against the glial marker Repo revealed a disorganized glia distribution in VNC regions disrupted by *dMRP* silencing or hABCC1 overexpression in post-mitotic neurons (**Fig. 29**). Nevertheless, we did not observe any evident phenotype upon *dMRP* silencing or hABCC1 overexpression in glial cells using the driver *repo-*

Gal4 (data not shown). This indicates that the dMRP/MRP1 level does not seem to have any role in glial cell biology.

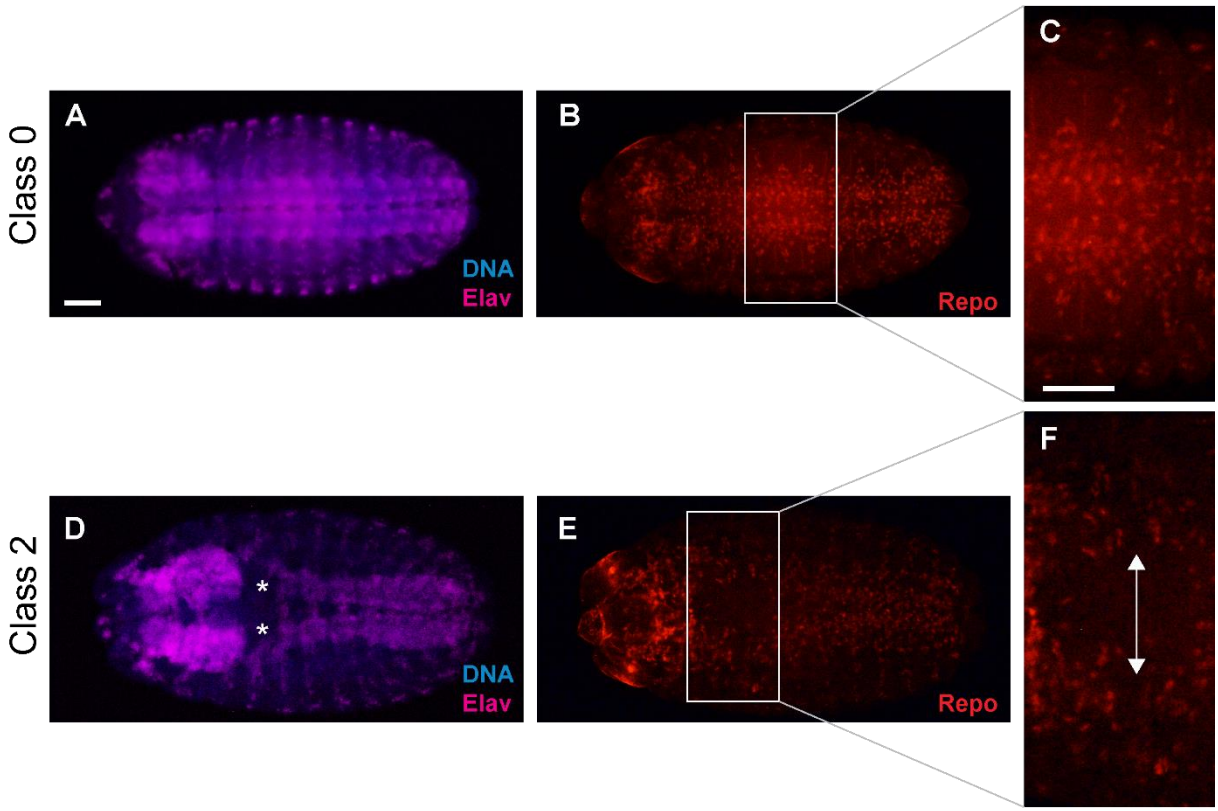

Figure 29 – CNS defects caused by altered dMRP/MRP1 levels affect glial cells. Ventral view of stage 16 embryos immunolabeled with the neuronal marker Elav (**A,D**) and the glial marker Repo (**B,C,E,F**). In (**C,F**) is shown the high magnification of the area indicated by the white rectangle in the corresponding low magnification image. In Class 0 embryos glial cells are correctly present and located in the VNC (**B-C**). In Class 2 embryos, showing defective CNS development (asterisks in **D**), glial cells are mis-located and faithfully follow the neuronal impairment (**E,F**). Scale bar: 25 μm

Altogether, our preliminary observations suggest for the first time a role of the ATP-binding cassette transporter dMRP in the embryonic nervous system development. Therefore, they reinforce the idea of a possible contribution of *ABCC1* amplification in the pathogenic effect of the duplicated genomic region 16p13.11.

DISCUSSION

Human pathologies like schizophrenia, ASD, ADHD and bipolar disorder are neuropsychiatric conditions characterized by altered nervous function. However, the neurobiological mechanisms underlying their onset are still poorly defined. Many studies have demonstrated a relevant genetic contribution to such diseases but their complex genetic landscape still represents a difficult challenge for the identification of susceptibility genes (Bray and O'Donovan 2019). Further identification of causative genetic variants may contribute to fully understand the neuropathological bases providing important indications for diagnosis and treatments. For this reason, human molecular geneticists have been long trying to unravel the genetic architecture of psychiatric disorders to identify risk genes accounting for the pathology onset using different strategies. Classical approaches such as linkage studies (based on the co-segregation of the disease with other markers) are best suited when one or a restricted number of loci are strongly associated with the disease. However, they are not appropriate for the polygenic nature of psychiatric disorders, where the contribution of single variants to the pathology onset is often very low and many variants cooperate to confer disease susceptibility. The development of technologies for high throughput genotyping of large samples has represented a significant advance in the study of risk genes associated with complex genetic disorders. These technologies allowed genome wide association studies (GWAS) to detect common risk factors by analysing an extraordinarily high number of SNPs broadly distributed in the genome (Bray and O'Donovan 2019). Moreover, genotyping arrays highlighted the relevant contribution of CNVs in shaping the genetic landscape of neuropsychiatric disorders. CNVs are unbalanced rearrangements consisting in duplications and deletions of genomic segments lager than 1 kb. Despite their presence in healthy individuals, where they provide an important source of genetic variability, some are known to be associated with human pathologies ranging from diabetes to neuropsychiatric conditions (Freeman et al. 2006). For instance, multiple studies have shown that *de novo* CNVs are carried by 5-15% of ASD-affected individuals compared to 1-2% in the general population (Bourgeron 2015).

ASD is a neurodevelopmental disease with a prevalence in the worldwide population of around 1% (Yuen et al. 2017). It is referred as an early onset disease since symptoms often arise within the first years of life. Clinical manifestations include a wide spectrum of deficits involving social interaction and communications, delayed speech development, stereotyped and repetitive behaviours and restricted range of interests. The ASD diagnosis is further complicated by the

continuous distribution of autistic traits in the general population and by the presence of comorbidities with intellectual disability, ADHD and epilepsy (Bourgeron 2015). Although ASD clinical features clearly rely on a defective nervous function, little is known about the brain regions that are affected and the neurobiological mechanisms underlying nervous dysfunction. Several studies have pointed out an altered neural connectivity compared to normal developing brain, suggesting an increase of short-range connections and a decrease of long-range connection (Courchesne and Pierce 2005) (Just et al. 2007). Recently, a fine mixture of hypo- and hyper-connectivity in autistic patients is emphasized depicting a more complex scenario (Kana et al. 2014). Epidemiological studies have long revealed a strong genetic contribution to ASD, nevertheless most ASD cases are still of unknown aetiology. Indeed, genetic variants contributing to ASD risk differ in type and frequency and this results in a very intricate genetics. Only 10-25% of ASD cases can be explained by single fully penetrant variants like chromosomal rearrangement, CNVs or single nucleotide variants. On the other hand, more than 1000 common low risk SNPs have been associated with ASD. Therefore, ASD genetic architecture appears to be modelled by the interplay between rare pathogenic variants buffered by a number of common low-risk variants (Bourgeron 2015). Understanding the biological meaning of susceptibility genes and assessing the functional interactions between ASD-associated variants are key challenges facing the scientific research in this field.

The 16p13.11 locus is among the genomic regions affected by duplications/deletions in ASD-individuals. The presence of low copy repeats all along the short arm of chromosome 16 predisposes this locus to recombination events underlying copy number variations (Martin et al. 2004). Ullmann and colleagues initially identified CNVs at 16p13.11, namely a 1.5 Mb duplication and reciprocal deletion, in four ASD-affected individuals and in unaffected or variable affected relatives, suggesting the involvement of this incompletely penetrant CNV in ASD susceptibility (Ullmann et al. 2007). Further studies confirmed the contribution of 16p13.11 CNVs to ASD susceptibility (Ramalingam et al. 2011) (Tropeano et al. 2013). Consistently, a CNV analysis recently performed by the Professor Maestrini's team in ASD-affected patients identified the 16p13.11 duplication in 1/128 probands and only in 1/365 controls. The pathogenic core of 16p13.11 region consists of nine protein coding genes of which *NDE1*, *MYH11*, *ABCC1* and *ABCC6* are ohnologs (Tropeano et al. 2013). Ohnologs are gene copies derived from genome wide duplications and referred to be dosage sensitive and often associated with human diseases (Makino and McLysaght 2010). Despite the so far unknown function of *ABCC1* in neurodevelopment, this gene shows several intriguing features which

prompted us to undertake the analysis of its possible contribution to the 16p13.11 duplication pathogenicity.

ABCC1 belongs to the ABC gene superfamily which includes genes encoding highly conserved ATP-binding cassette transporters: active pumps that move specific substrates across membranes using the energy released by ATP hydrolysis. The 49 human ABC genes are highly heterogeneous concerning transport direction, localization in plasma or vesicle membrane, substrate specificity and biological role. The dysfunction of some ABC genes has been already associated with different human pathologies. As an example, mutations involving the chloride ion channel encoded by the *ABCC7* gene (also referred as *CFTR*) are the cause of onset of cystic fibrosis (Vasiliou et al. 2009). Other members of the subfamily C are known to promote the efflux of a spectrum of anticancer agents out the plasma membrane, thus contributing to multidrug resistance of tumour cells and often leading to the failure of chemotherapeutic treatments (Gottesman et al. 2002). The multidrug resistance associated protein 1 (MRP1) encoded by *ABCC1* is overexpressed in different human tumours including the infancy cancer neuroblastoma, where high ABCC1 is associated with a poor outcome (Haber et al. 2006). Strikingly, the prognostic value of ABCC1 overexpression persists in untreated patients and neuroblastoma murine model. ABCC1 overexpression in neuroblastoma cell lines leads to increased cell motility and colony forming ability. These lines of evidence suggest that ABCC1 might contribute to tumour outcome through other functions besides its role in cytotoxic drug resistance and possibly acting on cell migration (Henderson et al. 2011). To date, the physiological function of MRP1 has been poorly investigated. However, multiple observations pointed out an important role played by MRP1 in immune cell migration. The pharmacological inhibition of MRP1 activity through the MK571 antagonist causes a decreased migration of dendritic cells and T cells from skin explants and blocks T cell chemotaxis in response to chemokine attractive signals (Leier et al. 1994) (Robbiani et al. 2000) (Honig et al. 2003). In developing and adult human brain MRP1 has been reported to be expressed in multiple cell populations including different types of neurons (Daood et al. 2008) (Bernstein et al. 2014) (Nies et al. 2004). This let us speculate a possible and still unknown function of *ABCC1* in the regulation of cell migration or other processes during neurodevelopment. Therefore, we chose *Drosophila* as powerful genetic and cellular model system to start investigating *ABCC1* function in physiological conditions with special regard to the nervous system.

Since precise null mutants of *dMRP*, the *Drosophila* orthologue of human *ABCC1*/MRP1, are not currently available, we adopted the binary system Gal4-UAS to express an RNAi construct

targeting *dMRP*. To activate the RNAi expression, we used the driver *en-Gal4*. expressed since embryogenesis in all posterior compartments of body segments, including the wing larval primordium (Alberts et al. 2002). This approach allowed us to disclose possible phenotypes in an unbiased manner using the anterior compartment as internal control. Strikingly, we observed the formation of a blister in the posterior compartment of the adult wing. This phenotype is specifically caused by *dMRP* silencing. Indeed, increasing the efficiency of the Gal4-UAS system by raising the growth temperature from 24°C to 29°C we observed a higher phenotypic penetrance. Moreover, in these conditions a higher number of animals showed the most severe phenotypic traits consisting in a blister occupying the entire posterior compartment. We further assessed the specificity of the *dMRP* downregulation phenotype by using different drivers to promote *dMRP-RNAi* expression: *nub-Gal4* (expressed in the proximal part of developing lateral appendages) and *tub-Gal4* (ubiquitously expressed) (Cifuentes and García-Bellido 1997). Consistently with the driver expression pattern, we observed the formation of wing blisters located in the proximal part of the wing in *nub-Gal4, dMRP-RNAi* animals and randomly distributed in the wing blade in *tub-Gal4, dMRP-RNAi* animals.

A blistered wing indicates a defective process of cell adhesion during wing development. At the end of the larval stage two well defined rounds of complex morphogenetic rearrangements transform the monolayered structure of the wing imaginal disc in a bilayered wing blade composed of a dorsal and a ventral epithelium. These epithelia overlap and adhere thanks to the establishment of basal junctions in which integrins anchor each wing layer to the interposed ECM (Fristrom et al. 1993). In *Drosophila* as in humans, integrin receptors are heterodimers of α and β subunits. The integrin subunits expressed in the fruit fly wing are encoded by the genes *myospheroid* (*mys* – βPS subunit expressed in both epithelia), *multiple edematous wing* (*mew* - αPS1 subunit expressed in the dorsal epithelium) and *inflated* (*if* - αPS2 subunit expressed in the ventral epithelium) (Brower et al. 1985). Clonal analysis of homozygous null mutations in one of these genes have long been reported to cause the detachment of the wing epithelia leading to a blistered wing (Brower and Jaffe 1989) (Brower et al. 1995) (Brabant and Brower 1993). Since *dMRP* silencing led to a phenocopy of integrin null mutant somatic clones we tested the genetic interaction between *dMRP* downregulation and integrin loss-of-function. Interestingly, we found that halving the gene dosage of either *mys* or *if* or *mew* (in mys^{1}, if^{B2}, mew^{M6} heterozygous null mutants) partially suppressed the wing blister phenotype caused by *dMRP* silencing. This suggests that *dMRP* silencing might lead to an over-activation of integrin function that is in part restored by integrin loss-of-function. As consequence, we can infer that

dMRP might act as an inhibitor of the integrin function. This evidence implies that the wing blister caused by *dMRP* silencing should be due to an overactivation of integrins. Notably, at least for αPS1 and αPS2, it has been demonstrated that both loss- and gain-of-function result in the same wing blister phenotype, emphasizing the importance of the integrin balance for a proper wing development (Brabant et al. 1996). *mys* mutant allele seems to show the strongest genetic interaction with *dMRP* downregulation. This could be explained by βPS being the only β subunit expressed in both wing epithelia and forming heterodimers with αPS1, in the dorsal layer, and with αPS2, in the ventral layer. According to that, the *mys* mutation possibly results in impaired activity of integrin receptors on both wing surfaces. Overall, our findings for the first time suggest a role of dMRP in wing morphogenesis and point out a possible physiological role of dMRP as negative modulator of integrin functions.

As mentioned before, *engrailed* is expressed in all posterior segments of animal body. Nevertheless, the appearance of a blistered wing represents the most clear and robust phenotype showed by adult flies. This could be due to the tremendously fine regulation of the wing development in which an unbalanced dosage of integrins could be sufficient to cause an evident phenotype. However, we cannot exclude a role of dMRP, conceivably related to integrin function, in other body parts, as suggested by the lethality caused by the ubiquitous *dMRP* silencing in animals raised at 29°C (data not shown). Indeed, integrins play many crucial roles in the cell. They underlie cell-cell and cell-matrix adhesion transducing the mechanical stimuli from the cell to the ECM and vice versa. They also activate signalling pathways (e.g. PI3K/AKT and ERK/CyclinD1) regulating cell proliferation, differentiation and apoptosis (Hynes 2002).

With regard to the nervous system, integrins regulate neural stem cell differentiation and the balance between neuronal and glial populations. They modulate neuron migration, neurite outgrowth, synaptogenesis and synaptic plasticity thanks to the interaction with ECM. They are also involved in axon myelinization, synaptic vesicle trafficking and remodelling of dendritic spines (Park and Goda 2016). It is worth noting that several ASD-associated mutations seem to converge on genes involved in neurite development, synapse and spine formation, stabilization and plasticity. Disruption of neurite outgrowth, defective synaptogenesis and alteration of dendritic branching have been indeed reported in ASD individuals (Lin et al. 2016). Remarkably, genetic variants of ITGB3 encoding the β3 integrin subunit have been found associated with autism spectrum disorder (Weiss et al. 2006) (Napolioni et al. 2011). Altogether, these observations lay the basis for a possible role of dMRP/MRP1 in neurodevelopment regulation.

Therefore, we started investigating this issue in the developing central nervous system of *Drosophila* embryos. The simple and stereotyped structure of the fruit fly embryonic CNS provides a suitable model to assess defects in neurons composing the ventral nerve cord (analogous to vertebrate spinal cord). We focused our analysis on alterations affecting neuron cell bodies and longitudinal and crossing nerves formed by their axon projection which we efficiently visualized using the anti-Elav and the BP102 antibodies, respectively. Strikingly, the downregulation of *dMRP* promoted by the *elav-Gal4* driver in all post mitotic neurons clearly affected the VNC development. In some cases, we observed mild phenotypic traits attributable to defective nerve fasciculation (i.e. extreme thinning or gaps in tracts of longitudinal nerves or disorganization of crossing nerve projections). In other cases, we observed more severe defects like the detachment between right and left side of the VNC or gaps of the VNC with consequent disorganized fasciculation of the nerves emerging from the affected regions. Further experiments are needed to better characterize the above-described phenotypes and to understand the underlying cellular mechanisms. However, this preliminary result for the first time suggests that dMRP might be required for proper nervous system development in *Drosophila*. Moreover, we are tempted to hypothesize that the dMRP expression level could be particularly important in this process, since both the silencing of the endogenous gene and the overexpression of the human ortholog result in the same phenotypic outcome. A possible explanation could rely on dMRP-mediated inhibition of the integrin function that we envisaged in *Drosophila* adult wing, and in the observation that both loss- and gain-of-function of αPS1 and αPS2 integrin subunits lead to an adult blistered wing (Brabant et al. 1996). If a similar mechanism would involve integrins also during CNS development, we could speculate that the repression (hABCC1 overexpression) or the hyperactivation (*dMRP* downregulation) of the integrin function might lead to the same phenotype. Consistently, defective CNS axons fairly similar to those described can be observed in null mutants for αPS1 and αPS2 integrin subunits expressed in the embryonic nervous system. Indeed, such mutations cause fasciculation defects including gaps in longitudinal nerves (Hoang and Chiba 1998). Upon overexpression of the human ABCC1 we obtained a stronger phenotypic effect compared to *dMRP* silencing. The more severe impact of hABCC1 could be due to a non-complete overlap between the sequences of the fruit fly and the human proteins. Otherwise, assuming a role of hABCC1 as integrin inhibitor likewise dMRP, it could also be related to a stronger effect of integrin inhibition rather than integrin overactivation. However, we cannot exclude a higher efficacy of the *UAS-hABCC1* construct compared to the *dMRP-RNAi* one. Future studies are needed to better define

the genetic interactions between hABCC1/dMRP and integrins and to assess the involvement of the integrins in dMRP-mediated phenotype in the developing CNS. Notably, the possible phenotypic effect of both *dMRP* silencing and overexpression in developing nervous system would be consistent with what reported about 16p13.11 CNVs in human neuropsychiatric disorders. Indeed, both 16p13.11 microdeletion and microduplication are known to be associated with a spectrum of psychiatric conditions including ASD (Ramalingam et al. 2011) (Tropeano et al. 2013).

It will be important to assess whether the overexpression of the endogenous dMRP can lead to the same phenotype than hABCC1, thereby confirming the functional conservation between the human and the *Drosophila* orthologs. Nevertheless, the good level of characterization of the human ABCC1 allowed us to generate and overexpress a mutated form of hABCC1 unable to bind ATP and undergo the conformational changes required to function as membrane transporter. The comparison between the phenotype caused by wild type hABCC1 or mutated hABCC1 expression provided important indications concerning the involvement of the efflux activity in hABCC1-mediated phenotype. In particular, we found that the overexpression of the mutated hABCC1 still affects CNS development, even though with a significantly weaker effect. This preliminary evidence suggests that the possible role of dMRP/MRP1 in regulating neurodevelopment might rely only in part on the efflux activity.

As previously mentioned, little is known about the physiological role of dMRP and it is not clear whether its function as efflux pump is strictly required. MRP1-deficient mice (*ABCC1*$^{-/-}$) show a strongly impaired migration of dendritic cells from epidermis to lymph nodes which can be rescued, albeit partially, by exogenous administration of LTC_4, a known physiological substrate of MRP1. This seems to suggest that the role of MRP1 on immune cell migration is, at least in part, dependent on the efflux activity promoted by MRP1 (Robbiani et al. 2000). Consistently, the increased motility of neuroblastoma cells upon ABCC1 overexpression is abrogated when the overexpressed ABCC1 is mutated at its ATP-binding site (Henderson et al. 2011). Nevertheless, the defective differentiation of dendritic cells caused by MRP1 pharmacological inhibition cannot be restored by LTC_4 administration, suggesting a role of MRP1 on immune cell differentiation independent from the leukotriene pathway and possibly efflux-independent (van de Ven et al. 2006).

Finally, we investigated the effect of *dMRP* downregulation and hABCC1 overexpression in glial cells using the driver *repo-Gal4.* Although dMRP/MRP1 altered levels in neurons led to the mis-localization of glial cells, the expression of *dMRP-RNAi* or *UAS-hABCC1* in glial cells

did not cause any obvious phenotype. According to this observation, the envisaged role of dMRP in nervous system development could be neuron specific.

Concluding, our results, albeit preliminary, suggest a novel physiological function of the ATP-binding cassette transporter dMRP/MRP1 beyond its well-established involvement in cytotoxic drug efflux. Based on the analysis of *dMRP* silencing phenotype and its genetic interaction with integrin mutants, we envisaged dMRP acting as an inhibitor of integrin function at least in the *Drosophila* adult wing. Integrins are well known key molecules for cell adhesion and migration. Hence, our findings might contribute to define the molecular bases of the enhanced cell motility shown by neuroblastoma cells upon ABCC1 overexpression. This could shed some light on the prognostic significance of high ABCC1 level in the poor outcome of neuroblastoma. Indeed, even in absence of chemotherapeutic treatments, ABCC1 might retain a substantial role in modulating metastasis formation and spreading. Moreover, during neurodevelopment integrins participate to the regulation of axon pathfinding and synapses establishment which are often disrupted in neurodevelopment disorder like autism. Notably, we found that both *dMRP* downregulation and hABCC1 overexpression in post mitotic neurons, but not in glial cells, are sufficient to affect embryonic nervous system development. Duplications and deletions of the genomic locus 16p13.11 are known to be associated with autism. This region encompasses few genes including *ABCC1* and little is known about which one could account for the phenotypic effect of 16p13.11 CNV. Our findings first suggest a possible function of *ABCC1* in the nervous system. Therefore, they lay the basis for a possible contribution of *ABCC1* to the pathogenicity of this genomic rearrangement and indicate that *ABCC1* might represent a risk factor for autism and other neuropsychiatric disorders associated with 16p13.11 unbalanced rearrangements.

MATERIALS AND METHODS

10.1 *Drosophila* strains

Flies were raised on standard corn-yeast medium and maintained at 22°C. Flies carrying genotypes of interest were generated from original lines or suitable intermediate stocks and raised at specific temperatures (24°C or 29°C) on corn-yeast medium (for analyses at adult stage) or on agar medium (for embryos collection and analysis). The used lines are listed below. *en-Gal4* (*P{en2.4-GAL4}e16E*, BL # 30564**)**, *nub-Gal4* (*nub2-Gal4*), *tub-Gal4* (*P{tubP-GAL4}LL7*, BL # 5138), *elav-Gal4* (*P{GAL4-elav.L}3*, BL # 8760), *repo-Gal4* (*P{GAL4}repo*, BL # 7415) *UAS-GFP* (*P{5xUAS-IVS-mCD8::GFP}attP2*, BL # 32192), mys^{1} (mys^{1} *P{neoFRT}19A/FM7c*, BL # 23862) if^{B2} (g^{2} if^{B2} f^{36a}/*FM7c*, BL # 2176), mew^{M6} (y^{1} mew^{M6} f^{36a} *P{neoFRT}18A/FM7c*, BL # 1483) lines were obtained from the Bloomington Drosophila Stock Center (BDSC, https://bdsc.indiana.edu). *dMRP-RNAi* (*5xUAS-dMRP-RNAi*, VDRC # 105419) was obtained from Vienna Drosophila Resource Center (VDRC, www.vdrc.at). All the lines are described at FlyBase (https://flybase.org). The transgenic lines *UAS-hABCC1* and *UAS-hABCC1mut* were generated in the lab. Plasmids for embryo microinjection had been obtained through molecular subcloning of the wild type human ABCC1 and the mutated human ABCC1 from pCMV14-3XFLAG-ABCC1 and pCMV14-3XFLAG-ABCC1-DE1454LL (Henderson et al. 2011) into a pUASTattpB vector using NotI restriction site. The cloned segments were sequenced to verify the integrity of coding sequence. The transgenic lines *5xUAS-hABCC1* (BestGene 13453/1-4M) and *5xUAS-hABCC1mut* (BestGene 15900/1-2M) were generated and verified by BestGene Inc - Drosophila Embryo Injection Services (https://www.thebestgene.com).

See Section 5.2 for a detailed explanation of the Gal4-UAS system adopted for genetic manipulation.

10.2 Phenotypic analysis of adult wings

The analysis of the wing blister phenotype in adult flies has been carried out through the observation of progeny of interest using conventional stereomicroscope. For each genotype at a specific temperature a minimum of 4 replicates were performed, with 50 up to 100 flies analysed per replica.

The statistical significance between different genotypes was evaluated through the Mann-Whitney Wilcoxon test. *p*-values are as follows: $p \leq 0.05$=*, $p \leq 0.01$=**, $p \leq 0.001$=***.
Images were acquired in bright field using a Nikon Eclypse T90i microscope with a 4X magnification for adults and 10X for wings. The images were captured through a z-stack acquisition then converted to focused images using the Enhanced Deep Focus (EDF) module of the NIS Elements AR 3.10 software (Nikon).

10.3 Analysis of wing imaginal discs

Fluorescent immunolabelling and imaging of wing imaginal discs were performed on wandering 3rd instar larvae as described in Section 5.4 for eye-antenna imaginal complex.

10.4 Phenotypic analysis of embryonic central nervous system

10.4.1 Fluorescence immunolabeling

Embryos were collected after 12 hours egg laying at 29°C, washed in H_2O and then incubated in 7,5% NaClO in H_2O for 3 minutes to remove the external chorion. After washes in H_2O embryos were incubated for 30 minutes in a mix composed by 50% heptane and 50% fixing solution (4% paraformaldehyde in 1X PBS) to permeabilize the vitelline membrane and fix embryonic tissues. Then, embryos were dehydrated in two steps. The aqueous phase of 4% paraformaldehyde in 1X PBS was removed and methanol were added. The heptane and the interface (containing vitelline membranes and non-devitelinized embryos) were also removed and fresh methanol was added again. Embryos were rehydrated with 3 washes in 0.1% Triton X-100 in 1X PBS (hereafter referred as 0.1% PBT) for 10 minutes, permeabilized in 0.3% Triton X-100 in 1X PBS (hereafter referred as 0.3% PBT) for 15 minutes and incubated in blocking solution (4% Normal Goat Serum in 0.3% PBT) for 30 minutes. The appropriate mix of primary antibodies diluted in blocking solution was added and let stand overnight at 4°C. The following primary antibodies were used: monoclonal rat anti-Elav (1:100; 7E8A10 - DSHB), monoclonal mouse BP102 anti-CNS axons (1:500, BP102 - DSHB), monoclonal mouse anti-Repo (1:100, 8D12 - DSHB) Embryos were washed in 0.3% PBT, incubated in blocking solution for 20 minutes and finally incubated in the specific mix of fluorescent-dye conjugated secondary antibodies properly diluted in blocking solution. The following secondary antibodies were used: Cy3 anti-mouse (1:400, Jackson Immunoresearch) and AlexaFluor 647 anti-rat (1:400, Jackson Immunoresearch), FITC anti-rat (1:400, Jackson

Immunoresearch). All the secondary antibodies were subtracted against the other hosts species to avoid cross-reactions. Cell nuclei were labelled through the incubation in HOECHST (Sigma-Aldrich) 2 μg/ml in 0.1% PBT for 5 minutes. After washes in 1X PBS, embryos were mounted on microscope slides using Fluoromount-G (Electron Microscopy Sciences). Slides were let stand overnight at room temperature (RT) to allow the mounting medium to polymerize then were stored at -20°C.

10.4.2 Imaging and statistical analysis

Immunolabelled embryos were observed at a conventional epifluorescence microscope (Nikon Eclypse T90i microscope) in order to assess embryonic stage and to perform the phenotypic analysis. For each genotype of interest, a minimum of 100 embryos were analysed in at least 2 independent replica.

The penetrance of the phenotypic classes was compared between different genotypes using the Mann-Whitney Wilcoxon test. *p*-values are as follows: $p \leq 0.05$=*, $p \leq 0.01$=**, $p \leq 0.001$=***.

Images were acquired with a 20X magnification as described in Section 10.2).

REFERENCES

Adhikary S, Eilers M. 2005. Transcriptional regulation and transformation by Myc proteins. *Nat Rev Mol Cell Biol* **6**: 635–645.

Alberts B, Johnson A, Lewis J, Raff M, Roberts K, Walter P. 2002. Drosophila and the Molecular Genetics of Pattern Formation: Genesis of the Body Plan. *Molecular Biology of the Cell 4th edition*. https://www.ncbi.nlm.nih.gov/books/NBK26906/ (Accessed September 28, 2019).

Amati B, Littlewood TD, Evan GI, Land H. 1993. The c-Myc protein induces cell cycle progression and apoptosis through dimerization with Max. *EMBO J* **12**: 5083–5087.

Ayer DE, Eisenman RN. 1993. A switch from Myc:Max to Mad:Max heterocomplexes accompanies monocyte/macrophage differentiation. *Genes Dev* **7**: 2110–2119.

Bakircioglu M, Carvalho OP, Khurshid M, Cox JJ, Tuysuz B, Barak T, Yilmaz S, Caglayan O, Dincer A, Nicholas AK, et al. 2011. The essential role of centrosomal NDE1 in human cerebral cortex neurogenesis. *Am J Hum Genet* **88**: 523–535.

Beira JV, Paro R. 2016. The legacy of Drosophila imaginal discs. *Chromosoma* **125**: 573–592.

Benassayag C, Montero L, Colombié N, Gallant P, Cribbs D, Morello D. 2005. Human c-Myc Isoforms Differentially Regulate Cell Growth and Apoptosis in Drosophila melanogaster. *Mol Cell Biol* **25**: 9897–9909.

Bernstein H-G, Hölzl G, Dobrowolny H, Hildebrandt J, Trübner K, Krohn M, Bogerts B, Pahnke J. 2014. Vascular and extravascular distribution of the ATP-binding cassette transporters ABCB1 and ABCC1 in aged human brain and pituitary. *Mech Ageing Dev* **141–142**: 12–21.

Bourgeron T. 2015. From the genetic architecture to synaptic plasticity in autism spectrum disorder. *Nature Reviews Neuroscience* **16**: 551–563.

Brabant MC, Brower DL. 1993. PS2 Integrin Requirements in Drosophila Embryo and Wing Morphogenesis. *Developmental Biology* **157**: 49–59.

Brabant MC, Fristrom D, Bunch TA, Brower DL. 1996. Distinct spatial and temporal functions for PS integrins during Drosophila wing morphogenesis. *Development* **122**: 3307–3317.

Brand AH, Perrimon N. 1993. Targeted gene expression as a means of altering cell fates and generating dominant phenotypes. *Development* **118**: 401–415.

Bray NJ, O'Donovan MC. 2019. The genetics of neuropsychiatric disorders. *Brain Neurosci Adv* **2**. https://www.ncbi.nlm.nih.gov/pmc/articles/PMC6551216/ (Accessed October 10, 2019).

Bridges CB. *Drosophila melanogaster*: legend for symbols, mutants, valuations. Drosophila Information Service 1935;3:5-19 [Google Scholar]

Brodeur GM. 2003. Neuroblastoma: biological insights into a clinical enigma. *Nat Rev Cancer* **3**: 203–216.

Brower DL. 1986. Engrailed gene expression in Drosophila imaginal discs. *EMBO J* **5**: 2649–2656.

Brower DL, Bunch TA, Mukai L, Adamson TE, Wehrli M, Lam S, Friedlander E, Roote CE, Zusman S. 1995. Nonequivalent requirements for PS1 and PS2 integrin at cell attachments in Drosophila: genetic analysis of the alpha PS1 integrin subunit. *Development* **121**: 1311–1320.

Brower DL, Jaffe SM. 1989. Requirement for integrins during Drosophila wing development. *Nature* **342**: 285–287.

Brower DL, Piovant M, Reger LA. 1985. Developmental analysis of Drosophila position-specific antigens. *Developmental Biology* **108**: 120–130.

Brown JL, Grau DJ, DeVido SK, Kassis JA. 2005. An Sp1/KLF binding site is important for the activity of a Polycomb group response element from the Drosophila engrailed gene. *Nucleic Acids Res* **33**: 5181–5189.

Brown JL, Kassis JA. 2010. Spps, a Drosophila Sp1/KLF family member, binds to PREs and is required for PRE activity late in development. *Development* **137**: 2597–2602.

Cagan R. 2009. Principles of Drosophila Eye Differentiation. *Curr Top Dev Biol* **89**: 115–135.

Chesler L, Schlieve C, Goldenberg DD, Kenney A, Kim G, McMillan A, Matthay KK, Rowitch D, Weiss WA. 2006. Inhibition of Phosphatidylinositol 3-Kinase Destabilizes Mycn Protein and Blocks Malignant Progression in Neuroblastoma. *Cancer Res* **66**: 8139–8146.

Cifuentes FJ, García-Bellido A. 1997. Proximo–distal specification in the wing disc of Drosophila by the nubbin gene. *PNAS* **94**: 11405–11410.

Cohn SL, Pearson ADJ, London WB, Monclair T, Ambros PF, Brodeur GM, Faldum A, Hero B, Iehara T, Machin D, et al. 2009. The International Neuroblastoma Risk Group (INRG) Classification System: An INRG Task Force Report. *J Clin Oncol* **27**: 289–297.

Cole SP, Bhardwaj G, Gerlach JH, Mackie JE, Grant CE, Almquist KC, Stewart AJ, Kurz EU, Duncan AM, Deeley RG. 1992. Overexpression of a transporter gene in a multidrug-resistant human lung cancer cell line. *Science* **258**: 1650–1654.

Comino-Méndez I, Gracia-Aznárez FJ, Schiavi F, Landa I, Leandro-García LJ, Letón R, Honrado E, Ramos-Medina R, Caronia D, Pita G, et al. 2011. Exome sequencing identifies *MAX* mutations as a cause of hereditary pheochromocytoma. *Nature Genetics* **43**: 663–667.

Conacci-Sorrell M, McFerrin L, Eisenman RN. 2014. An Overview of MYC and Its Interactome. *Cold Spring Harb Perspect Med* **4**. https://www.ncbi.nlm.nih.gov/pmc/articles/PMC3869278/ (Accessed September 4, 2019).

Corvi R, Amler LC, Savelyeva L, Gehring M, Schwab M. 1994. MYCN is retained in single copy at chromosome 2 band p23-24 during amplification in human neuroblastoma cells. *Proc Natl Acad Sci U S A* **91**: 5523–5527.

Courchesne E, Pierce K. 2005. Why the frontal cortex in autism might be talking only to itself: local over-connectivity but long-distance disconnection. *Curr Opin Neurobiol* **15**: 225–230.

Cowling VH, Chandriani S, Whitfield ML, Cole MD. 2006. A Conserved Myc Protein Domain, MBIV, Regulates DNA Binding, Apoptosis, Transformation, and G2 Arrest. *Mol Cell Biol* **26**: 4226–4239.

Daniel A, Dumstrei K, Lengyel JA, Hartenstein V. 1999. The control of cell fate in the embryonic visual system by atonal, tailless and EGFR signaling. *Development* **126**: 2945–2954.

Daood M, Tsai C, Ahdab-Barmada M, Watchko JF. 2008. ABC Transporter (P-gp/ABCB1, MRP1/ABCC1, BCRP/ABCG2) Expression in the Developing Human CNS. *Neuropediatrics* **39**: 211–218.

Davis AC, Wims M, Spotts GD, Hann SR, Bradley A. 1993. A null c-myc mutation causes lethality before 10.5 days of gestation in homozygotes and reduced fertility in heterozygous female mice. *Genes Dev* **7**: 671–682.

de Kovel CGF, Trucks H, Helbig I, Mefford HC, Baker C, Leu C, Kluck C, Muhle H, von Spiczak S, Ostertag P, et al. 2010. Recurrent microdeletions at 15q11.2 and 16p13.11 predispose to idiopathic generalized epilepsies. *Brain* **133**: 23–32.

Dehal P, Boore JL. 2005. Two rounds of whole genome duplication in the ancestral vertebrate. *PLoS Biol* **3**: e314.

Diederich RJ, Pattatucci AM, Kaufman TC. 1991. Developmental and evolutionary implications of labial, Deformed and engrailed expression in the Drosophila head. *Development* **113**: 273–281.

Diolaiti D, Bernardoni R, Trazzi S, Papa A, Porro A, Bono F, Herbert J-M, Perini G, Della Valle G. 2007. Functional cooperation between TrkA and p75NTR accelerates neuronal differentiation by increased transcription of GAP-43 and p21(CIP/WAF) genes via ERK1/2 and AP-1 activities. *Experimental Cell Research* **313**: 2980–2992.

Duffy JB. 2002. GAL4 system in Drosophila: a fly geneticist's Swiss army knife. *Genesis* **34**: 1–15.

Duman-Scheel M, Johnston LA, Du W. 2004. Repression of dMyc expression by Wingless promotes Rbf-induced G1 arrest in the presumptive Drosophila wing margin. *Proc Natl Acad Sci USA* **101**: 3857–3862.

Eilers M, Eisenman RN. 2008. Myc's broad reach. *Genes Dev* **22**: 2755–2766.

Ferrucci F, Ciaccio R, Monticelli S, Pigini P, di Giacomo S, Purgato S, Erriquez D, Bernardoni R, Norris M, Haber M, et al. 2018. MAX to MYCN intracellular ratio drives the aggressive phenotype and clinical outcome of high risk neuroblastoma. *Biochim Biophys Acta Gene Regul Mech* **1861**: 235–245.

Feuk L, Carson AR, Scherer SW. 2006. Structural variation in the human genome. *Nat Rev Genet* **7**: 85–97.

Frank SR, Parisi T, Taubert S, Fernandez P, Fuchs M, Chan H-M, Livingston DM, Amati B. 2003. MYC recruits the TIP60 histone acetyltransferase complex to chromatin. *EMBO Rep* **4**: 575–580.

Freeman JL, Perry GH, Feuk L, Redon R, McCarroll SA, Altshuler DM, Aburatani H, Jones KW, Tyler-Smith C, Hurles ME, et al. 2006. Copy number variation: new insights in genome diversity. *Genome Res* **16**: 949–961.

Fristrom D, Wilcox M, Fristrom J. 1993. The distribution of PS integrins, laminin A and F-actin during key stages in Drosophila wing development. *Development* **117**: 509–523.

Gallant P. 2013. Myc Function in Drosophila. *Cold Spring Harb Perspect Med* **3**. https://www.ncbi.nlm.nih.gov/pmc/articles/PMC3784813/ (Accessed September 7, 2019).

Gallant P, Shiio Y, Cheng PF, Parkhurst SM, Eisenman RN. 1996. Myc and Max Homologs in Drosophila. *Science* **274**: 1523–1527.

Gartel AL, Ye X, Goufman E, Shianov P, Hay N, Najmabadi F, Tyner AL. 2001. Myc represses the p21(WAF1/CIP1) promoter and interacts with Sp1/Sp3. *PNAS* **98**: 4510–4515.

Gatto CL, Broadie K. 2011. Drosophila modeling of heritable neurodevelopmental disorders. *Curr Opin Neurobiol* **21**: 834–841.

Gibson G, Gehring WJ. 1988. Head and thoracic transformations caused by ectopic expression of Antennapedia during Drosophila development. *Development* **102**: 657–675.

Gomez-Roman N, Grandori C, Eisenman RN, White RJ. 2003. Direct activation of RNA polymerase III transcription by c-Myc. *Nature* **421**: 290–294.

Gottesman MM, Fojo T, Bates SE. 2002. Multidrug resistance in cancer: role of ATP–dependent transporters. *Nat Rev Cancer* **2**: 48–58.

Grady EF, Schwab M, Rosenau W. 1987. Expression of N-myc and c-src during the development of fetal human brain. *Cancer Res* **47**: 2931–2936.

Grailles M, Brey PT, Roth CW. 2003. The Drosophila melanogaster multidrug-resistance protein 1 (MRP1) homolog has a novel gene structure containing two variable internal exons. *Gene* **307**: 41–50.

Grandori C, Mac J, Siëbelt F, Ayer DE, Eisenman RN. 1996. Myc-Max heterodimers activate a DEAD box gene and interact with multiple E box-related sites in vivo. *EMBO J* **15**: 4344–4357.

Guo Y, He J, Zhao S, Wu H, Zhong X, Sheng Q, Samuels DC, Shyr Y, Long J. 2014. Illumina human exome genotyping array clustering and quality control. *Nat Protoc* **9**: 2643–2662.

Haber M, Smith J, Bordow SB, Flemming C, Cohn SL, London WB, Marshall GM, Norris MD. 2006. Association of High-Level *MRP1* Expression With Poor Clinical Outcome in a Large Prospective Study of Primary Neuroblastoma. *JCO* **24**: 1546–1553.

Halder G, Callaerts P, Flister S, Walldorf U, Kloter U, Gehring WJ. 1998. Eyeless initiates the expression of both sine oculis and eyes absent during Drosophila compound eye development. *Development* **125**: 2181–2191.

Hannes FD, Sharp AJ, Mefford HC, de Ravel T, Ruivenkamp CA, Breuning MH, Fryns J-P, Devriendt K, Van Buggenhout G, Vogels A, et al. 2009. Recurrent reciprocal deletions and duplications of 16p13.11: the deletion is a risk factor for MR/MCA while the duplication may be a rare benign variant. *J Med Genet* **46**: 223–232.

Hartenstein V, Wodarz A. 2013. Initial neurogenesis in Drosophila. *Wiley Interdiscip Rev Dev Biol* **2**: 701–721.

Henderson MJ, Haber M, Porro A, Munoz MA, Iraci N, Xue C, Murray J, Flemming CL, Smith J, Fletcher JI, et al. 2011. ABCC Multidrug Transporters in Childhood Neuroblastoma: Clinical and

Biological Effects Independent of Cytotoxic Drug Efflux. *JNCI: Journal of the National Cancer Institute* **103**: 1236–1251.

Hermeking H, Rago C, Schuhmacher M, Li Q, Barrett JF, Obaya AJ, O'Connell BC, Mateyak MK, Tam W, Kohlhuber F, et al. 2000. Identification of CDK4 as a target of c-MYC. *PNAS* **97**: 2229–2234.

Hoang B, Chiba A. 1998. Genetic Analysis on the Role of Integrin during Axon Guidance in Drosophila. *J Neurosci* **18**: 7847–7855.

Honig SM, Fu S, Mao X, Yopp A, Gunn MD, Randolph GJ, Bromberg JS. 2003. FTY720 stimulates multidrug transporter- and cysteinyl leukotriene-dependent T cell chemotaxis to lymph nodes. *J Clin Invest* **111**: 627–637.

Hopewell R, Ziff EB. 1995. The nerve growth factor-responsive PC12 cell line does not express the Myc dimerization partner Max. *Mol Cell Biol* **15**: 3470–3478.

Housden BE, Muhar M, Gemberling M, Gersbach CA, Stainier DYR, Seydoux G, Mohr SE, Zuber J, Perrimon N. 2017. Loss-of-function genetic tools for animal models: cross-species and cross-platform differences. *Nat Rev Genet* **18**: 24–40.

Hurles ME, Dermitzakis ET, Tyler-Smith C. 2008. The functional impact of structural variation in humans. *Trends in Genetics* **24**: 238–245.

Hynes RO. 2002. Integrins: Bidirectional, Allosteric Signaling Machines. *Cell* **110**: 673–687.

Iafrate AJ, Feuk L, Rivera MN, Listewnik ML, Donahoe PK, Qi Y, Scherer SW, Lee C. 2004. Detection of large-scale variation in the human genome. *Nat Genet* **36**: 949–951.

Ingason A, Rujescu D, Cichon S, Sigurdsson E, Sigmundsson T, Pietiläinen OPH, Buizer-Voskamp JE, Strengman E, Francks C, Muglia P, et al. 2011. Copy number variations of chromosome 16p13.1 region associated with schizophrenia. *Mol Psychiatry* **16**: 17–25.

Iraci N, Diolaiti D, Papa A, Porro A, Valli E, Gherardi S, Herold S, Eilers M, Bernardoni R, Valle GD, et al. 2011. A SP1/MIZ1/MYCN Repression Complex Recruits HDAC1 at the TRKA and p75NTR Promoters and Affects Neuroblastoma Malignancy by Inhibiting the Cell Response to NGF. *Cancer Res* **71**: 404–412.

Jacquemont S, Reymond A, Zufferey F, Harewood L, Walters RG, Kutalik Z, Martinet D, Shen Y, Valsesia A, Beckmann ND, et al. 2011. Mirror extreme BMI phenotypes associated with gene dosage at the chromosome 16p11.2 locus. *Nature* **478**: 97–102.

Just MA, Cherkassky VL, Keller TA, Kana RK, Minshew NJ. 2007. Functional and anatomical cortical underconnectivity in autism: evidence from an FMRI study of an executive function task and corpus callosum morphometry. *Cereb Cortex* **17**: 951–961.

Kaczynski J, Cook T, Urrutia R. 2003. Sp1- and Krüppel-like transcription factors. *Genome Biol* **4**: 206.

Kana RK, Uddin LQ, Kenet T, Chugani D, Müller R-A. 2014. Brain connectivity in autism. *Front Hum Neurosci* **8**. https://www.frontiersin.org/articles/10.3389/fnhum.2014.00349/full#B28 (Accessed October 10, 2019).

Kohl NE, Kanda N, Schreck RR, Bruns G, Latt SA, Gilbert F, Alt FW. 1983. Transposition and amplification of oncogene-related sequences in human neuroblastomas. *Cell* **35**: 359–367.

Kuang S-Q, Guo D-C, Prakash SK, McDonald M-LN, Johnson RJ, Wang M, Regalado ES, Russell L, Cao J-M, Kwartler C, et al. 2011. Recurrent chromosome 16p13.1 duplications are a risk factor for aortic dissections. *PLoS Genet* **7**: e1002118.

Kumar JP. 2012. Building an Ommatidium One Cell at a Time. *Dev Dyn* **241**: 136–149.

Kumar JP, Moses K. 2001. EGF Receptor and Notch Signaling Act Upstream of Eyeless/Pax6 to Control Eye Specification. *Cell* **104**: 687–697.

Kurata S, Go MJ, Artavanis-Tsakonas S, Gehring WJ. 2000. Notch signaling and the determination of appendage identity. *PNAS* **97**: 2117–2122.

Lamka ML, Boulet AM, Sakonju S. 1992. Ectopic expression of UBX and ABD-B proteins during Drosophila embryogenesis: competition, not a functional hierarchy, explains phenotypic suppression. *Development* **116**: 841–854.

Landgraf M, Jeffrey V, Fujioka M, Jaynes JB, Bate M. 2003. Embryonic Origins of a Motor System: Motor Dendrites Form a Myotopic Map in Drosophila. *PLOS Biology* **1**: e41.

Leier I, Jedlitschky G, Buchholz U, Cole SP, Deeley RG, Keppler D. 1994. The MRP gene encodes an ATP-dependent export pump for leukotriene C4 and structurally related conjugates. *J Biol Chem* **269**: 27807–27810.

Lin Y-C, Frei JA, Kilander MBC, Shen W, Blatt GJ. 2016. A Subset of Autism-Associated Genes Regulate the Structural Stability of Neurons. *Front Cell Neurosci* **10**. https://www.ncbi.nlm.nih.gov/pmc/articles/PMC5112273/ (Accessed September 30, 2019).

Liu T, Tee AEL, Porro A, Smith SA, Dwarte T, Liu PY, Iraci N, Sekyere E, Haber M, Norris MD, et al. 2007. Activation of tissue transglutaminase transcription by histone deacetylase inhibition as a therapeutic approach for Myc oncogenesis. *Proc Natl Acad Sci USA* **104**: 18682–18687.

Loo LWM, Secombe J, Little JT, Carlos L-S, Yost C, Cheng P-F, Flynn EM, Edgar BA, Eisenman RN. 2005. The Transcriptional Repressor dMnt Is a Regulator of Growth in Drosophila melanogaster. *Mol Cell Biol* **25**: 7078–7091.

Lord C, Risi S, Lambrecht L, Cook EH, Leventhal BL, DiLavore PC, Pickles A, Rutter M. 2000. The autism diagnostic observation schedule-generic: a standard measure of social and communication deficits associated with the spectrum of autism. *J Autism Dev Disord* **30**: 205–223.

Lord C, Rutter M, Le Couteur A. 1994. Autism Diagnostic Interview-Revised: a revised version of a diagnostic interview for caregivers of individuals with possible pervasive developmental disorders. *J Autism Dev Disord* **24**: 659–685.

Makino T, McLysaght A. 2010. Ohnologs in the human genome are dosage balanced and frequently associated with disease. *PNAS* **107**: 9270–9274.

Mallo M, Alonso CR. 2013. The regulation of Hox gene expression during animal development. *Development* **140**: 3951–3963.

Malynn BA, de Alboran IM, O'Hagan RC, Bronson R, Davidson L, DePinho RA, Alt FW. 2000. N-myc can functionally replace c-myc in murine development, cellular growth, and differentiation. *Genes Dev* **14**: 1390–1399.

Mao DYL, Watson JD, Yan PS, Barsyte-Lovejoy D, Khosravi F, Wong WW-L, Farnham PJ, Huang TH-M, Penn LZ. 2003. Analysis of Myc Bound Loci Identified by CpG Island Arrays Shows that Max Is Essential for Myc-Dependent Repression. *Current Biology* **13**: 882–886.

Maris JM, Hogarty MD, Bagatell R, Cohn SL. 2007. Neuroblastoma. *The Lancet* **369**: 2106–2120.

Marshall GM, Gherardi S, Xu N, Neiron Z, Trahair T, Scarlett CJ, Chang DK, Liu PY, Jankowski K, Iraci N, et al. 2010. Transcriptional upregulation of histone deacetylase 2 promotes Myc-induced oncogenic effects. *Oncogene* **29**: 5957–5968.

Martin J, Han C, Gordon LA, Terry A, Prabhakar S, She X, Xie G, Hellsten U, Chan YM, Altherr M, et al. 2004. The sequence and analysis of duplication-rich human chromosome 16. *Nature* **432**: 988–994.

Merrill VK, Turner FR, Kaufman TC. 1987. A genetic and developmental analysis of mutations in the Deformed locus in Drosophila melanogaster. *Dev Biol* **122**: 379–395.

Meyer N, Penn LZ. 2008. Reflecting on 25 years with MYC. *Nat Rev Cancer* **8**: 976–990.

Miller DF, Rogers BT, Kalkbrenner A, Hamilton B, Holtzman SL, Kaufman T. 2001. Cross-regulation of Hox genes in the Drosophila melanogaster embryo. *Mech Dev* **102**: 3–16.

Mills RE, Walter K, Stewart C, Handsaker RE, Chen K, Alkan C, Abyzov A, Yoon SC, Ye K, Cheetham RK, et al. 2011. Mapping copy number variation by population-scale genome sequencing. *Nature* **470**: 59–65.

Morata G, Lawrence PA. 1975. Control of compartment development by the engrailed gene in Drosophila. *Nature* **255**: 614–617.

Mottis A, Mouchiroud L, Auwerx J. 2013. Emerging roles of the corepressors NCoR1 and SMRT in homeostasis. *Genes Dev* **27**: 819–835.

Nagaoka M, Shiraishi Y, Sugiura Y. 2001. Selected base sequence outside the target binding site of zinc finger protein Sp1. *Nucleic Acids Res* **29**: 4920–4929.

Napolioni V, Lombardi F, Sacco R, Curatolo P, Manzi B, Alessandrelli R, Militerni R, Bravaccio C, Lenti C, Saccani M, et al. 2011. Family-based association study of ITGB3 in autism spectrum disorder and its endophenotypes. *Eur J Hum Genet* **19**: 353–359.

Nienhaus U, Aegerter-Wilmsen T, Aegerter CM. 2012. In-Vivo Imaging of the Drosophila Wing Imaginal Disc over Time: Novel Insights on Growth and Boundary Formation. *PLoS One* **7**. https://www.ncbi.nlm.nih.gov/pmc/articles/PMC3473014/ (Accessed September 28, 2019).

Nies AT, Jedlitschky G, König J, Herold-Mende C, Steiner HH, Schmitt H-P, Keppler D. 2004. Expression and immunolocalization of the multidrug resistance proteins, MRP1–MRP6 (ABCC1–ABCC6), in human brain. *Neuroscience* **129**: 349–360.

Nooter K, Westerman AM, Flens MJ, Zaman GJ, Scheper RJ, Wingerden KE van, Burger H, Oostrum R, Boersma T, Sonneveld P. 1995. Expression of the multidrug resistance-associated protein (MRP) gene in human cancers. *Clin Cancer Res* **1**: 1301–1310.

Orian A, van Steensel B, Delrow J, Bussemaker HJ, Li L, Sawado T, Williams E, Loo LWM, Cowley SM, Yost C, et al. 2003. Genomic binding by the Drosophila Myc, Max, Mad/Mnt transcription factor network. *Genes Dev* **17**: 1101–1114.

Park SY, Stultz BG, Hursh DA. 2015. Dual Role of Jun N-Terminal Kinase Activity in Bone Morphogenetic Protein-Mediated Drosophila Ventral Head Development. *Genetics* **201**: 1411–1426.

Park YK, Goda Y. 2016. Integrins in synapse regulation. *Nature Reviews Neuroscience* **17**: 745–756.

Plaza S, Prince F, Jaeger J, Kloter U, Flister S, Benassayag C, Cribbs D, Gehring WJ. 2001. Molecular basis for the inhibition of Drosophila eye development by Antennapedia. *EMBO J* **20**: 802–811.

Porro A, Haber M, Diolaiti D, Iraci N, Henderson M, Gherardi S, Valli E, Munoz MA, Xue C, Flemming C, et al. 2010. Direct and Coordinate Regulation of ATP-binding Cassette Transporter Genes by Myc Factors Generates Specific Transcription Signatures That Significantly Affect the Chemoresistance Phenotype of Cancer Cells. *J Biol Chem* **285**: 19532–19543.

Price DH. 2000. P-TEFb, a Cyclin-Dependent Kinase Controlling Elongation by RNA Polymerase II. *Mol Cell Biol* **20**: 2629–2634.

Ramalingam A, Zhou X-G, Fiedler SD, Brawner SJ, Joyce JM, Liu H-Y, Yu S. 2011. 16p13.11 duplication is a risk factor for a wide spectrum of neuropsychiatric disorders. *J Hum Genet* **56**: 541–544.

Ratner N, Brodeur GM, Dale RC, Schor NF. 2016. The “Neuro” of Neuroblastoma: Neuroblastoma as a Neurodevelopmental Disorder. *Ann Neurol* **80**: 13–23.

Redon R, Ishikawa S, Fitch KR, Feuk L, Perry GH, Andrews TD, Fiegler H, Shapero MH, Carson AR, Chen W, et al. 2006. Global variation in copy number in the human genome. *Nature* **444**: 444–454.

Rickert C, Kunz T, Harris K-L, Whitington PM, Technau GM. 2011. Morphological Characterization of the Entire Interneuron Population Reveals Principles of Neuromere Organization in the Ventral Nerve Cord of Drosophila. *J Neurosci* **31**: 15870–15883.

Ripoll P, Messal ME, Laran E, Simpson P. A gradient of affinities for sensory bristles across the wing blade of. 11.

Ripoll P, Messal ME, Laran E, Simpson P. 1988. A gradient of affinities for sensory bristles across the wing blade of Drosophila melanogaster. *Development* **103**: 757–767.

Robbiani DF, Finch RA, Muller WA, Sartorelli AC, Randolph GJ. 2000 The Leukotriene C4 Transporter MRP1 Regulates CCL19 (MIP-3⊠, ELC)–Dependent Mobilization of Dendritic Cells to Lymph Nodes. 12.

Rusch DB, Kaufman TC. 2000. Regulation of proboscipedia in Drosophila by Homeotic Selector Genes. *Genetics* **156**: 183–194.

Sawai S, Shimono A, Wakamatsu Y, Palmes C, Hanaoka K, Kondoh H. 1993. Defects of embryonic organogenesis resulting from targeted disruption of the N-myc gene in the mouse. *Development* **117**: 1445–1455.

Schuettengruber B, Bourbon H-M, Di Croce L, Cavalli G. 2017. Genome Regulation by Polycomb and Trithorax: 70 Years and Counting. *Cell* **171**: 34–57.

Sebat J, Lakshmi B, Troge J, Alexander J, Young J, Lundin P, Månér S, Massa H, Walker M, Chi M, et al. 2004. Large-Scale Copy Number Polymorphism in the Human Genome. *Science* **305**: 525–528.

Secombe J, Li L, Carlos L, Eisenman RN. 2007. The Trithorax group protein Lid is a trimethyl histone H3K4 demethylase required for dMyc-induced cell growth. *Genes Dev* **21**: 537–551.

Seeger RC, Wada R, Brodeur GM, Moss TJ, Bjork RL, Sousa L, Slamon DJ. 1988. Expression of N-myc by neuroblastomas with one or multiple copies of the oncogene. *Prog Clin Biol Res* **271**: 41–49.

Soucek L, Jucker R, Panacchia L, Ricordy R, Tatò F, Nasi S. 2002. Omomyc, a Potential Myc Dominant Negative, Enhances Myc-induced Apoptosis. *Cancer Res* **62**: 3507–3510.

Staller P, Peukert K, Kiermaier A, Seoane J, Lukas J, Karsunky H, Möröy T, Bartek J, Massagué J, Hänel F, et al. 2001. Repression of p15INK4b expression by Myc through association with Miz-1. *Nat Cell Biol* **3**: 392–399.

Stanton BR, Perkins AS, Tessarollo L, Sassoon DA, Parada LF. 1992. Loss of N-myc function results in embryonic lethality and failure of the epithelial component of the embryo to develop. *Genes Dev* **6**: 2235–2247.

Stefansson H, Rujescu D, Cichon S, Pietiläinen OPH, Ingason A, Steinberg S, Fossdal R, Sigurdsson E, Sigmundsson T, Buizer-Voskamp JE, et al. 2008. Large recurrent microdeletions associated with schizophrenia. *Nature* **455**: 232–236.

Steiger D, Furrer M, Schwinkendorf D, Gallant P. 2008. Max-independent functions of Myc in *Drosophila melanogaster*. *Nature Genetics* **40**: 1084–1091.

Tabata T, Schwartz C, Gustavson E, Ali Z, Kornberg TB. 1995. Creating a Drosophila wing de novo, the role of engrailed, and the compartment border hypothesis. *Development* **121**: 3359–3369.

Tarnay JN, Szeri F, Iliás A, Annilo T, Sung C, Saux OL, Váradi A, Dean M, Boyd CD, Robinow S. 2004. The dMRP/CG6214 gene of Drosophila is evolutionarily and functionally related to the human multidrug resistance-associated protein family. *Insect Molecular Biology* **13**: 539–548.

Tropeano M, Ahn JW, Dobson RJB, Breen G, Rucker J, Dixit A, Pal DK, McGuffin P, Farmer A, White PS, et al. 2013. Male-Biased Autosomal Effect of 16p13.11 Copy Number Variation in Neurodevelopmental Disorders. *PLoS One* **8**. https://www.ncbi.nlm.nih.gov/pmc/articles/PMC3630198/ (Accessed September 19, 2019).

Trumpp A, Refaeli Y, Oskarsson T, Gasser S, Murphy M, Martin GR, Bishop JM. 2001. c-Myc regulates mammalian body size by controlling cell number but not cell size. *Nature* **414**: 768–773.

Ullmann R, Turner G, Kirchhoff M, Chen W, Tonge B, Rosenberg C, Field M, Vianna-Morgante AM, Christie L, Krepischi-Santos AC, et al. 2007. Array CGH identifies reciprocal 16p13.1 duplications and deletions that predispose to autism and/or mental retardation. *Hum Mutat* **28**: 674–682.

Valentijn LJ, Koster J, Haneveld F, Aissa RA, van Sluis P, Broekmans MEC, Molenaar JJ, van Nes J, Versteeg R. 2012. Functional MYCN signature predicts outcome of neuroblastoma irrespective of MYCN amplification. *Proc Natl Acad Sci USA* **109**: 19190–19195.

Van Arendonk KJ, Chung DH. 2019. Neuroblastoma: Tumor Biology and Its Implications for Staging and Treatment. *Children (Basel)* **6**. https://www.ncbi.nlm.nih.gov/pmc/articles/PMC6352222/ (Accessed September 2, 2019).

van de Ven R, de Jong MC, Reurs AW, Schoonderwoerd AJN, Jansen G, Hooijberg JH, Scheffer GL, de Gruijl TD, Scheper RJ. 2006. Dendritic cells require multidrug resistance protein 1 (ABCC1) transporter activity for differentiation. *J Immunol* **176**: 5191–5198.

Vaqué JP, Fernández-García B, García-Sanz P, Ferrandiz N, Bretones G, Calvo F, Crespo P, Marín MC, León J. 2008. c-Myc Inhibits Ras-Mediated Differentiation of Pheochromocytoma Cells by Blocking c-Jun Up-Regulation. *Mol Cancer Res* **6**: 325–339.

Vasiliou V, Vasiliou K, Nebert DW. 2009. Human ATP-binding cassette (ABC) transporter family. *Hum Genomics* **3**: 281–290.

Velinov M. 2019. Genomic Copy Number Variations in the Autism Clinic—Work in Progress. *Front Cell Neurosci* **13**. https://www.ncbi.nlm.nih.gov/pmc/articles/PMC6389619/ (Accessed October 3, 2019).

Vennstrom B, Sheiness D, Zabielski J, Bishop JM. 1982. Isolation and characterization of c-myc, a cellular homolog of the oncogene (v-myc) of avian myelocytomatosis virus strain 29. *J Virol* **42**: 773–779.

Wada RK, Seeger RC, Brodeur GM, Einhorn PA, Rayner SA, Tomayko MM, Reynolds CP. 1993. Human neuroblastoma cell lines that express N-myc without gene amplification. *Cancer* **72**: 3346–3354.

Wartiovaara K, Barnabé-Heider F, Miller FD, Kaplan DR. 2002. N-myc Promotes Survival and Induces S-Phase Entry of Postmitotic Sympathetic Neurons. *J Neurosci* **22**: 815–824.

Weiss LA, Kosova G, Delahanty RJ, Jiang L, Cook EH, Ober C, Sutcliffe JS. 2006. Variation in ITGB3 is associated with whole-blood serotonin level and autism susceptibility. *Eur J Hum Genet* **14**: 923–931.

Wellcome Trust Case Control Consortium, Craddock N, Hurles ME, Cardin N, Pearson RD, Plagnol V, Robson S, Vukcevic D, Barnes C, Conrad DF, et al. 2010. Genome-wide association study of CNVs in 16,000 cases of eight common diseases and 3,000 shared controls. *Nature* **464**: 713–720.

Wert M, Kennedy S, Palfrey HC, Hay N. 2001. Myc drives apoptosis in PC12 cells in the absence of Max. *Oncogene* **20**: 3746–3750.

Wiese KE, Walz S, von Eyss B, Wolf E, Athineos D, Sansom O, Eilers M. 2013. The Role of MIZ-1 in MYC-Dependent Tumorigenesis. *Cold Spring Harb Perspect Med* **3**. https://www.ncbi.nlm.nih.gov/pmc/articles/PMC3839600/ (Accessed August 28, 2019).

Wilcox M, Brower DL, Smith RJ. 1981. A position-specific cell surface antigen in the drosophila wing imaginal disc. *Cell* **25**: 159–164.

Wirz J, Fessler LI, Gehring WJ. 1986. Localization of the Antennapedia protein in Drosophila embryos and imaginal discs. *EMBO J* **5**: 3327–3334.

Yuen RK, Merico D, Bookman M, Howe JL, Thiruvahindrapuram B, Patel RV, Whitney J, Deflaux N, Bingham J, Wang Z, et al. 2017. Whole genome sequencing resource identifies 18 new candidate genes for autism spectrum disorder. *Nat Neurosci* **20**: 602–611.

Zaffran S, Chartier A, Gallant P, Astier M, Arquier N, Doherty D, Gratecos D, Semeriva M. 1998. A Drosophila RNA helicase gene, pitchoune, is required for cell growth and proliferation and is a potential target of d-Myc. *Development* **125**: 3571–3584.

Zarrei M, MacDonald JR, Merico D, Scherer SW. 2015. A copy number variation map of the human genome. *Nature Reviews Genetics* **16**: 172–183.

Zimmerman KA, Yancopoulos GD, Collum RG, Smith RK, Kohl NE, Denis KA, Nau MM, Witte ON, Toran-Allerand D, Gee CE, et al. 1986. Differential expression of myc family genes during murine development. *Nature* **319**: 780–783.